

**EFFECT OF WELDING ON
LATERAL-TORSIONAL BUCKLING RESISTANCE OF
I-SHAPED BUILT-UP STEEL BEAMS**

By
Raja Muhammed Younes

Supervisor
Dr. Yasser M. Hunaiti, Prof.

Co-Supervisor
Dr. Ghazi Abu-Farsakh, Prof.

Submitted in Partial Fulfillment of the Requirement for the
Degree of Doctor in Philosophy in Civil Engineering

Faculty of Graduate Studies
The University of Jordan

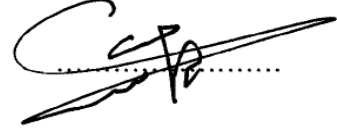
January, 2008

This thesis (Effect of Welding on Lateral-Torsional Buckling Resistance of I-shaped Built-Up Steel Beams) was successfully defended and approved on: 3rd January 2008.


Examination Committee

Signature

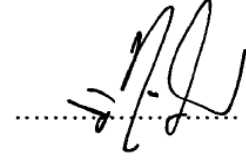
Dr. Yasser Hunaiti, Chairman
Prof. of Civil Engineering
Jordan



Dr. Ghazi Abu-Farsakh, Co-supervisor
Prof. of Civil Engineering
Jordan University of Science and Technology



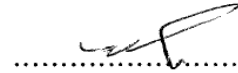
Dr. Raed M. Samra, Member
Prof. of Civil Engineering
Jordan



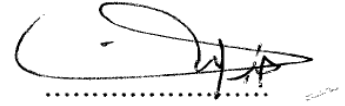
Dr. Samih S. Qaqiach, Member
Prof. Of Civil Engineering
Jordan



Dr. Mutasim S. Abdel-Jaber, Member
Assist. Prof. of Civil Engineering
Jordan



Dr. Khairedin M. Nussairat, Member
Assoc. Prof. of Civil Engineering
Jordan University of Science and Technology



DEDICATION

To my family, friends and husband, engineer Nabil Bitawi, without his consistent support and encouragement, it is impossible for me to finish this work.

For all of them I dedicate this work with love and respect.

Raja

ACKNOWLEDGMENT

First I would like to express my grateful thanks to my God for helping me and giving me the power to overcome all the difficulties during this study.

There are so many people to thank and I find it difficult to know where to begin. I firstly thank my supervisor Professor Yasser M. Hunaiti, for his invaluable suggestions and guidance throughout my graduate work. I have come to value his integrity and professionalism.

I also want to thank Professor Ghazi Abu-Farsakh, for all he has done to assist me during my candidature. He has provided expert advice and support.

I am indebted to those who provided financial support to this project. The experimental program conducted during this study was financially supported by the Deanship of Scientific Research at the University of Jordan. Test specimens were sponsored (fabricated and supplied) by Steel Building Company Ltd. I owe much to the efficient and high quality work of the staff of this company. I especially thank Engineer Ramzi Haffar for his help and support.

Thanks go to those who have provided help especially Dr. Ibraheem Asi and Dr. Muhammed Abdel Gader, Engineers Shadi, Jamal and Muhammed Abas.

The valuable reviews of the committee members, Prof. Raed Samra, Prof. Samih Qaqiach, Assoc. Prof. Khairedin Nussairat and Assist. Prof. Mutasim Abdel-Jaber are greatly acknowledged.

LIST OF CONTENTS

EXAMINATION COMMITTEE	ii
DEDICATION	iii
ACKNOWLEDGMENT	iv
LIST OF CONTENTS	v
LIST OF FIGURES	viii
LIST OF TABLES	xii
ABBREVIATIONS AND NOTATIONS	xiv
LIST OF SYMBOLS	xv
ABSTRACT	xvii
CHAPTER 1 INTRODUCTION	1
1.1 General	1
1.2 Research Significance	1
1.3 Literature Review	3
1.4 Objectives of the Study	12
CHAPTER 2 BUCKLING OF I-BEAMS	14
2.1 Introduction	14
2.2 Local Buckling	15
2.2.1 Local Buckling Requirements	18
2.2.1.1 Canadian Standard CSA-S16-01-2001	18
2.2.1.2 European Standard - EC3 (2005) (ENV 1993) Part 1.1	18
2.2.1.3 American Specification AISC LRFD-2005	20
2.3 Lateral-Torsional Buckling	21
2.3.1 Elastic Lateral-torsional buckling	22
2.3.1.1 Moment Gradient	24
2.3.1.2 Effect of Load Height	25
2.3.1.3 End Restrained Doubly Symmetric Beams	26
2.3.2 Inelastic Lateral Torsional Buckling	29
2.3.3 American Specification AISC LRFD-2005	32
2.3.4 Canadian Standard CSA-S16-01-2001	34
2.3.5 European Standard - EC3 (2005) (ENV 1993) Part 1.1	36

2.3.6 Australian Standard -AS4100-98	38
2.4 Comparison of Design Specifications	40
CHAPTER 3 MECHANICAL-PROPERTY TESTS	43
3.1 Residual Stress Measurements	43
3.1.1 Introduction	43
3.1.2 Background	44
3.1.3 Principle of Hole-Drilling Method	46
3.1.4 Computation of Stresses	49
3.1.5 Test for non-uniformity	50
3.1.6 Equivalent Uniform Stress Method (EUS)	52
3.1.7 Experimental Approach	54
3.2 Tension Tests	60
3.2.1 Introduction	60
3.2.2 Test procedure	61
CHAPTER 4 EXPERIMENTAL PROGRAM	67
4.1 Introduction	67
4.2 Test Beams	67
4.3 Supported System	71
4.4 Initial Imperfections	73
4.5 Test Set-Up	74
4.6 Instrumentation	74
4.6.1 Load Measurements	74
4.6.2 Displacement Measuring Instruments	76
4.6.3 Strain Measurement	76
4.7 Experimental Procedure	78
CHAPTER 5 EXPERIMENTAL RESULTS AND DISCUSSION	80
5.1 Introduction	80
5.2 Behavior of Specimens and Failure Loads	80
5.3 Support Conditions	91
5.4 Effect of Residual Stress	92

5.5 Load-Strain Behavior and Strain Distribution	93
5.6 Load-Deflection Behavior	105
5.7 Evaluation of Test Results	124
5.7.1 Comparison with Available Test Data of welded Beams	124
5.7.2 Comparison with Available Test Data of Rolled Beams	126
5.7.3 Comparison with Current Standards	126
CHAPTER 6 CONCLUSIONS AND RECOMONDATIONS	130
6.1 Summary	130
6.2 Conclusions	131
6.3 Recommendations	133
REFERENCES	135
APPENDICES	139
Appendix A	140
Appendix B	159
ARABIC ABSTRACT	167

LIST OF FIGURES

<u>Figure</u>	<u>Description</u>	<u>Page</u>
2.1	Local Buckling of I-Beams	15
2.2	Classification of Beam Sections According to Canadian Standard CSA S16.1-94 and American (LRFD) Specifications	17
2.3	Lateral -Torsional Buckling of a Beam Subjected to Uniform Moment	21
2.4	Plan View of Idealized End Restraints	28
2.5	Lateral Buckling Strength of Simply Supported-Beams	31
2.6	Schematic Plot of Beam Curve in LRFD	32
2.7	The Design Rules in Different Standards for Lateral-Torsional Buckling of I-Sections Beams	42
3.1	Strain Gage Rosette Arrangement for Determining Residual Stresses	45
3.2	Data-Reduction Coefficients, as Functions of Non-Dimensional Hole Depth and Diameter (From Technical Notes TN-503-2)	48
3.3	Percent Strain Versus Normalized Hole Depth for Uniform Stress With Depth (From ASTM E 837-2001)	52
3.4	Data-Reduction Coefficients, as Functions of Non Dimensional Hole Depth and Diameter (From Schajer ,1988)	53
3.5	Allotment of Test Specimens and Locations of Rosettes	55
3.6	Hole Size Measurement	56
3.7	Instrumentation of Residual Stress Measurement	57
3.8	The Application of Rosette	57
3.9	Percent Strain Versus Normalized Hole Depth for Specimen AA30	58
3.10	Tension Test Coupon	63
3.11	Universal Testing Machine	64
3.12	Tension Test Specimen with Extensometer	65
3.13	Tension Test Specimen after Fracture	65
3.14	Tension Test Specimens with Strain Gages	66
3.15	Portable Data Logger TDS-303	66
4.1a	Beam Specimens With Fillet Welds on Both Side of the Web	69
4.1b	Beam Specimens With Fillet Weld on One Side of the Web	69

4.2	Figure 4.2: Automatic Submerged Arc Welding process	69
4.3	Support System	72
4.4	Schematic Diagram of Test Set-Up	75
4.5	Buckling Test Apparatus	75
4.6	Strain Gage Identification Numbers and Locations	77
5.1	Combined Buckling Mode in Beam AB1A.	84
5.2	Local Buckling Mode in Beam AB1	84
5.3	Typical Wave shapes for Beams AB1 and AB1A at Collapse	85
5.4	Combined Buckling Mode in Beam BB2	85
5.5	Combined Buckling Mode in Beam BB1A	86
5.6	Combined Buckling Mode in Beam BB1	86
5.7	Local Buckling Mode in Beam AB3	88
5.8	Combined Buckling Mode in Beam AB3A	88
5.9	Combined Buckling Mode in Beam BB4A	89
5.10	Local Buckling Mode in Beam BB4	89
5.11	Lateral-Torsional Buckling Mode in Beam CB4A	90
5.12	Lateral-Torsional Buckling Mode of Beam CB4	90
5.13	Load-Strain Curves for Beam AB1	96
5.14	Load-Strain Curves for Beam AB1A	97
5.15	Load-Strain Curves for Beam AB2	98
5.16	Load-Strain Curves for Beam AB2A	99
5.17	Load-Strain Curves for Beam BB1	100
5.18	Load-Strain Curves for Buckling of Beam BB1A	101
5.19	Load-Strain Curves for Buckling of Beam BB2	102
5.20	Load-Strain Curves for Buckling of Beam BB2A	103
5.21	Load-Strain Curves for Buckling of Beam AB3	106
5.22	Load-Strain Curves for Buckling of Beam AB3A	106
5.23	Load-Strain Curves for Buckling of Beam BB3	107
5.24	Load-Strain Curves for Buckling of Beam BB3A	108
5.25	Load-Strain Curves for Buckling of Beam BB4	109
5.26	Load-Strain Curves for Buckling of Beam BB4A	110
5.27	Load-Strain Curves for Buckling of Beam CB3	111
5.28	Load-Strain Curves for Buckling of Beam CB3A	112

5.29	Load-Strain Curves for Buckling of Beam CB4	113
5.30	Load-Strain Curves for Buckling of Beam CB4A	114
5.31	Load-Deflection Curves for Beam AB1	115
5.32	Load-Deflection Curves for Beam AB1A	115
5.33	Load-Deflection Curves for Beam AB2	116
5.34	Load-Deflection Curves for Beam AB2A	116
5.35	Load-Deflection Curves for Beam BB1	117
5.36	Load-Deflection Curves for Beam BB1A	117
5.37	Load-Deflection Curves for Beam BB2	118
5.38	Load-Deflection Curves for Beam BB2A	118
5.39	Load-Deflection Curves for Beam AB3	119
5.40	Load-Deflection Curves for Beam AB3A	119
5.41	Load-Deflection Curves for Beam BB3	120
5.42	Load-Deflection Curves for Beam BB3A	120
5.43	Load-Deflection Curves for Beam BB4	121
5.44	Load-Deflection Curves for Beam BB4A	121
5.45	Load-Deflection Curves for Beam CB3	122
5.46	Load-Deflection Curves for Beam CB3A	122
5.47	Load-Deflection Curves for Beam CB4	123
5.48	Load-Deflection Curves for Beam CB4A	123
5.49	Comparison of Test Results with Available Test Data for Welded Beams	127
5.50	Comparison of Test Results with Available Test Data for Hot Rolled Beams	128
5.51	Comparison of Test Results with Current Standards	129
A.1	Maximum and Minimum Stresses for Specimen AA30 at Point 1	141
A.2	Maximum and Minimum Stresses for Specimen AA30 at Point 2	141
A.3	Maximum and Minimum Stresses for Specimen AA30 at Point3	142
A.4	Maximum and Minimum Stresses for Specimen A30 at Point 1	142
A.5	Maximum and Minimum Stresses for Specimen A30 at Point 2	143
A.6	Maximum and Minimum Stresses for Specimen A30 at Point 3	143
A.7	Maximum and Minimum Stresses for Specimen BB40 at Point 1	144
A.8	Maximum and Minimum Stresses for Specimen BB40 at Point 2	144

A.9	Maximum and Minimum Stresses for Specimen BB40 at Point 3	145
A.10	Maximum and Minimum Stresses for Specimen B40 at Point 1	145
A.11	Maximum and Minimum Stresses for Specimen B40 at Point 2	146
A.12	Maximum and Minimum Stresses for Specimen B40 at Point 3	146
B.1	Stress-Strain Curve for Specimen CP4-T1	160
B.2	Stress-Strain Curve for Specimen CP4-T2	160
B.3	Stress-Strain Curve for Specimen CP5-T3	161
B.4	Stress-Strain Curve for Specimen CP5-T4	161
B.5	Stress-Strain Curve for Specimen CP5-T5	162
B.6	Stress-Strain Curve for Specimen CP5-T6	162
B.7	Stress-Strain Curve for Specimen CP6-T7	163
B.8	Stress-Strain Curve for Specimen CP6-T8	163
B.9	Stress-Strain Curve for Specimen CP6-T9	164
B.10	Stress-Strain Curve for Specimen CP8-T10	164
B.11	Poisson Ratio from Tensile Coupon Test CP5-T11	165
B.12	Poisson Ratio from Tensile Coupon Test CP6-T12	165
B.13	Poisson Ratio from Tensile Coupon Test CP8-T13	166

LIST OF TABLES

<u>Table</u>	<u>Description</u>	<u>Page</u>
2.1	Coefficients for Transverse Loads	26
2.2	Moment Reduction Factor for Different Load Cases	27
3.1	Nominal Dimensions of Test Specimens for Residual Stress Measurement	56
3.2	Experimental Results of Residual Stress	59
3.3	Tensile Materials Properties	62./
4.1	Dimensions of Beam Specimens	70
5.1	Failure Loads and Failure Modes	83
5.2	Summary of Test Result	125
A.1	Measurement of Residual Stress by the Hole-Drilling Method Specimen AA30 at Point 1	147
A.2	Measurement of Residual Stress by the Hole-Drilling Method Specimen AA30 at Point 2	148
A.3	Measurement of Residual Stress by the Hole-Drilling Method Specimen AA30 at Point 3	149
A.4	Measurement of Residual Stress by the Hole-Drilling Method Specimen A30 at Point 1	150
A.5	Measurement of Residual Stress by the Hole-Drilling Method Specimen A30 at Point 2	151
A.6	Measurement of Residual Stress by the Hole-Drilling Method Specimen A30 at Point 3	152
A.7	Measurement of Residual Stress by the Hole-Drilling Method Specimen BB40 at Point 1	153
A.8	Measurement of Residual Stress by the Hole-Drilling Method Specimen BB40 at Point 2	154
A.9	Measurement of Residual Stress by the Hole-Drilling Method Specimen BB40 at Point 3	155
A.10	Measurement of Residual Stress by the Hole-Drilling Method Specimen B40 at Point 1	156

A.11	Measurement of Residual Stress by the Hole-Drilling Method Specimen B40 at Point 2	157
A.12	Measurement of Residual Stress by the Hole-Drilling Method Specimen B40 at Point 3	158

LIST OF ABBREVIATIONS AND NOTATIONS

AISC	American Institute of Steel Construction
AS	Australian Standard
AWS	American Welding Society
CSA	Canadian Standard
ECCS	European Convention for Constructional Steelwork
EUS	Equivalent Uniform Stress
FWB	Fillet Weld on Both sides
FWO	Fillet Weld on One side
LRFD	Load Resistance Factor Design
LTB	Lateral Torsional Buckling
Max.	Maximum
Min.	Minimum
SAW	Submerged Arc Welding
SMAW	Shielded Metal Arc Welding

LIST OF SYMBOLS

a_{LT}	Imperfection factor for lateral-torsional buckling
C_w	Warping constant
E	Elastic modulus
$(EC_w)_e$	Effective warping rigidity
$(EI_y)_e$	Effective bending rigidity
F_u	Maximum stress
F_r	Compressive residual stress in the flange
F_Y	Yield stress
F_{yf}	Minimum specified yield stress for the flange plate material
G	Shear modulus
$(GJ)_e$	Effective torsional rigidity
GPa	Gega Pascal
I_y	Minor axis moment
J	Sant venant torsion
l_e	Effective length
M_A	Absolute value of moment at quarter point of the unbraced beam segment
M_B	Absolute value of moment at centerline point of the unbraced beam segment
M_b	Flexural resistance to lateral-torsional buckling
M_c	Absolute value of moment at three-quarter point of the unbraced beam segment
M_{cr}	Elastic critical moment for lateral-torsional buckling
M_E	Elastic critical moment
M_m^*	Maximum design bending moment in the segment
M_{max}	Absolute value of maximum moment in the unbraced segment
M_o	Elastic buckling moment
M_p	Full plastic moment
MPa	Mega Pascal

M_s	Nominal section capacity
M_u	Ultimate moment
M_{ocr}	Critical elastic lateral-torsional buckling moment
r_y	Radius of gyration about the minor axis
S	Standard deviation
S_x	Elastic section modulus about strong axis
t	Flange thickness
ν	Poisson's ratio
X_{LT}	Reduction factor for lateral-torsional buckling
w	Web thickness
ϵ_r	Measured strain relaxation
σ_y	Maximum principal stress
σ_x	Minimum principal stress
λ_p	Slenderness limits for compact
λ_r	Slenderness limits for non-compact
$\bar{\lambda}$	Modified slenderness ratio
α_m	A moment modification factor
α_s	A slenderness reduction factor

**EFFECT OF WELDING ON
LATERAL-TORSIONAL BUCKLING RESISTANCE OF
I-SHAPED BUILT-UP STEEL BEAMS**

By

Raja Muhammed Younes

Supervisor

Dr. Yasser M. Hunaiti, prof.

Co-Supervisor

Dr. Ghazi Abu-Farsakh, prof.

ABSTRACT

An experimental investigation was made of the inelastic lateral-torsional buckling of built-up steel I-beams. All beams were carefully fabricated with controlled levels of initial crookedness. Nineteen beams were tested in five groups under same loading conditions with two points load applied at the top flange. Specially designed supports allowed the end cross sections of each test beam to rotate about the major and minor axis, but restrained them against twisting about the longitudinal axis. Result of a number of subsidiary experiments such as residual stresses and tensile coupons are also presented. The results confirmed that built-up beams of intermediate slenderness with fillet welds on one side of the web are sometimes stronger than their counterpart beams with fillet welds on both sides of the web. It was found that design loads predicted by the Australian Standard provided good lower bounds estimates to failure loads of the test beams.

CHAPTER I

INTRODUCTION

1.1 General

Metal beams and columns are extensively used in engineering applications ranging from skyscraper buildings to offshore structures. Several reasons contribute to the wide use of metal structures such as the production of new high quality metal structural members with increasing yield stresses, smaller thicknesses and lower weight, also, the development of efficient industrial process in forming specific sizes and shapes of structural members. It becomes common practice in some areas of the world to build up or fabricate W-shapes from plates as alternates to rolled W-shapes.

One of the key feathers of metal building systems is their primary frames being made up of built-up plate rigid frames. Steel plates are cut using lasers into tapered shapes for webs and prismatic shapes for flanges. Then these shapes are placed into a ConRac submerged arc welder that welds both flanges to the web at one time. This weld is a fillet weld in one side of the thickness of the web.

1.2 Research Significance

Today, metal building systems dominate the low-rise (1 or 2-story) non residential building construction in the world with several advantages such as cost efficiency, ability to long spanning, fast construction, and so on. Since the primary cornerstone of

metal building construction is to minimize the building cost, the goal is usually achieved through optimization of steel weight and the fabrication process by adopting the built-up I-shaped web-tapered primary framing members with bolted end-plate connections and the cold-formed secondary structural members. Since no design procedure for metal building systems exists in the current codes, the industry takes advantage of all allowed code exceptions and options that frequently result in lighter and more economical structures.

It is common practice in the metal building industry in Jordan to fabricate built-up beams from continuous web and flange plates. The plates are hydraulically cut to the required width and length. The flange to web fillet welds was made on one side of the web only using Submerged Arc Welding (SAW) process or Shielded Metal Arc Welding (SMAW). SAW is more common shop-welding process and yields larger heat-affected zone, resulting in higher strength fillet weld than the same fillet weld made using SMAW. American Welding Society (AWS) and American Institute of Construction (AISC) prescribe larger effective throats and design strength for fillet welds using SAW than those using SMAW. This method of fabrication is not explicitly explained in the related specifications (Load Resistance Factor Design specification LRFD (2005); European Standard Eurocode 3 (2005) Part 1.1 ; Canadian Standard CSA-S16-01 (2001); Australian Standard AS4100 (1998); etc.). Moreover, limited information about this subject causes ambiguity among practicing engineers.

Some engineers believe that the weld between the flange and webs of a fabricated built-up section that is a flexural or compression member should be determined by the computed shear between the flange and the web. If the computed shear can be carried

out by welds on one side of the joint there is no reason to arbitrarily weld both sides.

They based on the following:

1. Millions of welded members in rigid frames with one-side welds are performing well all over the world and have been for over fifty years.
2. According to AWS D1.1 AWS (2000) sec 2.27 Prohibited Joint and Welds, one-sided Groove Welds are prohibited while one-sided fillet welds are not mentioned as prohibited joints.

Other engineers believe that connecting the flanges and webs by fillet weld only on one side is not an acceptable practice because the cross section of the beam loses its symmetry and there is nothing mentioned in modern standards which is crucial to illuminate the acceptance of this method of fabrication.

1.3 Literature Review

Over the past several years the lateral–torsional buckling of beams of rigid cross section has been thoroughly investigated and summarized in many text books (Timoshenko and Gere ,1961); (Galambos, 1988) ; (Trahair, 1993), while methods of design are presented in modern standards (Load Resistance Factor Design specification LRFD (2005); European Standard Eurocode 3 (2005) Part 1.1; Canadian Standard CSA-S16-01 (2001); Australian Standard AS4100 (1998) .

Research on the lateral torsional buckling of I-beams has focused on hot-rolled sections or welded sections with fillet welds on both sides of the web. There does not

appear to be any published data in the international literature on lateral buckling of doubly-symmetric I-beams with fillet welds only on one side of the web.

Cherry (1960) investigated experimentally the interaction of local and lateral-torsional buckling. He carried out five series of tests on aluminum I-beams of varying length under conditions of pure end couples. The actual support conditions associated with the experimental work corresponded to simply supported ends with full restraint against warping. Cherry supported his experimental work with a theoretical analysis based on the lateral stability of a transformed monosymmetric section. The transformed section was obtained from an effective plate width formulation in the post-locally buckled range. He suggested that the strength of beams after the occurrence of local buckling in the compression flange can be estimated by the lateral buckling of the transformed monosymmetric I-section based on the concept of effective compression plate width.

Galambos (1963) studied the problem of inelastic lateral-torsional buckling of wide flanges beams subjected to equal end moment. He studied the effect of residual stresses in as-rolled member on their lateral-torsional buckling strength. He concluded that residual stresses have a considerable influence on buckling strength and that they may reduce the critical moment by 30%. He also derived an exact formulation for calculating the inelastic lateral-torsional buckling strength for the considered beam case. Then he reported a simplified formula that would reduce the calculation efforts for design without loss of accuracy.

The interaction between flange local and lateral buckling was considered by Lay and Galambos (1965) for beams under moment gradients. They considered the case where local

buckling had formed in the yielded region, but lateral buckling had not yet taken place. When lateral deflections occurred, the half flange undergoing compression during the process of lateral deformation would be inactive because of the flange local buckling. Thus, the effective bending stiffness of the flange would be reduced by a factor of eight leading to lateral buckling of the flange. They concluded that local buckling in a beam under a moment gradient would lead to lateral buckling and that the two effects, in combination, would cause unloading.

Graham and Richard (1971) studied the elastic buckling of steel beams numerically. A general numerical method for investigating the lateral-torsional stability of beams of arbitrary configuration was presented based on finite element concept. Although only elastic I-beams were considered, the method can be extended to include inelastic effects and a variety of cross-sectional shapes.

The effect of in-plane deformations on the critical moment which cause lateral buckling of beams have been studied theoretically and experimentally by Vacharajittiphan *et. al.* (1974). A closed form solution was obtained for the buckling of a simply supported beam subjected to two equal and opposite end moments. The results obtained indicate that the classical critical moments are generally conservative, except for members which are highly restrained laterally. In those beams investigated which are laterally unrestrained, the magnitude of the effect of the in-plane deformations is substantially independent of the major axis moment distribution, and of the member length if the loading is centroidal and the beams are not short, but increases significantly as the height of the point of load application above the centroid decreases.

An experimental investigation of the inelastic buckling of full-scale simply supported steel I – beams under central concentrated loads was conducted by Kitipornchai *et al.* (1975). A total of six buckling tests were carried out. Two of the six testes were carried out on stress-relieved beams. It was found that the effect of the experimental residual stresses was not very important while the geometrical imperfections in the beams were found to be significant in reducing the strength of the beam below their theoretical buckling loads.

Fukumoto and kubo (1977) carried out an extensive survey of literature on the lateral buckling tests that had been conducted at various institution. A summary of surveyed results was presented in tables and figures for 159 rolled beams and 119 welded beams, and the scattered test points were compared with the design formulas of lateral buckling strength recommended by the European Convention for Constructional Steelwork (ECCS) for laterally unsupported beam which is given by:

$$\frac{M_u}{M_p} = (1 + \lambda^{2n})^{-1/n} \quad (1.1)$$

Where:

$$\lambda = \sqrt{\frac{M_p}{M_e}}$$

M_u, M_p = ultimate and full plastic moments, respectively

M_e = elastic critical moment

n = system factor

They recommended from the tests survey that the system factor $n = 2.5$ and 1.5 , respectively, for mean M and $M-2S$ ($S =$ standard deviation) for rolled beams and $n = 2$ and 1 for welded beams.

Fukumoto *et al.* (1980) conducted an experimental investigation on laterally unsupported beams from the statistical consideration. Twenty-five simply supported rolled beams with nominally identical cross sections I - $200 \times 100 \times 5.5 \times 8$ mm were tested in three groups, each group having different span lengths. These beams were tested under a concentrated load applied vertically at the midspan of the compression flange.

The variation of the geometrical and material imperfections was measured. The mean values of initial crookedness of 75 beams about major and minor axis were found to be $(0.084 \times 10^{-3}) L$ and $(0.08 \times 10^{-3}) L$ respectively, and the mean values of residual stresses were. $0.69F_{yf}$, $0.08F_{yf}$, and $0.62F_{yw}$ at the upper flange center, flange end and web center, respectively.

In order to present the test data in the non-dimensional form, three different values of M_p were used by the authors for comparisons. First, they used the measured F_y of tensile coupons in the flange and in the web and the nominal cross-sectional dimensions. Second, they used the measured F_y and the measured cross-sectional dimensions. Third, they used the nominal F_y and nominal cross-section. They found that the main parameter that highly influences the variation of the ultimate strength is the variable value of actual full plastic moment that contains actual yield stresses and cross-sectional dimensions.

The authors proposed the following general formula:

$$\frac{M_p}{M_e} = 1 - 0.412(\lambda - 0.2) \quad (1.2)$$

which insure empirically the lower bound for the test points and other tests that had been conducted before by Fukumoto and Kubo (1977).

Fukumoto and Itoh (1981) investigated experimentally the buckling strength of laterally-unsupported welded beams. Thirty-four, nominally-identical welded beams for each group of two different lengths, are tested under a concentrated load applied vertically at the midspan of compression slab. The loading and supporting conditions are the same as for the rolled beams of Fukumoto *et al.* (1980). The obtained test results have indicated that the welded beams have a lower ultimate strength in the mean value than rolled beams. Measurements of the compression residual stresses and initial crookedness in the welded beams have shown that the mean and the coefficient of variation are significantly large in welded beams, as compared with those of hot rolled.

Bradford and Trahair (1981) studied the effect of different end conditions and distortional buckling using finite element. They found that the buckling modes of beams with end restraint which allow lateral displacement of compression flange may vary with the member length. For short-length beam the flange in-plane stiffness is high, buckling occurs in an antisymmetric mode in which the compressive flange deflects laterally as a near-rigid body. For longer beams, the beam prefers to buckle in symmetric mode. This means that the buckling modes for long beams with partial end restraint will approach those of beams with total end restraint.

Fukumoto *et al.* (1982) conducted a series of experiments on the buckling of continuous welded I-beams with single-run weld by manual of size 6 was used. These continuous beams were tested under a concentrated load on the midspan of the one side span. The geometrical and material imperfections were also measured. The test results were compared directly with the buckling behavior of simple beams.

Yoshida and Maegawa (1984) presented a method for analyzing the ultimate strength of beams. They examined five models of I-beams, simply supported at both ends against lateral displacement and twist. They studied the relationship between the lateral-torsional buckling and the ultimate load-carrying of beams and the effect of initial imperfections such as initial horizontal deflection, eccentricity of loading and the types of residual stress distributions on the ultimate load-carrying capacity. They proposed that the ultimate strength of beams with initial out-of-plane deflection is considerably lower than the buckling strength of straight beams in the range of a relative large modified slenderness $\bar{\lambda}$ and the ultimate strength in the region of small $\bar{\lambda}$ depends not only on the magnitude of initial out-of plane deflection, but also on the reduction of stiffness due to the extent of yielded zones. They also concluded that the ultimate strength curves of beams with residual stress types of welded shapes are below those of beams with residual stress types of rolled shapes for almost the whole range of $\bar{\lambda}$ and the lateral-torsional buckling strengths are intensely affected by the residual stresses distribution while the ultimate strengths are relatively less affected.

Bradford and Hancock (1984) developed analytical models to assess the nonlinear interaction of local and lateral buckling. The analytical models were compared against the experimental test results of Cherry (1960). They pointed out that the interaction of

local and lateral-torsional buckling is not only sensitive to the width thickness ratio of the flange or web, but also to the ratio of thicknesses of the flange and the web.

Kemp (1986) summarized his derived theoretical models of flange local buckling, web local buckling, and lateral-torsional buckling where he included the effect of the different modes on one another. Based on test observations, he proposed interaction criteria for the different buckling modes.

Bradford (1987) presented a finite strip method of analysis for the inelastic local buckling of I-beams fabricated by welding. The residual stresses induced by such welding are included in the analysis based on the so-called (tendon force concept). He concluded that the flexural stiffness of the welded beams is reduced by 30% below the linear elastic response due to the presence of residual stresses.

The interactive behavior of local and lateral-torsional buckling was investigated in the inelastic buckling range by Kubo *et al.* (1988). A total of 22 thin-walled welded I-beams with four different cross-sectional sizes were tested under a concentrated load at the center of a simply supported span. The beams were restrained at their end support against lateral displacement and twist but not against warping. The flange width-thickness ratios were 14.7 and 17.5, and those of the webs vary from 62.3-96. The slenderness ratio about the minor and major axis are approximately 50, 70, and 100. The mean values of the maximum measured initial out-of-straightness in each beam was $(0.137 \times 10^{-3}) L$ in the major axis plane and $(0.188 \times 10^{-3}) L$ in the minor axis plane where L is the length of the beam.

Based on test observations they concluded that for the beams with intermediate length, the combined failure mode of local flange and lateral-torsional buckling was obtained while the long beams failed only by lateral-torsional buckling. Web buckling was not observed on any of the beams tests, local flange buckling with a short wave length occurred near the span center of the beams.

Trahair and Hancock (2002) provided a simple advanced out-of-plane analysis method in which the elastic moduli E , G are reduced by a reduction factor γ_{IM} to allow for imperfections and residual stresses as well as yielding. The reduced moduli are derived from the basic beam and column strength curves of the Australian steel code AS4100 (1998). They found that the strengths predicted for simply supported beams are exactly the same as those of AS4100 while the strength predicted for simply supported beams under double curvature bending are less than those of AS4100 method of design by buckling analysis.

Suryoatmono and Ho (2002) have solved the governing differential equation using finite differences technique. They have shown how equivalent uniform moment factor provided by AISC-LRFD are very conservative for most moment diagram but may be non-conservative in particular cases.

Lim *et al.* (2003) have conducted an extensive investigation into elastic buckling in I-beams. They focused on linear moment diagram, lateral bending prevention and warping prevention. They proposed new equations to be used in determining the moment gradient correction factor for those particular cases.

Finite-element method buckling analyses of I-shaped beams were conducted by Park *et al.* (2004). The beams were subjected to a concentrated load or uniformly distributed load at top flange along with end moments. Traditional moment gradient factors were reviewed and compared with the Finite-element method results. They proposed a new design equation for obtaining the lateral-torsional buckling resistance capacity of beams with continuous lateral top bracing subjected to a concentrated load at the top flange.

1.4 Objectives of the Study

When flexural members are dimensioned so that instability occurs after the section yielded, many parameters that do not affect or are not significant in the case of elastic stability come into play; materials properties, material imperfections and geometric imperfection, moreover, local buckling, distortional buckling and lateral-torsional buckling often interact with one another. All above, make the inelastic behavior of member too complex for rigorous mathematical representation that would account for all parameters which affect it. This is why most of our knowledge about inelastic lateral buckling of members arises from experimental research.

In view of the limited information available on the behavior of built-up steel beams with one fillet welds on one side of the web, an experimental program was conducted in collaboration with Jordan University of Science and Technology (JUST). The general scope of the program aims at investigating the validity of using fillet welds only on one side of the web of the beam and to study the effect of this way of fabrication on the failure modes and the ultimate strength of these beams.

The overall objective of the research project described in this thesis will be achieved through testing nineteen built-up steel beams under two symmetrical point loads acting in the middle third of the span and placing the central third under a constant moment. The beams are not braced against lateral translation or torsional twisting at loading points. The support condition associated with this work corresponded to simply supported ends.

Specific objectives of the research project include:

- Studying the load-deflection and the load-strain behavior of the specimens.
- Studying the failure modes and the ultimate strength of the specimens.
- Comparing the behavior of built-up beams with fillet welds only on one side of the web with built-up beams having fillets welds on both sides of the web.
- Comparing the experimental results with the design approaches in several current specifications such as Load Resistance Factor Design specification LRFD (2005); European Standard Eurocode 3 (2005) Part 1.1; Canadian Standard CSA-S16-01 (2001) and Australian Standard AS4100 (1998).
- Comparison with available test results will also be done.

CHAPTER 2

BUCKLING OF I-BEAMS

2.1 Introduction

Thin-walled I-shaped beams are usually accompanied by bending moments about the strong axis due to the applied loads, and they deform vertically with an increase of the loads. When the magnitude of the loads approaches a certain value, lateral deflection and twist of the beams increase rapidly, and then the beams experience an unstable state and they may lose their ability to carry the loads Yoshido and Maegawa (1984). At this stage, the beams are considered to have buckled. Research into buckling of structural members has generally been considered as either plate buckling of components or overall buckling. Plate buckling of components, normally called local buckling, assumes that the line junctions between intersecting plates remain straight. Overall members buckling usually takes the form of lateral-torsional buckling. The main assumption in lateral-torsional buckling is that the cross section of the beam remains undistorted. That is each cross section of a beam deforms as if it was a rigid body with only three degree of freedom in the plane of the cross section. It is also possible for a beam to buckle into modes which combine lateral displacement and twist, together with local changes in the cross section geometry. This type of buckling is referred to as distortional buckling Bradford and Trahair (1981).

The width-thickness ratio of the plate elements and the slenderness ratio about the weak axis for unbraced beams are the basic buckling parameters for local and lateral-

torsional buckling modes respectively. The interaction of local and lateral-torsional buckling is not sensitive to the width-thickness ratio of the flange or web, but also to the ratio of the thicknesses of the flange and the web.

2.2 Local Buckling

Local buckling of a thin plate element of a structural member, such as the flange in Fig. 2.1 or web of I-beams, involves deflections of the plate out of its original plane. It is characterized by changes in the cross-sectional geometry without overall lateral displacement or twist. Usually, local buckling is concentrated at one small region along the length of the structural member. The half wave length of the buckle is much smaller than the length of the beams. Local buckling can be sub-divided into flange buckles, web buckling in which only the web buckles, and coupled local buckling in which the flange and the web buckle together.



Figure 2.1: Local Buckling of I-Beam

Local buckling of structural elements is usually controlled or prevented in design standards by setting limits for the slenderness ratios of these elements. These slenderness limits form the basis on which the classification of flexural members is made. According to the Canadian Standard CSA S16-01 (2001) these slenderness limits separate structural sections, used in flexural design, into the four distinct classes shown in Fig. 2.2.

These classes are:

- Class 1 sections: permit the attainment of the plastic moment capacity of members and also allow for sufficient (but unspecified) rotational capacity for subsequent redistribution of loads in the structure before local buckling occurs,
- Class 2 sections: are required to attain the plastic moment capacity with no requirements for rotational capacity,
- Class 3 sections: permit the attainment of the yield moment, at least, before local buckling takes place, and
- Class 4 sections: the limit state of strength is the elastic post-local buckling capacity of the element in compression.

Before the adoption of the above terminology for the classification of sections in Canadian Standard CSA S16-01 (2001), the section categories were known as plastic design, compact, non-compact and slender sections, respectively. These designations are still used in the American Institute of Steel Construction Load Resistance Factor Design (LRFD) Specifications (2005). The European Standard, Eurocode 3 (2005) Part

1.1, uses similar designations to those in Canadian Standard CSA S16-01 (2001). F_y at all three standards is the specified minimum yield stress for the steel used.

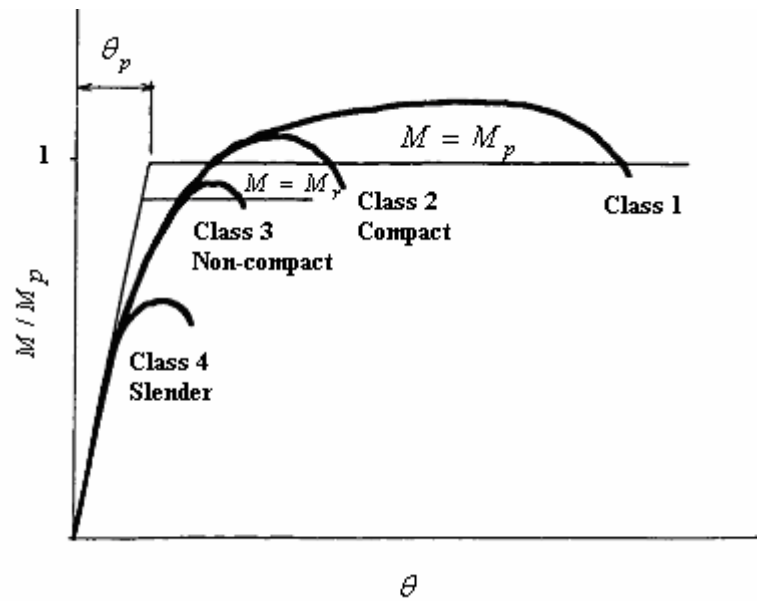


Figure 2.2: Classification of Beam Sections According to Canadian Standard CSA S16-01 and American (LRFD) Specifications.

2.2.1 Local Buckling Requirements

2.2.1.1 Canadian Standard CSA-S16-01-2001

Flexural members are classified into Class 1, Class 2, Class 3, and Class 4 sections. They are bound by the following slenderness limits:

$$b/t \leq \frac{145}{\sqrt{F_y}} \quad \text{and} \quad \frac{h}{w} \leq \frac{1100}{\sqrt{F_y}} \quad \text{for Class 1}$$

$$b/t \leq \frac{170}{\sqrt{F_y}} \quad \text{and} \quad \frac{h}{w} \leq \frac{1700}{\sqrt{F_y}} \quad \text{for Class 2}$$

$$b/t \leq \frac{200}{\sqrt{F_y}} \quad \text{and} \quad \frac{h}{w} \leq \frac{1900}{\sqrt{F_y}} \quad \text{for Class 3}$$

$$b/t \geq \frac{200}{\sqrt{F_y}} \quad \text{and} \quad \frac{h}{w} \geq \frac{1900}{\sqrt{F_y}} \quad \text{for Class 4}$$

(2.1)

where b = half width of the compression flange

h = web depth measured as the clear distance between flanges

t = flange thickness

w = web thickness

2.2.1.2 European Standard-EC3 (2005) (ENV 1993) Part 1.1

Flexural members are classified into Class 1, Class 2, Class 3, and Class 4 sections.

The definitions of the different classes are similar to the same designations in the

Canadian Standard. Like the Canadian Standard, Eurocode 3 does not specify a minimum value for the rotational capacity expected of Class 1 sections.

The section classes are bound by the following slenderness limits:

$$\begin{aligned}
 c/t &\leq \frac{153}{\sqrt{F_y}} && \text{rolled sections} && \text{and} && \frac{h}{w} \leq \frac{1104}{\sqrt{F_y}} && \text{for Class 1 sections} \\
 c/t &\leq \frac{138}{\sqrt{F_y}} && \text{welded sections} && && && \\
 c/t &\leq \frac{169}{\sqrt{F_y}} && \text{rolled sections} && \text{and} && \frac{h}{w} \leq \frac{1272}{\sqrt{F_y}} && \text{for Class 2 sections} \\
 c/t &\leq \frac{153}{\sqrt{F_y}} && \text{welded sections} && && && \\
 c/t &\leq \frac{230}{\sqrt{F_y}} && \text{rolled sections} && \text{and} && \frac{h}{w} \leq \frac{1900}{\sqrt{F_y}} && \text{for Class 3 sections} \\
 b/t &\leq \frac{215}{\sqrt{F_y}} && \text{welded sections} && && &&
 \end{aligned}$$

(2.2)

where c = half width of the compression flange for rolled sections, or, the distance from the edge of weld to the flange tip for welded sections.

h = the clear distance between flanges less the fillet or corner radius for each flange for rolled sections, or the distance between edges of welds for welded section

2.2.1.3 American Specification AISC LRFD-2005

Flexural members are categorized into compact, non-compact, and slender sections, bound by the following slenderness limits:

$$b/t \leq \lambda_r = \frac{170}{\sqrt{F_y}} \quad \text{and} \quad \frac{h}{w} \leq \lambda_p = \frac{1680}{\sqrt{F_y}} \quad \text{for compact sections.}$$

For rolled sections

$$b/t \leq \lambda_r = \frac{370}{\sqrt{F_y - 69}} \quad \text{and} \quad \frac{h}{w} \leq \lambda_p = \frac{2547}{\sqrt{F_y}} \quad \text{for non-compact sections}$$

For welded section

$$b/t \leq \lambda_r = \frac{425}{\sqrt{(F_{yf} - 114)/k_c}}$$

where

λ_p Slenderness limits for compact

λ_r Slenderness limits for non-compact

(2.3)

where $k_c = \frac{4}{\sqrt{h/w}}$

$0.35 \leq k_c \leq 0.763$ is a factor reflecting the effect of web slenderness on flange

buckling in the elastic range.

b = half width of the compression flange

h = the clear distance between flanges less the fillet or corner radius for each flange, or, the clear distance between flanges for welded sections

F_{yf} = minimum specified yield stress for the flange plate material.

The above limits are presented in this format to make them compatible with their Canadian counterparts for ease of comparison.

2.3 Lateral-Torsional Buckling

Lateral-torsional buckling consists of simultaneous deflection perpendicular to the plane of bending plus twisting of a beam without deformation of the cross section as shown in Figure 2.3

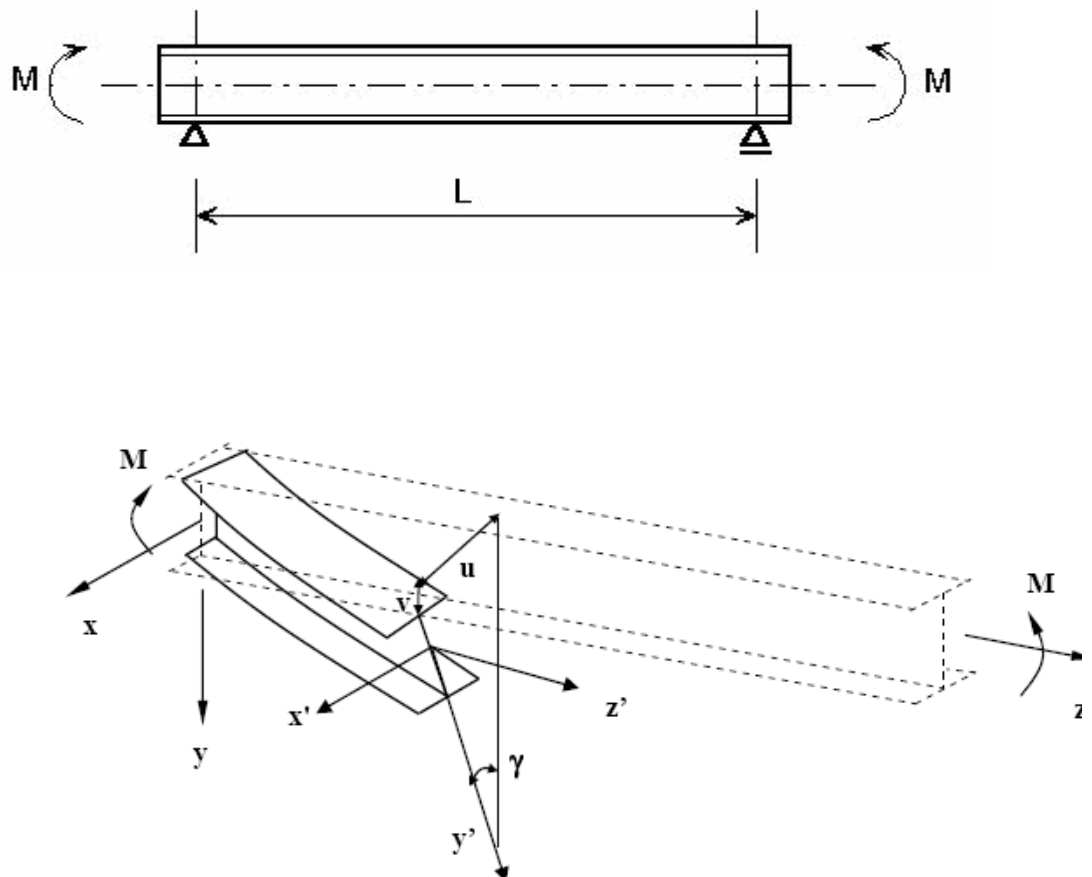


Figure 2.3: Lateral-Torsional Buckling of a Beam Subjected to Uniform Moment.

Beams that have relatively small lateral and torsional stiffnesses compared to their stiffness in the plane of loading or that have inadequate lateral restrains may buckle out of plane of the transverse load. For a perfectly straight, elastic beam, there is no out-of-plane deformation until the applied load reaches a critical value. However, as the critical load is reached, lateral deflection and twist begin suddenly and the beams become unstable. This critical load is the lateral-torsional buckling load obtained as an eigenvalue for the bifurcation problem of beams. For real beams usually used in practice, which has not only geometrical imperfections, but also material imperfections, lateral deflection and twist begin with the commencement of load, and increased rapidly as the critical load is approached. Thus the beam enters an unstable state and cannot resist any additional load. Such a load as the maximum value on load deformation curve is called the ultimate load carrying capacity, or ultimate load of a beam Yoshido and Maegawa (1984).

2.3.1 Elastic Lateral-Torsional Buckling

The perfectly straight beam which is subjected to bending moments about the strong axis will deflect in the plane of applied moments until moments reach a critical value. When the buckling moment is reached, lateral-torsional buckling is initiated by lateral deflection and twisting of the beam. Elastic lateral-torsional buckling strength of beams was solved mathematically by Timoshenko and Gere (1961) using differential equations. For a simply supported beam under constant moment, the elastic lateral-torsional buckling moment M_{ocr} is given by Timoshenko and Gere as:

$$M_{ocr} = \frac{\pi}{L_b} \sqrt{EI_y GJ} \sqrt{\left(1 + \frac{\pi^2 EC_w}{L_b^2 GJ}\right)} \quad (2.4)$$

where:

L_b = unbraced length of beam

E = elastic modulus

G = shear modulus

J = torsional constant

I_y = minor axis moment

C_w = warping inertia

The above equation assumes that the in-plane deflection has no effect on the lateral-torsional buckling behavior of the beam. This assumption is well justified if the major axis rigidity is greater than that of minor axis. However, if rigidities of minor and major axes are of the same order of magnitude, the solution becomes more complicated. An approximate solution was given by (Vacharajittiphan *et al.*, 1974) as:

$$M_{ocr} = \frac{\pi}{L_b} \sqrt{\frac{EI_y GJ}{(1 - EI_y / EI_x)(1 - (GJ + \pi^2 EC_w / L_b^2)) / 2EI_x}} \sqrt{\left(1 + \frac{\pi^2 EC_w}{L_b^2 GJ}\right)} \quad (2.5)$$

This correction factor, which is just less than unity for most beam sections but may be significantly less than unity for column sections, is usually neglected in design. Nevertheless, its value approaches zero as I_y approaches I_x (major axis moment) so that the true elastic buckling moment approaches infinity. Thus an I-beam in uniform bending about its weak axis does not buckle, which is intuitively obvious.

2.3.1.1 Moment Gradient

Uniform bending moments rarely occur in real beams, which usually have concentrated or distributed loads and varying bending moment diagrams. For such cases closed-form solution is not available and recourse must be had to numerical and approximate procedures to obtain critical load. The effect of moment gradient on critical moment can easily be accounted for by the use of equivalent uniform moment factor C_b .

The formula for this factor according to LRFD (2005)-Appendix F1 is:

$$C_b = \frac{12.5M_{max}}{2.5M_{max} + 3M_A + 4M_B + 3M_C} R_m \leq 3 \quad (2.6)$$

where:

M_{max} = absolute value of maximum moment in the unbraced segment

M_A = absolute value of moment at quarter point of the unbraced beam segment

M_B = absolute value of moment at centerline point of the unbraced beam segment

M_C = absolute value of moment at three-quarter point of the unbraced beam segment

R_m = cross section monosymmetry parameter. It is 1.0 for doubly symmetric members and for singly symmetric members subjected to single curvature bending

And the nominal moment for the beam in this case can be obtained from

$$M_n = C_b M_{ocr} \quad (2.7)$$

2.3.1.2 Effect of Load Height

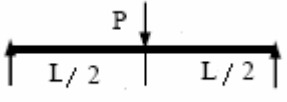
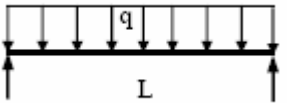
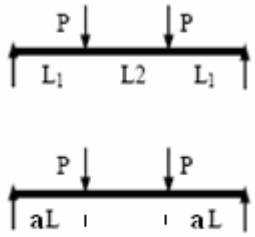
In some cases a beam may have gravity loads which act at the top flange, and which move laterally with the flange during buckling. These loads induce additional torques about the beam axis which increase the twist rotation and decrease the resistance to elastic buckling. Approximations for the effect of load height on the maximum moment at buckling have been suggested by Nethercot and Rocky (1971) and Nethercot (1983) as taking the form of

$$M_{cr} = AB^{2y/h} M_{ocr} \quad (2.8)$$

$$W = \left(\frac{\pi}{L}\right) \sqrt{\frac{EC_w}{GJ}} \quad (2.9)$$

Where A and B are taken from Table 2.1, h is the beam depth, and y is the distant from the mid height to point of load application. The distant y is negative for load applied above midheight, and positive for loading applied below midheight.

Table 2.1 Coefficients for Transverse Loads.

Loading	A	B
	1.35	$I + 0.649W - 0.180W^2$
	1.12	$I + 0.535W - 0.154W^2$
	$1 + \left(\frac{L_1}{2L_1 + L_2}\right)^2$	$I + 1.636aW - 0.465aW^2$

2.3.1.3 End Restrained Doubly Symmetric Beams

End restraint has a pronounced effect on the elastic lateral-torsional buckling strength of a beam. The closed form solutions for beams subjected to uniform bending moment are based on the following boundary conditions:

- Both ends are fixed against in-plane vertical deflection but unrestrained against in-plane rotation, and one end is fixed against longitudinal horizontal displacement.
- Both ends are fixed against out-of-plane horizontal deflection and twist rotation but unrestrained against minor axis rotation and warping displacement.

Nethercot and Rocky (1971) have presented the following method of solution for loading cases shown in Table 2.2.

$$M_{cr} = C_{bs} M_{ocr} \quad (2.10)$$

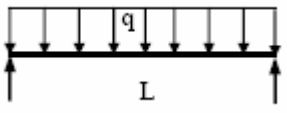
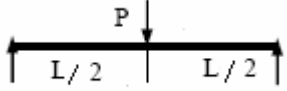
Where C_{bs} is the moment gradient factor but it also accounts for different end conditions of the beam.

$$C_{bs} = A/B \text{ for-top flange loading}$$

$$C_{bs} = A \text{ for loading through the mid height}$$

$$C_{bs} = AB \text{ for-bottom flange loading}$$

Table 2.2 Moment Reduction Factor for Different Load Cases

Loading	Case #	A	B
	1	$1.643 + 1.771W - 0.405W^2$	$1 + 0.625W - 0.339W^2$
	2	$1.2 + 0.402W + 0.416W^2$	$1 + 0.571W - 0.225W^2$
	3	$1.9 + 0.006W - 0.125W^2$	$1 + 0.806W - 0.1W^2$
	1	$1.916 + 1.851W - 0.424W^2$	$1 + 0.923W - 0.466W^2$
	2	$1.43 + 0.463W + 0.485W^2$	$1 + 0.619W - 0.317W^2$
	3	$2 + 0.304W - 0.074W^2$	$1 + 1.047W - 0.207W^2$

Special cases of idealized end condition are shown in Fig. 2.4. In restrained condition case #2 the end is free to rotate laterally but is prevented from warping. Such a condition can be effectively achieved by welding boxed stiffeners at or near the end support Ojalvo and Chambers (1977).

When the lateral and the warping end restraints are unequal, the following general approximate method can be used:

$$M_{ocr} = \frac{\pi}{K_y L_b} \sqrt{EI_y GJ} \sqrt{\left(1 + \frac{\pi^2 EC_w}{(K_z L_b)^2 GJ}\right)} \quad (2.11)$$

For end condition case #2 in Figure 2.4 $K_y = 1$ and $K_z = 0.5$. When one end is fixed and the other is pinned $K_z = 0.7$.

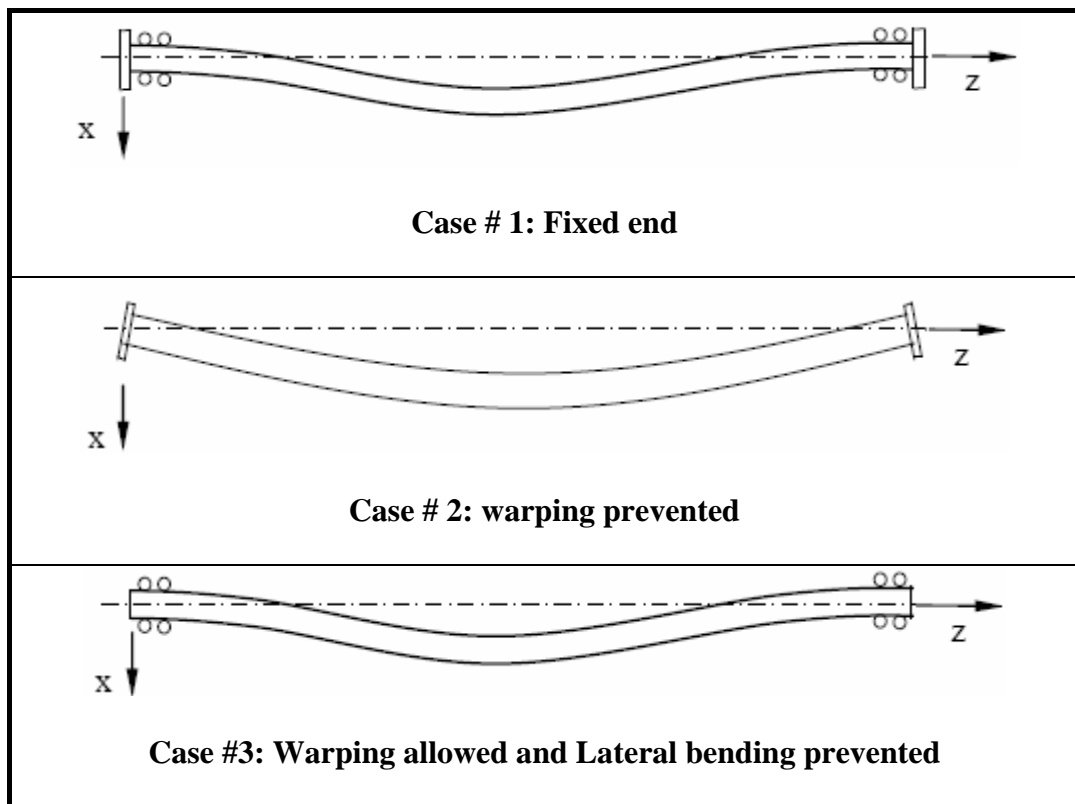


Figure 2.4: Plan View of Idealized End Restraints

2.3.2 Inelastic Lateral Torsional Buckling

The solution for the buckling moment M_{ocr} of a perfectly straight simply supported I-beam with equal end moments given by equations 2.4 is only valid for relatively slender beams in which yielding of material does not take place anywhere in the beam. However, for beams of intermediate slenderness ratios, yielding will occur in some fibers of the beam before the attainment of the critical load. Since some portions of the beam are inelastic when buckling commences, only the elastic portion of the cross section will remain effective in providing resistance to lateral buckling. As a result, effective rigidities of these inelastic portions are reduced by yielding, and consequently, the buckling moment is also reduced.

For beams with equal and opposite end moments, the distribution of yield across the section does not vary along the beam, and when there are no residual stresses, the inelastic buckling moment can be calculated from a modified form of equation 2.4 (Chen and Lui, 1987) as:

$$M_{ocr} = \frac{\pi}{L_b} \sqrt{(EI_y)_e (GJ)_e} \sqrt{\left(1 + \frac{\pi^2 (EC_w)_e}{L_b^2 (GJ)_e}\right)} \quad (2.12)$$

Where $(EI_y)_e$, $(GJ)_e$, $(EC_w)_e$ are the effective bending rigidity, torsional rigidity and warping rigidity. Estimates of these rigidities can be obtained by using the tangent modulus of elasticity which is appropriate to the varying stress levels throughout the section. It is assumed that, once beams' fibers have yielded, the stiffness of fibers depends on the tangent modulus while no elastic unloading is considered.

It should be mentioned that equation (2.12) is not applicable for beams with residual stresses. If residual stresses are considered in the analysis, the inelastic buckling moment of a beam with residual stresses can be obtained in a similar manner, except that the pattern of yielding is not symmetrical about the section major axis, so that a modified form of a critical moment equation valid for monosymmetric I-beam must be used instead of equation 2.12.

It can be seen from Fig. 2.5 that the presence of residual stresses greatly reduces the lateral-torsional buckling strength of the beam in the inelastic range. For hot-rolled beam the inelastic buckling moment decreases in an approximately linear fashion as the slenderness increases because, the flange tip residual stresses are comparatively high, and the inelastic buckling is initiated early in these beams, so the residual stresses in these beams decrease away from the flange tip, and the effective rigidities $(EI_y)_e$, $(EC_w)_e$ steadily decrease as the applied moment increases.

For welded beams the compressive residual stresses at the flange tips, which increase with the welding heat input, are usually somewhat smaller than those in hot-rolled beams, and so the initiation of inelastic buckling is delayed. However, the variations of the residual stresses across the flanges are nearly uniform in welded beams, and so, once flange yielding is initiated, it spreads quickly through the flange with little increase in moment.

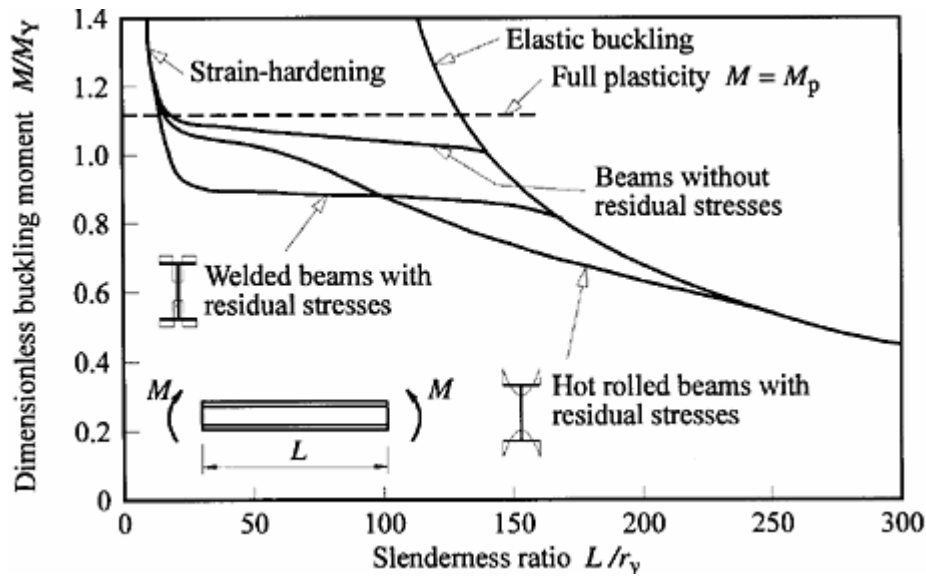


Figure 2.5: Lateral Buckling Strength of Simply-Supported Beams (Trahair, 1993)

When a beam has a more general loading than that of equal and opposite end moments, the in-plane bending moment varies along the beam, and so when yielding occurs its distribution also varies. Because of this the beam acts as if non-uniform, and the torsion equilibrium equation becomes more complicated. Nevertheless, the numerical solutions have been obtained for some hot-rolled beams with a number of different loading arrangements. Trahair (1993) has summarized the numerical methods used for inelastic buckling. They include finite differences, finite integral, transfer matrix and finite element methods. Among all the numerical methods, 3D finite element analysis provided the most comprehensive solution.

2.3.3 American Specification AISC LRFD-2005

For beams of compact sections, there are two possible types of failure: (1) plastic yielding, (2) lateral torsional buckling. The design curve is shown in Fig. 2.6. The beam design curve is divided into three sections. If $L_b \leq L_p$, the beam is considered to have adequate lateral support. If $L_p \leq L_b \leq L_r$, the beam is considered to be laterally unsupported and inelastic lateral-torsional buckling may occur. When $L_b \geq L_r$, the nominal moment M_n is equal to elastic buckling solution. For double symmetric I-sections, the nominal moment capacity is defined as in AISC LRFD (2005) for various ranges of L_b . The flexural resistance is then calculated by multiplying the nominal resistance by the resistance factor $\phi_b = 0.9$

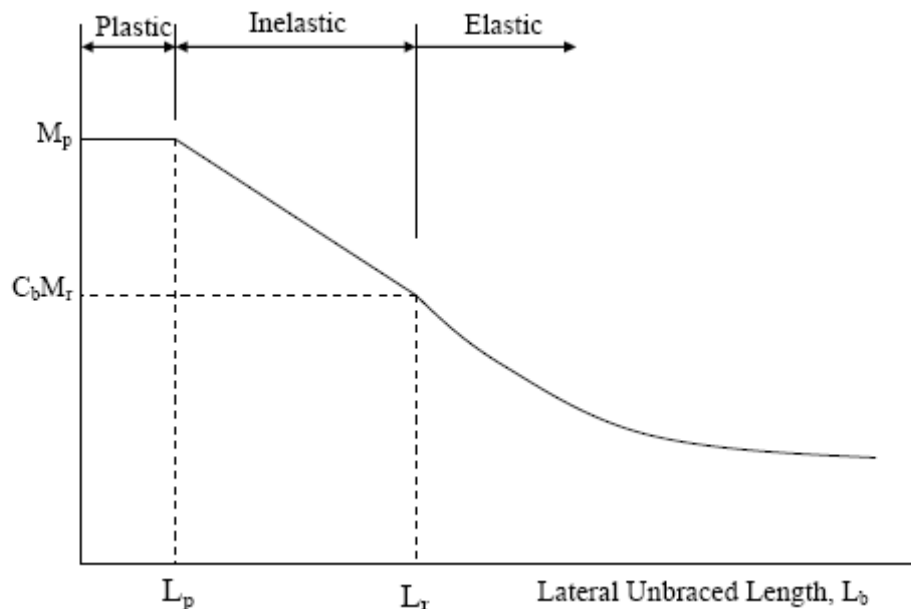


Figure 2.6: Schematic Plot of Beam Curve in LRFD

The nominal flexural strength of a beam is calculated according to the unbraced length, L_b , as

follows:

$$\text{When } L_b \leq L_p \quad M_n = M_p = F_y Z \leq 1.5 M_y \quad (2.13 \text{ a})$$

$$\text{When } L_p \leq L_b \leq L_r \quad M_n = C_b \left[M_p - (M_p - M_r) \left(\frac{L_b - L_p}{L_r - L_p} \right) \right] \leq M_p \quad (2.13 \text{ b})$$

$$\text{When } L_b \geq L_r \quad M_n = M_{cr} \leq M_p \quad (2.13 \text{ c})$$

$$\text{where } L_p = \frac{790 r_y}{\sqrt{F_{yf}}} \quad (2.14 \text{ a})$$

is the limiting unbraced length for full plastic bending capacity, and

$$L_r = \frac{\pi r_y \sqrt{EGJA/2}}{S_x F_L} \sqrt{1 + \sqrt{\left(1 + \frac{4C_w}{I_y} \left(\frac{S_x}{GJ}\right)^2 F_L^2\right)}} \quad (2.14 \text{ b})$$

is the limiting unbraced length for inelastic lateral-torsional buckling

$$F_L = F_{yf} - F_r \text{ or } F_{yw} \quad (2.15)$$

In equation (2.13 b),

$$M_r = S_x F_L \quad (2.16)$$

where S_x Elastic section modulus about strong axis

$$C_b = \frac{12.5M_{max}}{2.5M_{max} + 3M_A + 4M_B + 3M_C} R_m \leq 3 \quad (2.17)$$

For non-compact and slender sections, the LRFD Specification considers two additional limit states: the limit state of local flange buckling and that of local web buckling. The limit state of lateral-torsional buckling is checked using equations (2.13) as in the case of compact sections.

Assuming λ to be the controlling slenderness parameter (representing flange slenderness for flange local buckling or web slenderness for web local buckling limit states), the local buckling limit states are checked as follows:

$$\text{when } \lambda_b \leq \lambda_p \quad M_n = M_p \quad (2.18 \text{ a})$$

$$\text{when } \lambda_p \leq \lambda_b \leq \lambda_r \quad M_n = C_b \left[M_p - (M_p - M_r) \left(\frac{\lambda_b - \lambda_p}{\lambda_r - \lambda_p} \right) \right] \leq M_p \quad (2.18 \text{ b})$$

Where λ_p and λ_r are as given in equation (2.3) in section 2.2.1.3

2.3.4 Canadian Standard CSA-S16-01-2001

The Canadian Standard considers two cases in beam design: the first is for laterally supported members (where continuous lateral support is provided to the compression flange), and the moment resistance is determined as follows (in all cases, the resistance factor $\phi_b = 0.9$)

$$\text{For Class 1 and Class 2 sections} \quad M_r = \phi M_p = \phi Z F_Y \quad (2.19 \text{ a})$$

$$\text{For Class 3 sections} \quad M_r = \phi M_y = \phi S F_Y \quad (2.20 \text{ b})$$

Canadian Standard CSA S16-01 2001 allows no transition in strength from the yield moment capacity to the plastic moment capacity. Thus, flexural strength undergoes a sudden jump when either cross-sectional slenderness parameters fall on the Class 2 limit.

The second case is for laterally unsupported members. Here a distinction is made between doubly symmetric and mono-symmetric shapes. The following equations apply to doubly symmetric sections.

For Class 1 and Class 2 sections:

$$\text{when } M_u > 0.67 M_p \quad M_r = 1.15 \phi M_p \left(1 - \frac{.28 M_p}{M_u} \right) \leq \phi M_p \quad (2.21 \text{ a})$$

$$\text{when } M_u \leq 0.67 M_p \quad M_r \leq \phi M_u \quad (2.21 \text{ b})$$

where M_u is the critical elastic lateral-torsional buckling moment given by:

$$M_u = \frac{\omega_2 \pi}{L} \sqrt{EI_y GJ + \left(\frac{\pi E}{L} \right)^2 I_y C_w} \quad (2.22)$$

where L is the unbraced length of the beam, C_w is the warping constant.

$$\omega_2 = 1.75 + 1.05\kappa + 0.3\kappa^2 \leq 2.5 \quad \text{for unbraced lengths subjected to end moments.}$$

$\omega_2 = 1$ when the bending moment within L is larger than the larger end moment or when there is no effective lateral support for the compression flange at one end.

κ is the ratio of smaller to larger factored moments at opposite ends of the unbraced length, positive for double curvature.

Equation (2.21 a) represents a transition curve between the elastic lateral-torsional buckling moment and plastic moment capacities.

For Class 3 sections, equations (2.21 b) apply after replacing M_p by M_y

2.3.5 European Standard - EC3 (2005) (ENV 1993) Part 1.1

Eurocode 3 considers two flexural ultimate limit states for the design of beams: the flexural resistance of the cross section and the resistance to lateral-torsional buckling. The first limit state implies continuous lateral support for the compression flange, and as such, the moment resistance is determined as follows:

$$\text{For Class 1 and Class 2 sections} \quad M_r = \frac{1}{\gamma_{M_0}} ZF_Y \quad (2.23a)$$

$$\text{For Class 3 sections} \quad M_r = \frac{1}{\gamma_{M_0}} S F_Y \quad (2.23b)$$

where $\gamma_{M_0} = 1.1$ (resistance factor)

Here as well, like in CSA S16.1-94, no transition in flexural strength is allowed from the yield moment to the plastic moment capacity.

For the limit state of lateral-torsional buckling, the flexural resistance of a doubly symmetric beam is calculated as follows:

$$M_b = \frac{I}{\gamma_{MI}} B_w Z X_{LT} F_y \quad (2.24)$$

where M_b = flexural resistance to lateral-torsional buckling

γ_{MI} = resistance factor = 1.1

$B_w = 1$ for Class 1 and 2 section

$B_w = \frac{Z}{S}$ for Class 3 sections

X_{LT} = reduction factor for lateral-torsional buckling; calculated from:

$$X_{LT} = \frac{I}{\phi_{LT} + \left[\phi_{LT}^2 - \bar{\lambda}_{LT}^2 \right]^{1/2}} \leq 1 \quad (2.25)$$

where $\phi_{LT} = .5 \left[1 + a_{LT} (\bar{\lambda}_{LT} - .2) + \bar{\lambda}_{LT}^2 \right]$ (2.26)

a_{LT} = imperfection factor for LTB,

= 0.21 for rolled sections, and

= 0.49 for welded sections

$\bar{\lambda}_{LT}$ = non-dimensional lateral slenderness; determined from:

$$\bar{\lambda}_{LT} = \sqrt{\frac{B_w Z F_y}{M_{cr}}} \quad (2.27)$$

where M_{cr} = elastic critical moment for lateral-torsional buckling; similar to M_u of equation (2.22).

Eurocode 3 states that equation (2.24) need not be checked if the value of the non-dimensional lateral slenderness, is less than or equal to 0.4.

2.3.6 Australian Standard -AS4100-98

The nominal member moment capacity for bending (M_b) is defined in Clause 5.6.1.1 AS4100-98 as:

$$M_b = \alpha_m \alpha_s M_s \leq M_s \quad (2.28)$$

where: α_m = a moment modification factor

α_s = a slenderness reduction factor

M_s = nominal section capacity

The moment modification factor can be obtained from AS 4100 Table 5.6.1, or by using the following equation:

$$\alpha_m = \frac{1.7M_m^*}{\sqrt{(M_2^*)^2 + (M_3^*)^2 + (M_4^*)^2}} \leq 2.5 \quad (2.29)$$

M_m^* = maximum design bending moment in the segment

$M_2^* M_4^*$ = design bending moments at the quarter points of the segment

M_3^* = design bending moment at the midpoint of the segment

The slenderness reduction factor is given as:

$$\alpha_s = 0.6 \left[\sqrt{\left(\frac{M_s}{M_o} \right) + 3} - \left(\frac{M_s}{M_o} \right) \right] \leq 2.5 \quad (2.30)$$

M_o is called the reference buckling moment which is obtained from elastic analysis of simply supported beams under a uniform bending moment

$$M_o = \sqrt{\left(\frac{\pi^2 EI_y}{l_e^2} \right) \left[GJ + \left(\frac{\pi^2 EI_w}{l_e^2} \right) \right]} \quad (2.31)$$

where:

E, G = the elastic moduli

I_y , I_w and J = section constants

l_e = the effective length

The effective length is given by:

$$l_e = k_t k_l k_r l \quad (2.32)$$

where:

k_t is a twist restraint factor, k_l is a load height factor and k_r is a lateral rotation restraint factor.

l is taken as:

- a) The segment length, for segments without intermediate restraints, or for segment unstrained at one end, with or without intermediate lateral restraints.
- b) The sub-segment length, for sub-segments formed by intermediate lateral restraints in a segment which is fully or partially restrained at both ends.

2.4 Comparison of Design Specifications

All of the design codes are based on the well established theory of elastic lateral torsional buckling, which is the upper bound for all design criteria. The plastic moments are taken as the ultimate compact beam capacities at short unbraced length for all three design specification. For intermediate and long members, different forms of imperical transition are used to obtain the ultimate capacities from the elastic buckling curves.

Those in the American Institute of Steel Construction (AISC) Load Resistance Factor Design LRFD (2005) are based on the means of the test results, those in the Australian Standard AS4100-1998 are based on the lower bounds of the test results, those in the Canadian Standard CSA-S16-01-2001 are based on the upper bounds of the test results, and those in the European Standard Eurocode 3 (2005) Part 1.1 lie between the lower bounds and the means of test results.

In comparison, the beam curve used in the Australian design specification (AS4100) adapts a lower bound approach. Various effects including residual stresses, initial geometrical imperfections, etc. are taken into considerations. In the beam capacity formula, the separation of moment modification factor and slenderness reduction with AS4100 is significantly different to other codes.

The M_u / M_P versus the non dimensional slenderness ratio $\bar{\lambda} = \sqrt{M_P / M_o}$ for different standards are plotted in Fig. 2.7.

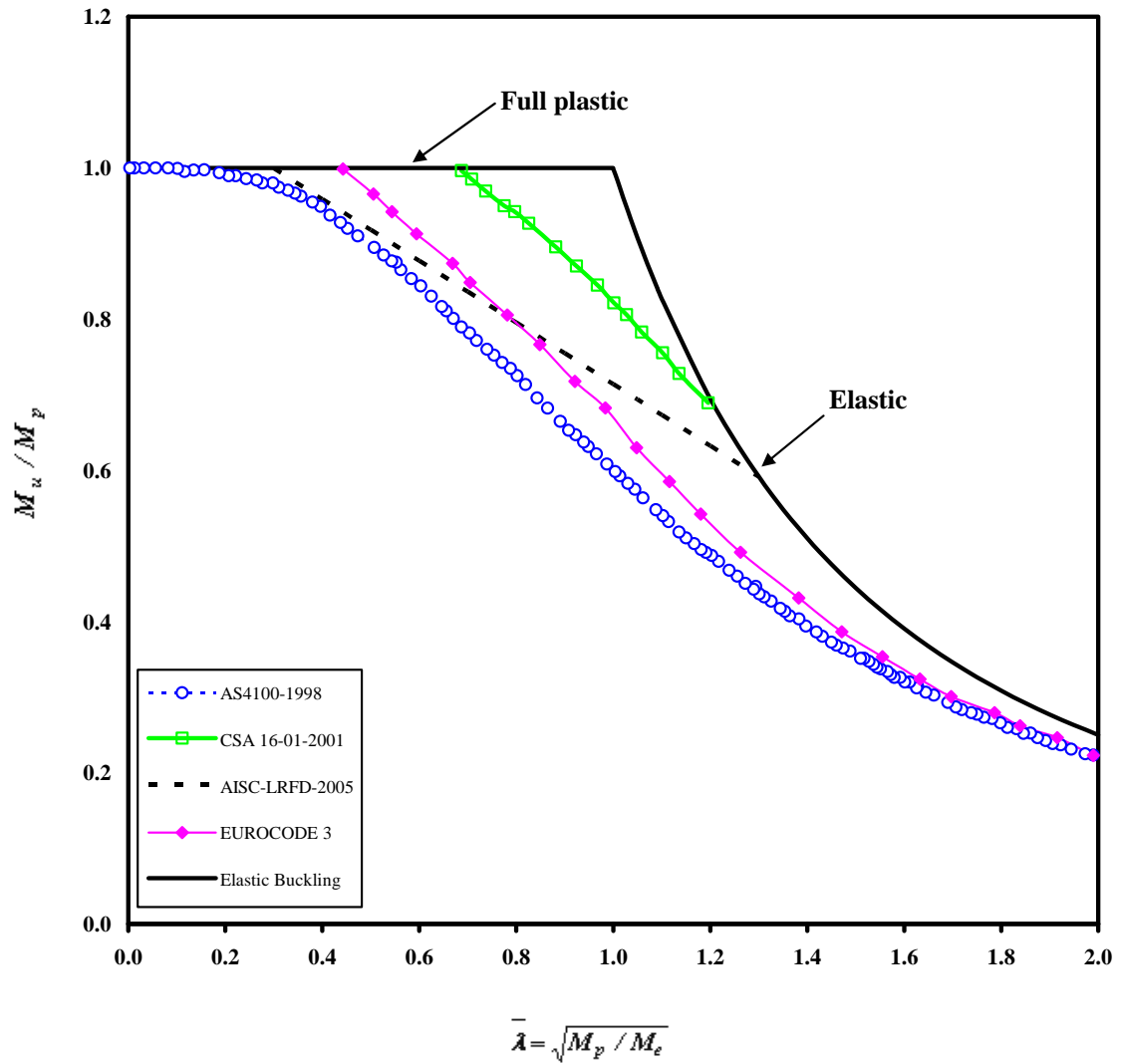


Figure 2.7: The Design Rules in Different Standards for Lateral-Torsional Buckling of I-Sections Beams

CHAPTER 3

MECHANICAL-PROPERTY TESTS

3.1 Residual Stress Measurements

3.1.1 Introduction

Residual stresses are those stresses which already exist in a component before any external or service loads are applied. They may be present as a result of manufacturing and fabricating processes or they may occur during the life time of the structure. Sometimes residual stresses are deliberately introduced into the material surface, through techniques such as controlled shot-peening, in order to enhance the mechanical or corrosion performance. Manufacturing processes are the most common causes of residual stresses. Virtually all manufacturing and fabricating processes including welding, casting, machining, molding heat treatment, etc. introduce residual stresses into the manufactured object.

For a welded I-profile the residual stresses may develop as follows: During solidification and further cooling the material of the weld zone experiences a larger shrinkage than the surrounding colder and more rigid base metal due to volume differences in the liquid and solid states and due to thermal contraction. The larger shrinkage of the weld zone induces tensile stresses in a magnitude limited by the momentary yield strength of the material in a warmer weld zone. The contraction of the

weld and heat affected zone induces in turn compressive stresses in the cross section of the surrounding colder base material.

Parameters that influence welding residual stresses include welding voltage, electrode speed, weld size, welding procedures, type of welding, fabrication procedure, manual or automatic welding and material properties.

Whether the residual stress is a consequence of the manufacturing processes, or it is introduced deliberately, it is important to know its distribution, i.e. the magnitude and orientation of its components with respect to geometry, in order to understand its performance.

A wide variety of residual stress measurement techniques exist, but hole drilling strain-gage method which belongs to semi-destructive methods, is the most popular and widely used technique for measuring residual stresses, its popularity stems largely from its ease of use in many different application and materials, its limited damage to the specimen, and its general reliability. This technique has been quoted in ASTM Standard E837 since 1981.

3.1.2 Background

The hole-drilling method for measuring residual stress was first introduced in the 1930s. Mathar (1934) based his technique on the fact that the shape of a circular hole drilled into a stressed structure will change as the result of stress. Mathar used mechanical and optical extensometer. Soete and Vancrombrugge (1954) employed a

similar concept using electrical strain gages rosette type EA-09-125E around the hole rather than measuring changes in the hole diameter with an extensometer. Further work on measuring non-uniform residual stresses by hole drilling method was performed by Kelsey (1956). The method is empirical and depends on experimental calibration. Schajer (1981) provided the first generalized finite element analysis of the hole-drilling method. Comprehensive practical information and further references are given in Technical Note TN-503-2. Supplied by Measurements Group, manufacturer of the specialized strain gage rosette shown in Fig. 3.1.

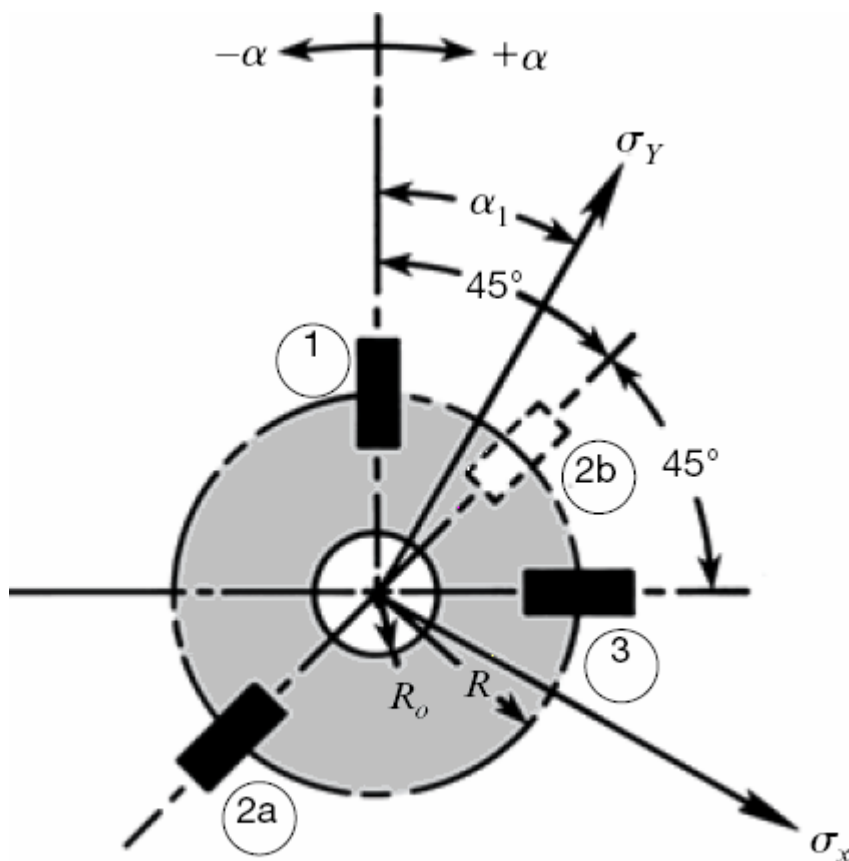


Figure 3.1: Strain Gage Rosette Arrangement for Determining Residual Stresses

(from Technical Notes TN-503-2).

3.1.3 Principle of Hole-Drilling Method

The hole-drilling method is based on the fact that drilling a hole in a stress field disturbs the equilibrium of the stresses, thus resulting in a measurable deformation on the surface of the part, adjacent to the hole. This occurs because every perpendicular to a free surface is necessarily a principal axis on which the shear and normal stresses are zero. The elimination of these stresses on the hole surface changes the stresses in the immediately surrounding region, causing the local strains on the surface of the test object to change correspondingly.

For a linear elastic isotropic material, it may be shown theoretically that the following general formula relates the strain relaxation measured at any of the strain gages in the rosette in Fig. 3.1 to the principal residual stresses and the angle relative to the maximum principal stress direction (Technical Notes TN-503-2).

$$\varepsilon_r = A(\sigma_x + \sigma_y) + B(\sigma_x - \sigma_y)\cos 2\alpha \quad (3.1)$$

where,

ε_r = measured strain relaxation

σ_y = maximum principal stress

σ_x = minimum principal stress

α = angle measured counterclockwise from the nearer principal stress direction to the axis of strain gauge no. 1

A, B = calibration constants

The two calibration constants A and B depend on the geometry of the strain gage used, the elastic properties of the material of the specimen, the radius and depth of the hole. These coefficients cannot be calculated directly from theoretical considerations, they must be obtained by empirical means; that is by experimental calibration or by numerical procedures such as finite-element analysis. Since the strain gage geometry is constant when using the specialized rosette in Fig. 3.1, only the specimen elastic properties, the hole radius and depth remain as variable. Several different approaches have been taken in attempting to remove the material dependency from A and B, leaving only the geometric dependence. One of these, proposed by Schajer (1981) is adopted in our calculations. He introduced two new coefficients, denoted as \bar{a} and \bar{b} , which are defined as follows:

$$\bar{a} = -\frac{2EA}{1+\nu} \quad (3.2a)$$

$$\bar{b} = -2EB \quad (3.2b)$$

Schajer has determined from finite-element calculation that for blind holes, \bar{a} and \bar{b} vary by less than 2% for range of Poisson's ratio from 0.25 to 0.35.

The \bar{a} and \bar{b} coefficients for Vishay Micro-Measurement residual stress rosettes type RE and UL are provided graphically in Fig. 3.2, where the solid lines apply to full-depth blind holes and the dashed lines to through holes assuming, in both cases, that the initial residual stress is uniform with depth. Both the through-hole and full-depth blind holes coefficients plotted in Fig. 3.2 have been determined by a combination of finite element

analysis and experimental calibration. These coefficients are also supplied numerically in tabular form in ASTM E 837-99.

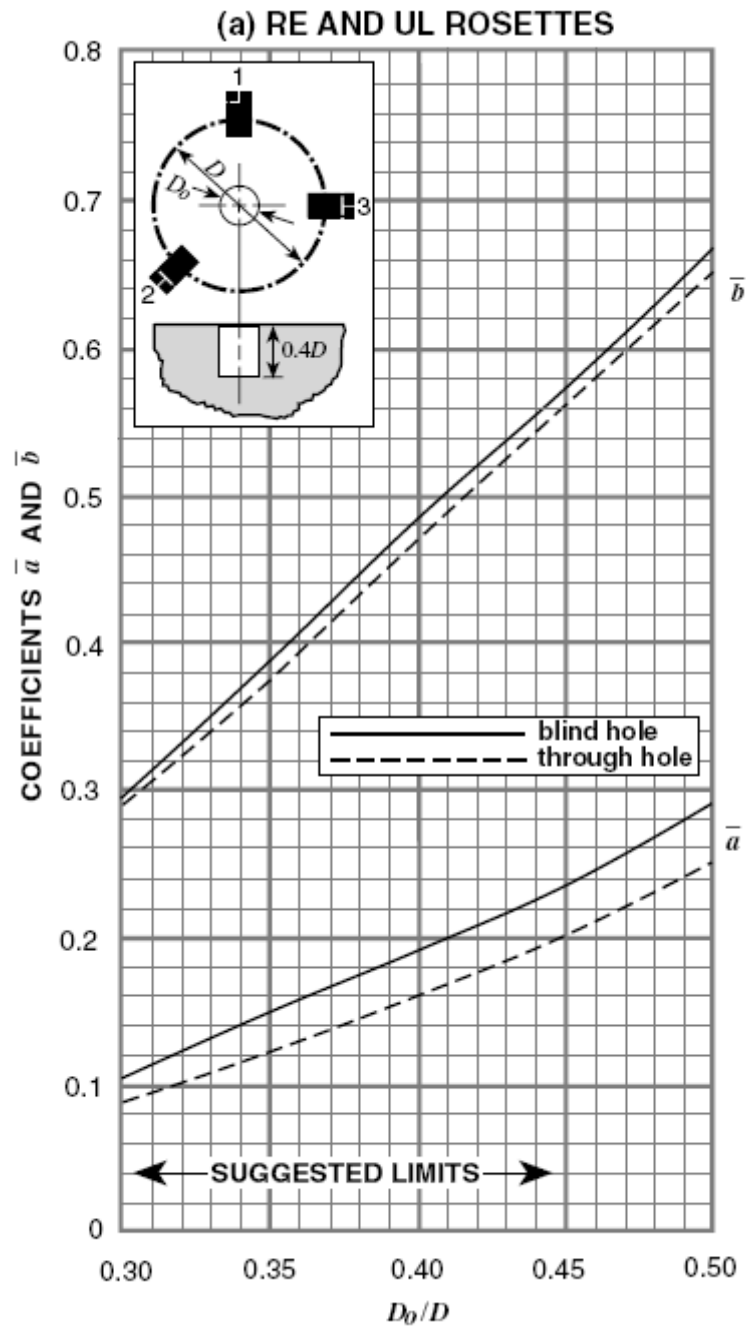


Figure 3.2: Data-Reduction Coefficients, as Functions of Non-Dimensional Hole Depth and Diameter (from Technical Notes TN-503-2)

3.1.4 Computation of Stresses

The common procedure for measuring the relieved strains is to mount three resistance strain gages in the form of a rosette around the site of the hole before drilling. Such a rosette is shown schematically in Fig. 3.1, where three radially oriented strain gages are located with their centers at the radius R from the center of the hole site.

Although the angles between gages can be arbitrary (but must be known), a 45-degree angular increment leads to the simplest analytical expressions, and thus has become the standard for commercial residual stress rosettes. As indicated in Fig. 3.1, α_1 is the acute angle from the nearer principal axis to gage No.1, while $\alpha_2 = \alpha_1 + 45^\circ$ and $\alpha_3 = \alpha_1 + 90^\circ$ with positive angles measured in the direction of gage numbering. It should be noted that the direction gage numbering for the rosette type sketched in Fig. 3.1 is clockwise.

Equation (3.1) can now be written three times, once for each gage in the rosette:

$$\varepsilon_1 = A(\sigma_x + \sigma_y) + B(\sigma_x - \sigma_y)\cos 2\alpha \quad (3.3a)$$

$$\varepsilon_2 = A(\sigma_x + \sigma_y) + B(\sigma_x - \sigma_y)\cos 2(\alpha + 45^\circ) \quad (3.3b)$$

$$\varepsilon_3 = A(\sigma_x + \sigma_y) + B(\sigma_x - \sigma_y)\cos 2(\alpha + 90^\circ) \quad (3.3c)$$

When equations (3.3) are solved simultaneously for the principal stresses and their direction, the results can be expressed as:

$$\sigma_{\max} = \frac{\varepsilon_1 + \varepsilon_3}{4A} - \frac{1}{4B} \sqrt{(\varepsilon_3 - \varepsilon_1)^2 + (\varepsilon_3 + \varepsilon_1 - 2\varepsilon_2)^2} \quad (3.4a)$$

$$\sigma_{\min} = \frac{\varepsilon_1 + \varepsilon_3}{4A} + \frac{1}{4B} \sqrt{(\varepsilon_3 - \varepsilon_1)^2 + (\varepsilon_3 + \varepsilon_1 - 2\varepsilon_2)^2} \quad (3.4b)$$

$$\tan 2\alpha = \frac{\varepsilon_1 - 2\varepsilon_2 + \varepsilon_3}{\varepsilon_3 - \varepsilon_1} \quad (3.4c)$$

where α is the angle from gage number 1 to the nearer principal axis. The following rules can be used to determine which principal stress is referred to gage number 1.

$$\varepsilon_3 \rangle \varepsilon_1 : \alpha \text{ refers to } \sigma_{\max}$$

$$\varepsilon_3 \langle \varepsilon_1 : \alpha \text{ refers to } \sigma_{\min}$$

$$\varepsilon_3 = \varepsilon_1 : \alpha = \pm 45^\circ$$

$$\varepsilon_2 \langle \varepsilon_1 : \sigma_{\max} \text{ at } 45^\circ$$

$$\varepsilon_2 \langle \varepsilon_1 : \sigma_{\min} \text{ at } 45^\circ$$

3.1.5 Test for Non-Uniformity

In general, the nature of the residual stresses is not known in advance of the measurement. Good judgment combined with acknowledgment of the stresses expected should be used to choose the most appropriate calculation method.

As recommended in ASTM E837-2001, it is always preferable to drill the hole in small increments of depth, recording the observed strains and measured hole depth at each increment. This is done to obtain data for judging whether the residual stress is essentially uniform with depth, thus validating the use of the standard full-depth coefficients \bar{a} and \bar{b} for calculating the stress magnitudes.

There is currently no absolute criterion for verifying stress uniformity from the surface of the test piece to the bottom of a full-depth hole. However, the incremental data, consisting of relieved strain versus hole depth, can be used to aid in detecting a non-uniform stress distribution. For each depth increment, the sums and differences of the measured strain data have to be calculated, $\varepsilon_3 + \varepsilon_1$ and $\varepsilon_3 - \varepsilon_1$ respectively. Express each set of data as fractions of their values when the hole depth equals 0.4 times the mean diameter of the strain gage circle. Plot these percent strains versus normalized hole depth. These graphs should yield data points very close to the curves presented in ASTM E837-2001 shown below in Fig. 3.3. Data points that deviates by more than $\pm 3\%$ from the curve presented below indicate either substantial stress non-uniformity through the material thickness, or strain measurements errors. In either case the measured data are not acceptable for residual stress calculations using full-depth coefficients shown in Fig. 3.2.

When a principal residual stress direction is closer to the axial direction of gage number 2 in the strain gage rosette arrangement than to either gage numbers 1 or 3, the strain sum $\varepsilon_3 + \varepsilon_1 - 2\varepsilon_2$, will be numerically larger than $\varepsilon_3 - \varepsilon_1$. In such a case, the percent strain data check should be done using $\varepsilon_3 + \varepsilon_1 - 2\varepsilon_2$ instead of $\varepsilon_3 - \varepsilon_1$.

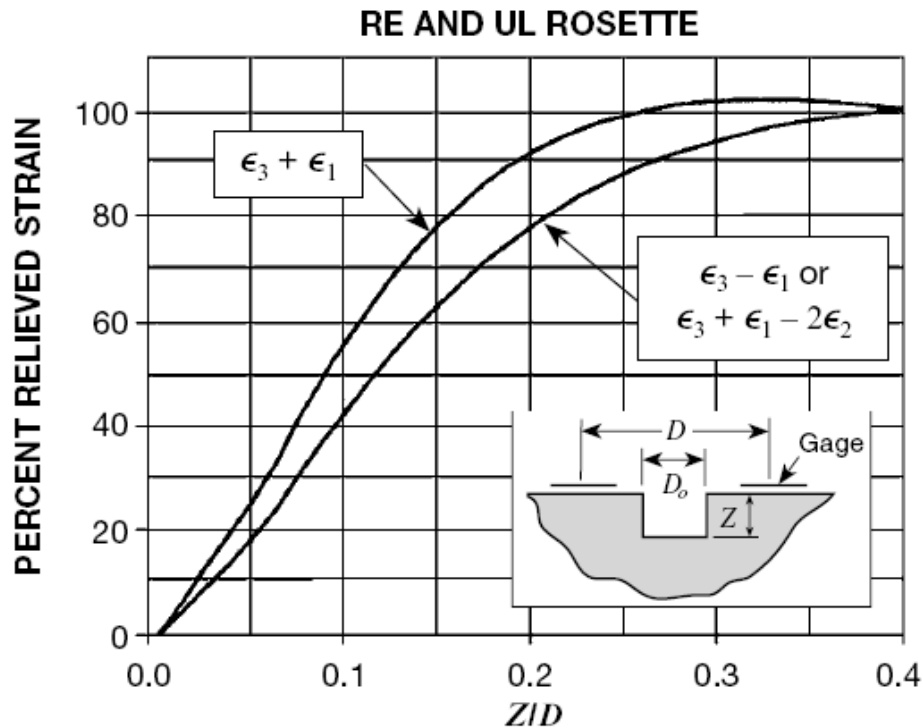


Figure 3.3: Percent Strain Versus Normalized Hole Depth for Uniform Stress with Depth (from ASTM E 837-2001)

3.1.6 Equivalent Uniform Stress Method (EUS)

This method of data analysis is described in the Measurements Group Technical Note TN-503-2. The equivalent uniform stress is defined as that stress magnitude, which, if uniformly distributed through the thickness would produce the same total relieve strain, at any depth, as measured during hole drilling. If the residual stresses varies with depth, the stresses at the incremental depths do not represent the actual residual stresses, but the equivalent uniform stress that would produce the same relieved strain. This technique can provide qualitative information about stress variation with depth.

In order to calculate the equivalent uniform stresses at each increment, the uniform stress coefficients \bar{a} and \bar{b} , as functions of hole depth, must be available. These have been determined by Schajer (1988), based on finite-element studies. The partial-depth coefficients obtained by Schajer have been plotted against the dimensionless hole depth, Z/D , for different values of the diameter ratio, D_o/D , as shown below in Fig. 3.5. When it is known that the residual stress is uniform with depth, the coefficients applicable to any combination of Z/D , and D_o/D can, in principle, be read directly from the graphs shown below and used to calculate the residual stress by substitution into equations (3.2) and then into equations (3.4).

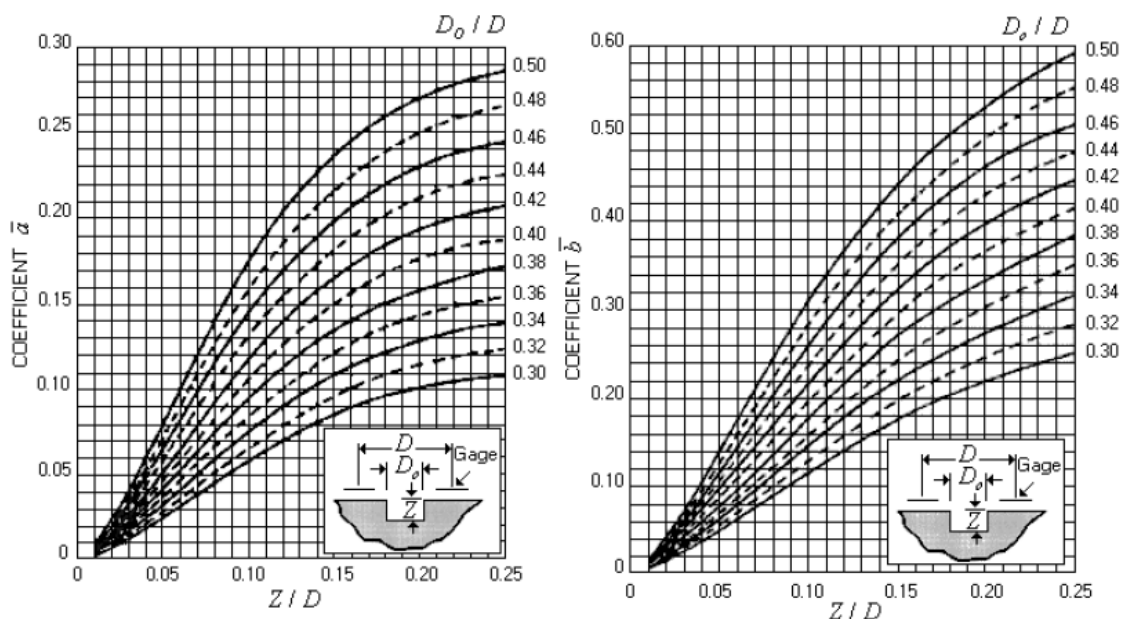


Figure 3.4: Data-Reduction Coefficients, as Functions of Non-Dimensional Hole Depth and Diameter (from Schajer, 1988)

When the residual stress apparently varies with depth, the stresses at partial depths (calculated with the coefficients shown above) do not represent the actual residual

stress, but the equivalent uniform stress (from the surface to depth) which would produce the same relieved strain at that depth. Calculated EUS can provide at least qualitative information about the stress variation with depth. Furthermore, for the first small increment of depth, the calculated EUS is the best available estimate of the actual average stress in that layer. The EUS calculated for the second and subsequent depth increments are ever less subject to quantitative interpretation. This is so because the cumulative relieved strain at any depth is affected in a complex way by the relaxed stresses at all lesser.

3.1.7 Experimental Approach

A total of four specimens of residual strain measurements were made from four built-up beams. As shown in Fig. 3.6 from 5.5 meter long member, beams having two different span lengths of 3 m and 2 m, and a short beam for residual stress measurements, have been cut out. Residual stresses in the flanges and the webs were measured at three points (1, 2, and 3) for all specimens as shown in Fig. 3.6. The dimensions of the specimens are given in Table 3.1. Each specimen is referred to by a code number, such as A30, which denotes the specimen type A, means (the first group with single fillet weld on one side of the web), and its depth (30 cm, means that the specimen has a depth of 30 cm), and (AA, means the first group with double fillet weld on both sides of the web).

The experimental results described here were obtained using EA-06-062RE-120 gage made by Measurement Group. The design of this rosette has centering pattern for precisely positioning the boring tool at the center of the gage. The gages were applied using the manufactures recommended procedure. The MANFORD VMC 610 machine

with 6000 rpm was used for drilling the hole using 2 mm central drill. The drilling was done in increments $0.05D$ up to a depth of $0.4D$ (Max depth for blind hole method as recommended by ASTM E837-2001), where D is the diameter of rosette. The size of the hole was measured after drilling using a special device as shown in Fig. 3.7. The average measured value of holes sizes was found to be 2 mm. The data acquisition system was used to record strains. The instrumentation used in residual stress measurements and rosette applications are shown in Fig. 3.8 and Fig. 3.9 respectively.

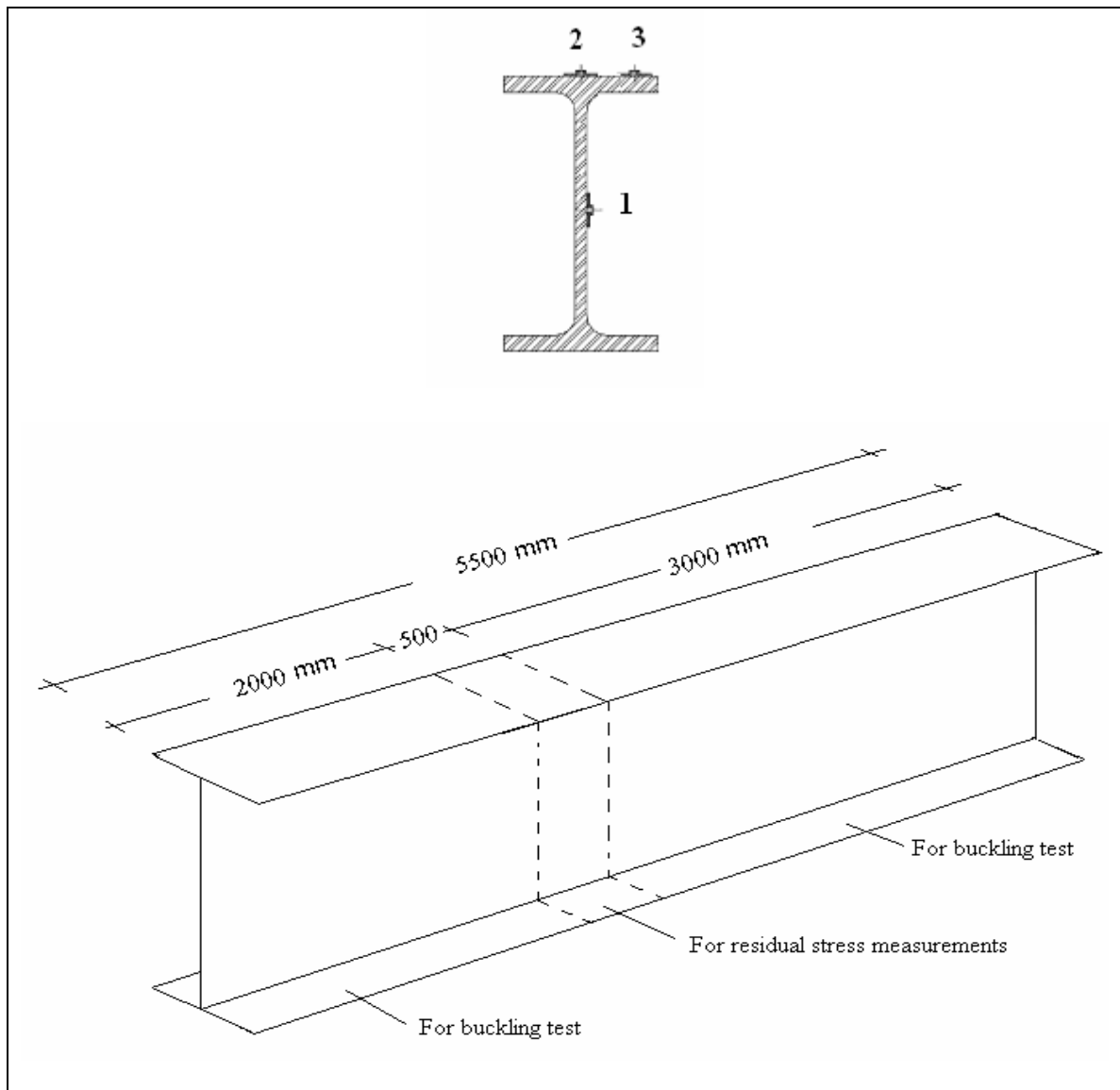


Figure 3.5: Allotment of Test Specimens and Locations of Rosettes

Table 3.1 Nominal Dimensions of Test Specimens for Residual Stress Measurement

Specimens	d (mm)	b_f (mm)	t_f (mm)	t_w (mm)	L (mm)
A30	300	150	5	4	500
AA30	300	150	5	4	500
B40	400	150	6	5	500
BB40	400	150	6	5	500

**Figure 3.6: Hole Size Measurement**



Figure 3.7: Instrumentation of Residual Stress Measurement

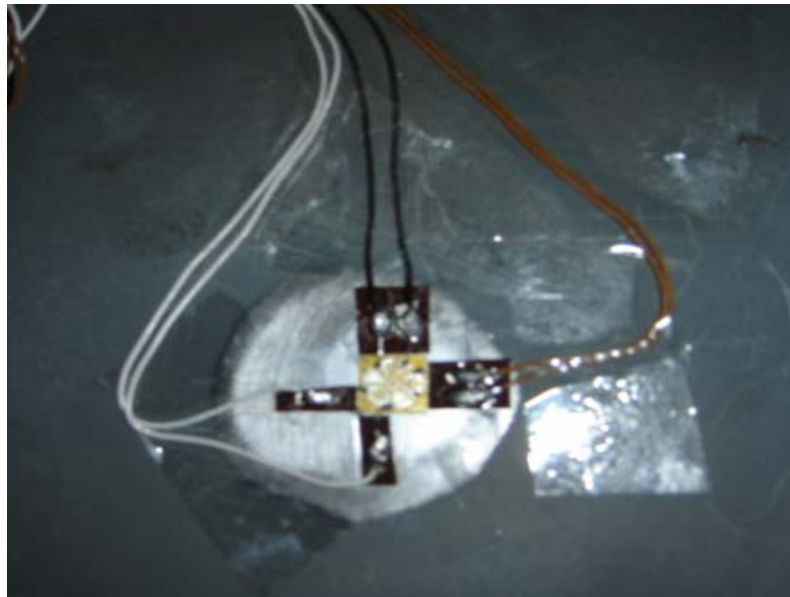


Figure 3.8: The Application of Rosette

Two specimens with 6 mm thickness were saw cut to approximately (25 mm x 200 mm) dimensions had been subjected to relieved treatment at 315 C°, as per standard (AWS D1.1, 2000) to measure the induced stresses by the drilling machine. The average of these stresses was found to have a little effect on the residual stress calculation.

It is clear from Fig. 3.9 that the stress field for the specimen AA30 does not satisfy the validity criteria, the theoretical and measured values do not coincide and therefore the assumption of uniform stress field is invalid. In general weld residual stresses are highly non-uniform.

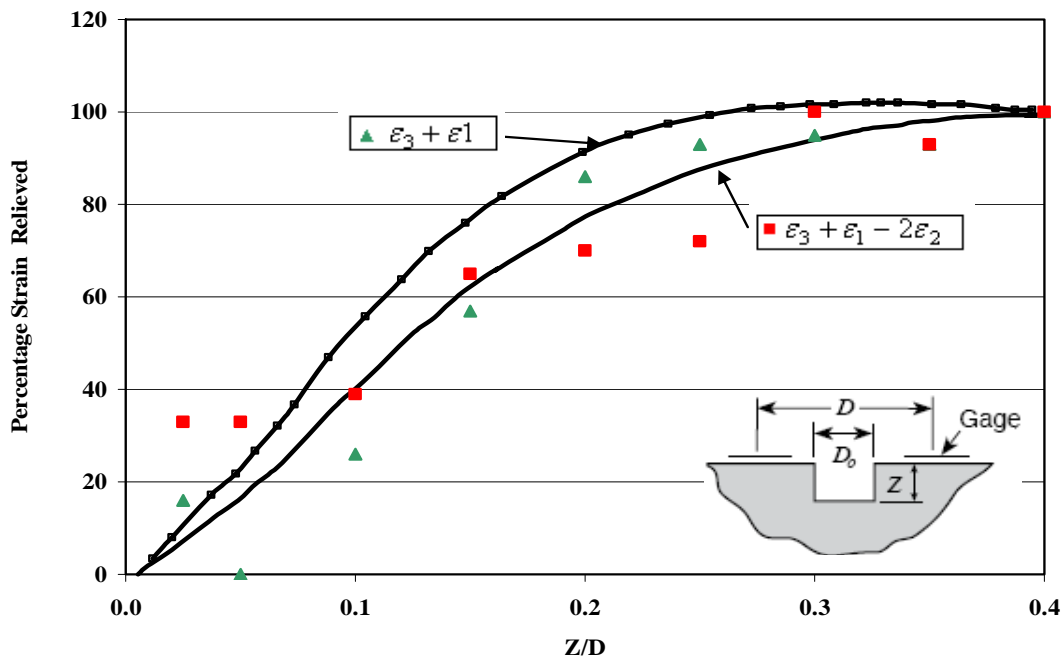


Figure 3.9: Percent Strain Versus Normalized Hole Depth for Specimen AA30

Tables A.1-A.12 show the measured relieved strains via incremental hole-drilling to a depth of 2 mm. The equivalent uniform principal stresses are calculated for each increment using the mean Young's modulus of 204000 MPa and Poisson's ratio .29. The data-reduction coefficients \bar{a} and \bar{b} were taken from ASTM E837-2001. The average measured values were used to represent the residual state of the tested specimens are listed in Table 3.2. and the stresses versus the dimensionless hole depth, Z/D are shown in Figs. A.1-A.12.

From the experimental results shown in Table 3.2, the expected pattern of residual stresses shows compressive residual stresses occurring at the mid-height of the web and high tensile residual at the flange-to-web junctions. This feature conforms to that reported by other researchers (Fukumoto, 1971).

Table 3.2 Experimental Results of Residual Stresses

Specimens	Point 1 MPa	Point 2 MPa	Point 3 MPa
A30	-11	135	-92
AA30	-40	195	-192
B40	-14	216	-113
BB40	-153	292	-116

3.2 Tension Tests

3.2.1 Introduction

The flanges and the webs of the buckling test beams were made from six original plates by using a hydraulic cutting machine. Thirteen tension tests were carried on specimens prepared from the original plates to determine their material properties. The coupons were prepared and tested in accordance with ASTM E8 Standard Test Methods and Definitions for Mechanical Testing of Steel Products (ASTM, 2001). The type of coupon specimen used of the ATSM plate-type for testing plates, shapes, and flat materials having a normal thickness of 4 mm and over. This specimen type has a gage length of 200 mm and a reduced width of 40 mm to ensure that the failure occurs within the designed gage length. The dimensions shown in Fig. 3.10 are the standard specimen used for this purpose. The mean value of the results obtained from the tension tests were used in calculating the buckling loads and residual stresses for the test beams.

After both surfaces of the central part of the coupon were cleaned and prepared so that they were completely smooth, the exact cross-sectional dimensions were measured at four locations along the gage length using digital calliper. These results as well as the original plate to which each coupon corresponds are shown in Table 3.3.

3.2.6 Test procedure

The tension tests were carried out in a 2000 kN capacity Universal Testing Machine located in the construction material laboratory at Al-Hashemite University as shown in Fig. 3.11. The specimens were placed between the upper movable head and the lower fixed head with friction grips to apply the loading. One LVDT was mounted on the tensile coupon to measure the longitudinal elongation of 200 mm gage length as shown in Fig. 3.12 and Fig. 3.13 respectively. Double grid electrical resistance strain gauges type and AP-11-TS50N-120-EL were used on three coupons with different thicknesses. These gages were positioned centrally on the central part of coupons to measure axial and transverse strains as shown in Fig. 3.14. The reason for this was to determine a correct value for Poisson's ratio, ν , because the accuracy of the determination of Poisson's ratio is usually limited by the accuracy of the transverse strain measurements. The strain gages wires were connected to TDS-303 data acquisition systems which recorded the loads and strain gages readings at two second interval as shown in Fig. 3.15. The strain gages for these coupons remained functional until a load close to the yield ultimate load was reached. The stress was calculated using the cross-sectional dimensions listed in a column (3) of Table 3.3 in which the following mechanical properties are listed: (4) Yield stress, F_Y ; (5) ultimate stress, F_u ; (6) modulus of elasticity, E; and (7) Poisson's ratio, ν .

Average yield stresses have been found from minimum lower yield stresses. Values of modulus of elasticity, E, were determined from the slope of the plot of the axial stresses versus the axial strains. The stress-strain curves for the ten coupons are shown in Figs. B.1-B.10. Poisson's ratio was calculated for three coupons by taking the

negative ratio of the transverse strain to its corresponding axial strain. Figs. B.11-B.13 show the axial and transverse strains for these coupons.

Table 3.3 Tensile Materials Properties

Coupon No.	Coupon Name	Cross-Sectional Dimensions mm	Yield-Stress F_Y MPa	Ultimate-Stress F_u MPa	E GPa	Poisson's Ratio ν
1	CP4-T1	42.9 x 4.2	341	506	221	-
2	CP4-T2	42.9 x 4.15	348	499	206	-
3	CP5-T3	41.5 x 5.2	356	513	206	-
4	CP5-T4	41.9 x 5.1	442	568	192	-
5	CP5-T5	40.3 x 5.2	359	507	193	-
6	CP5-T6	42 x 5.3	494	543	227	-
7	CP6-T7	40.3 x 6.3	333	496	209	-
8	CP6-T8	40.4 x 6.3	328	494	208	-
9	CP6-T9	40.4 x 6.2	341	510	190	-
10	CP8-T9	42.3 x 8.5	410	567	201	-
11	CP5-T11	41.9 x 5.2	360	520	204	0.29
12	CP6-T12	40.2x6.2	345	520	218	0.28
13	CP8-T13	42 x 8.4	407	554	191	0.29
Average			378	524	204	0.29

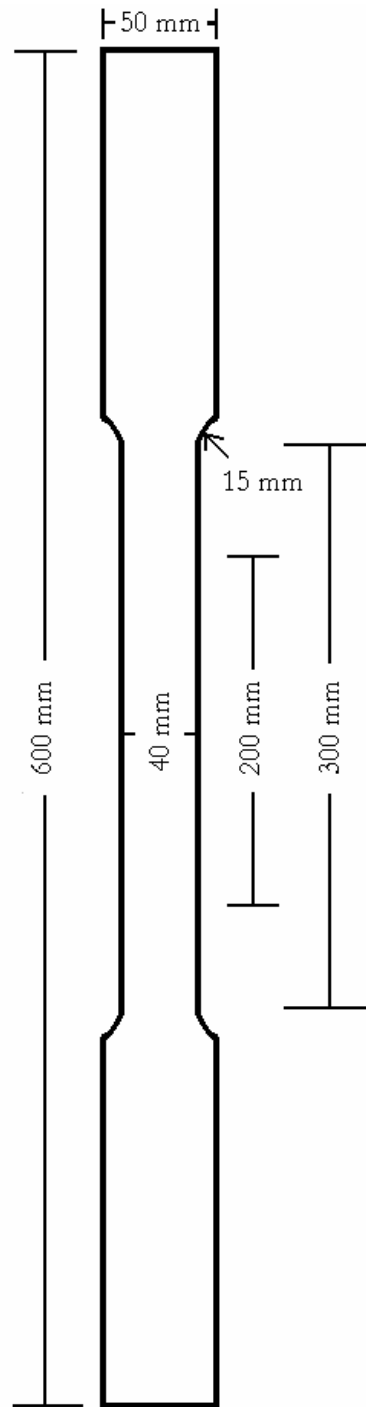


Figure 3.10: Tension Test Coupon



Figure 3.11: Universal Testing Machine



Figure 3.12: Tension Test Specimen with Extensometer



Figure 3.13: Tension Test Specimen after Fracture

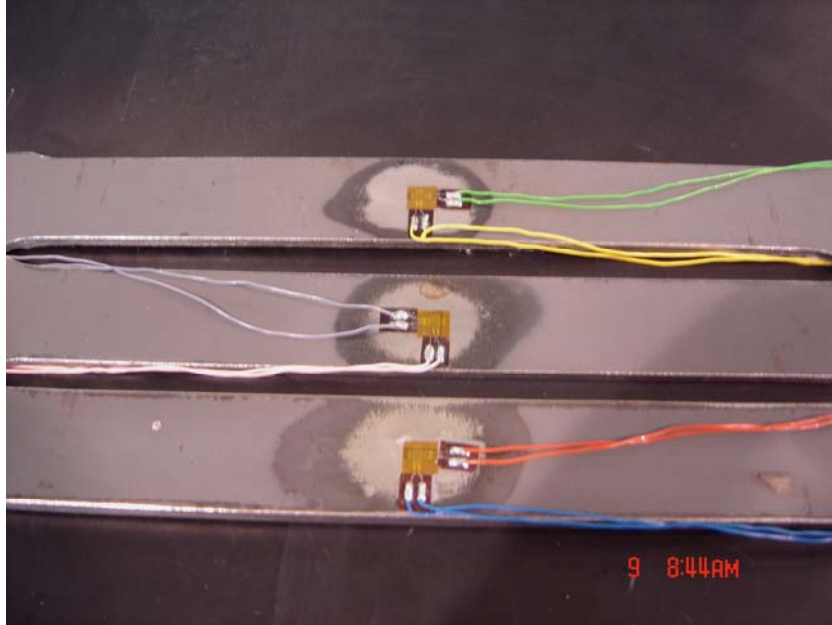


Figure 3.14: Tension Test Specimens with Strain Gages



Figure 3.15: Portable Data Logger TDS-303

CHAPTER 4

EXPERIMENTAL PROGRAM

4.1 Introduction

In order to achieve the study objectives given earlier in chapter 1, an experimental program was devised and constructed in collaboration with Jordan University of Science and Technology (JUST). To study the lateral buckling behavior of simply supported built-up beams with fillet weld: 1) on one side of the web; 2) on both sides of the web as shown in Figs. 4.1a - 4.1b respectively. Nineteen buckling tests were carried out on five groups of built-up I-beams with two symmetrical concentrated loads applied vertically at third point of the compression flange. The first group of specimens was composed of four beams with 2 m length and the second group of specimens had identical length to the first group but differed in cross sections. The third group is similar to the first group but the beam span was 3 m, while the fourth and the fifth groups specimens had identical depths and spans but differed in plate thicknesses.

This chapter describes in detail the experimental program including specimen details, specimen instrumentations, test setup and applied loads.

4.2 Test Beams

Built-up I-section members used in this investigation were fabricated from continuous web and flange plates. A pair of transverse stiffeners was attached to the

web at the loading points. The flange-to-web, stiffeners-to-web and stiffeners-to-flange fillet welds undermatched and made with automatic Submerged Arc Welding process as shown in Fig. 4.2. Fillet weld of size 5 mm leg length was used for all specimens. All welding was performed in accordance with AWS structural welding Code D1.1-2000 (AWS, 2000). A total of nineteen specimens were tested under two concentrated loads at third points, placing the central third under a constant moment. The ratio of thicknesses of the flange and the web (t_f / t_w) was varied from 1.2-1.33, while the ratio (b_f / h) was varied from 0.39-0.52. The width-thickness ratio of the flanges ($b_f / 2t_f$) were approximately 9, 12 and 14, and those of the webs (h / t_w) were approximately 60, 75 and 77. The span lengths L of the beams were such that the lateral torsional-buckling failure occurred in the inelastic region, and the slenderness ratios, L / r_y (r_y = the radius of gyration about the minor axis), were approximately 60, 67, 90, and 100. The geometric dimensions of each specimen, including the overall length, height, width of the flange, thickness of the flange and of the web were measured using standard instruments. The measured dimensions of all the tested beams are listed in Table 4.1.

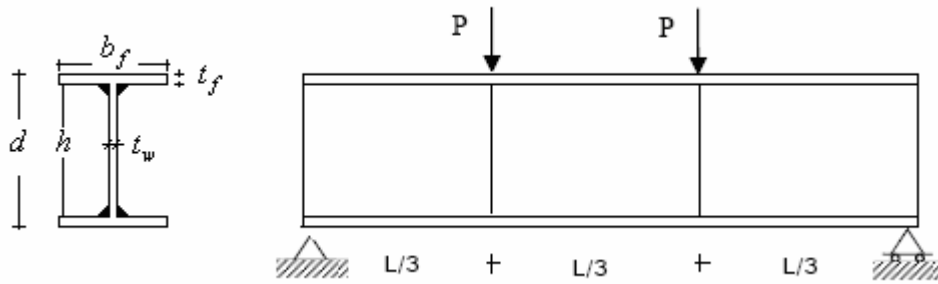


Figure 4.1a: Beam Specimens With Fillet Welds on Both Side of the Web

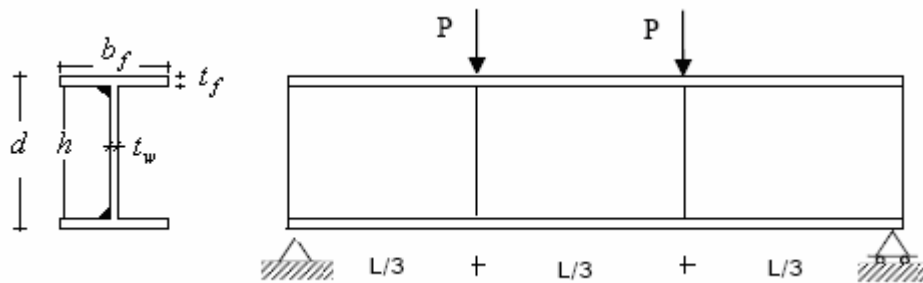


Figure 4.1b: Beam Specimens With Fillet Weld on One Side of the Web

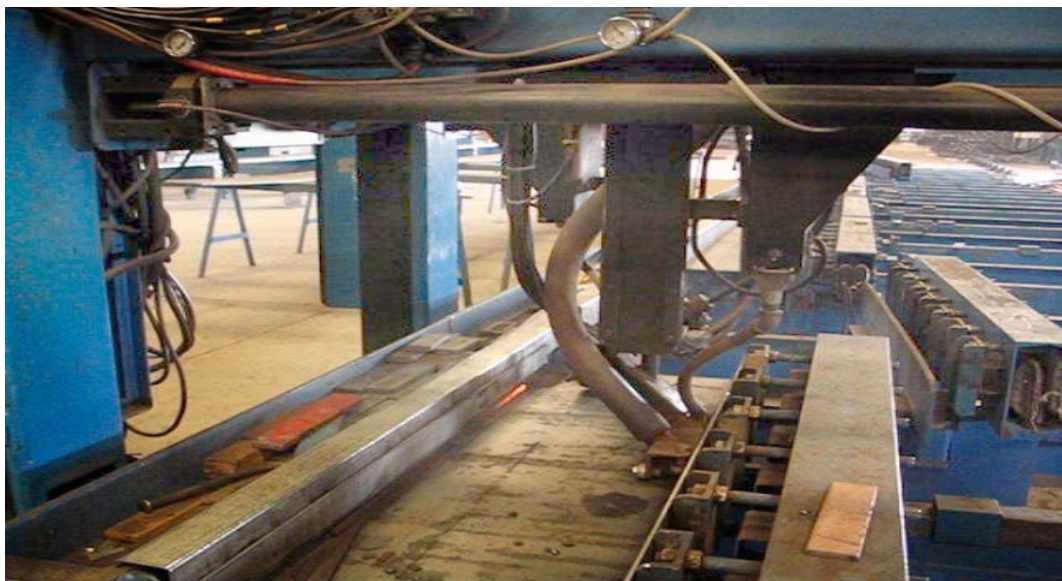


Figure 4.2: Automatic Submerged Arc Welding process

Table 4.1 Dimensions of Beam Specimens

Group	Specimens	d <i>mm</i>	b_f <i>mm</i>	t_f <i>mm</i>	t_w <i>mm</i>	$b_f / 2t_f$	h / t_w	L <i>m</i>	L / r_y
1	AB1	300.10	150.80	4.10	5.30	14.23	70.61	2	60.9
	AB2	300.12	150.94	4.20	5.27	14.32	68.95	2	61.2
	AB1A	300.14	150.44	4.30	5.22	14.41	67.37	2	62.2
	AB2A	300.17	150.58	4.25	5.35	14.07	68.11	2	61.6
2	BB1	400.11	150.13	5.11	6.04	12.43	75.94	2	66.9
	BB2	400.20	150.00	5.14	6.12	12.25	75.48	2	66.9
	BB1A	400.13	150.11	5.03	6.12	12.26	77.12	2	66.7
	BB2A	400.15	149.99	5.11	6.14	12.21	75.90	2	66.9
3	AB3	300.10	150.14	4.20	5.15	14.58	69.00	3	92.9
	AB3A	300.20	150.10	4.13	5.10	14.72	70.22	3	93.2
	AB4A	300.00	150.20	4.00	5.20	14.44	72.40	3	92.1
	BB3	400.23	150.20	5.15	6.20	12.11	75.31	3	99.9
4	BB4	400.15	150.13	5.18	6.10	12.31	74.89	3	100.5
	BB3A	400.10	150.02	5.17	6.14	12.21	75.01	3	100.7
	BB4A	400.10	150.03	5.22	6.10	12.29	74.31	3	101.1
	CB3	400.17	150.12	6.18	8.11	9.26	62.16	3	97.5
5	CB4	400.1	150	6.14	8.08	9.28	62.56	3	97.5
	CB3A	400.21	150.14	6.11	8.13	9.23	62.9	3	97.4
	CB4A	400.01	150.2	6.2	8.1	9.27	61.94	3	97.7

4.3 Supported System

The support system was designed to insure the beam was simply supported in-plane and out-of-plane. A beam that is simply supported in-plane has a single span with ends fixed against in-plane vertical deflections, but unrestrained against in-plane rotation. The ends of a beam that are simply supported out-of-plane are fixed against out-of-plane (lateral) deflection and twist rotations, but are unrestrained against minor axis rotations.

Specially designed supports as shown in Fig. 4.3 with a horizontal and a vertical axis has been fabricated to approach these simply supported conditions. It can be seen from Fig. 4.3 that the test beams were simply supported both in-plane and out-of-plane. The in-plane vertical deflections were prevented by the supporting sides with bolted end-plate connections. The in-plane rotations were not restrained because the beam could rotate freely about the horizontal axis ($x_1 - x_1$) through two roller bearing. The out-of-plane deflection and twist rotation were prevented. The minor axis rotations were not restrained, because the beam could rotate freely about the vertical axis ($y_1 - y_1$) through a thrust ball bearing which transmits the end reaction. The two supports ends were the same except that the beam at one end was prevented from running by horizontal stops while the beam at other end was allowed to run.

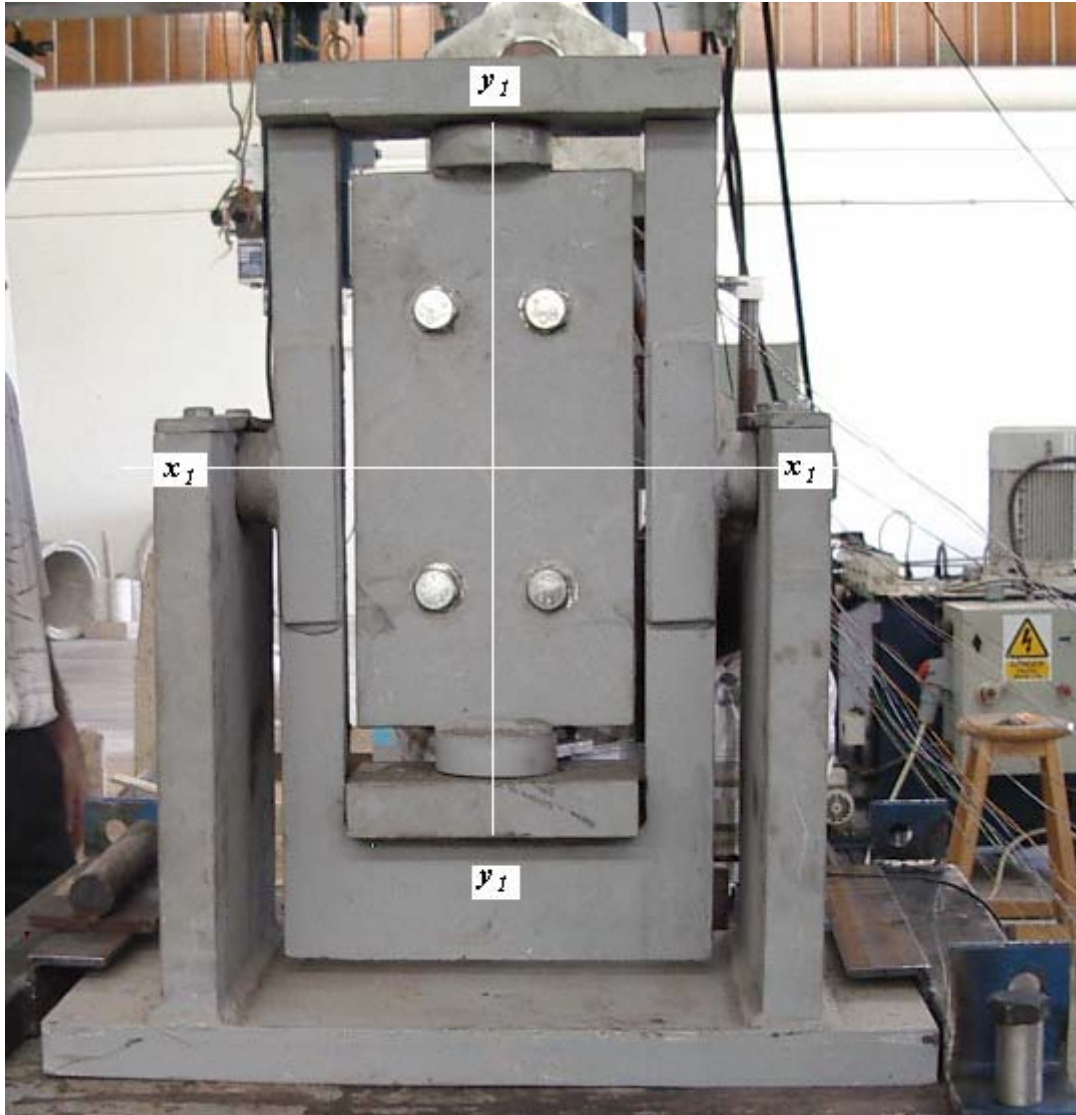


Figure 4.3: Support System

4.4 Initial Imperfections

All specimens in this research were carefully fabricated with controlled levels of initial crookedness to reduce its effect on load capacity of the beam in order to clarify the effect of residual stresses.

Nominally straight specimens were fabricated such that the maximum offset of each flange was less than $L/1000$, in which L is the distance between points of lateral support, corresponding to the fabricated tolerance limits specified in (AS4100, 1998).

The structural welding code-steel AWS D1.1-2000 AWS (2000) which for (the imperfection of the web plate) provides the value of $D/100$ for d/t_w equal to or less than 150 and $D/80$ for d/t_w equal to or less than 100. d and t_w are the beam depth and thickness respectively and D is the least panel dimension bounded by the stiffeners or flanges or both. The same codes also provide the max offset or tilt of the flange plate which is 1% of the total flange width or 6 mm, whichever is greater, and for built-up I-members, the allowed variation between the center line of the web and the centerline of the flange at contact surface is 6 mm.

The imperfections of the test beams were measured in the lab as a part of the test program. This was done by measuring the distance between a plastic wire held tautly over the specimens by means of weights tied to each end and to the specimens itself. The distances were measured by a digital caliper with an accuracy of 0.02 mm. The measured out-of-straightness of the flange and the web was less than $L/1000$ for all specimens and within the limits specified by (AWS, 2000).

4.4 Test Set-Up

Experimental test were carried out in a rig (designed and fabricated in DARTIC limited). This rig consists of two portal frames, supports, a strong floor with matrix of fixing holes in both directions @ 500 mm and two loading hydraulic actuators, each of these actuators had a load capacity of 417 kN in compression and a built-in load cell. Figs. 4.4-4.5 show elevation, instrumentation, supports and details of set up.

4.6 Instrumentation

The test specimens were instrumented in with a variety of sensors. The targeted measurements include load measurements, displacement measurements and strain measurements, the nineteen built-up beams were instrumented at different selected positions to obtain the data necessary to describe their strength and behavior. All electronic measuring devices such as load cells, Linear Variable Displacement Transducer LVDTs, and cable transducers were calibrated before use.

4.6.1 Load Measurements

The two hydraulics actuators were provided with load cells which furnished direct measurements of the applied vertical forces. The loading cells are connected to the data acquisition system.

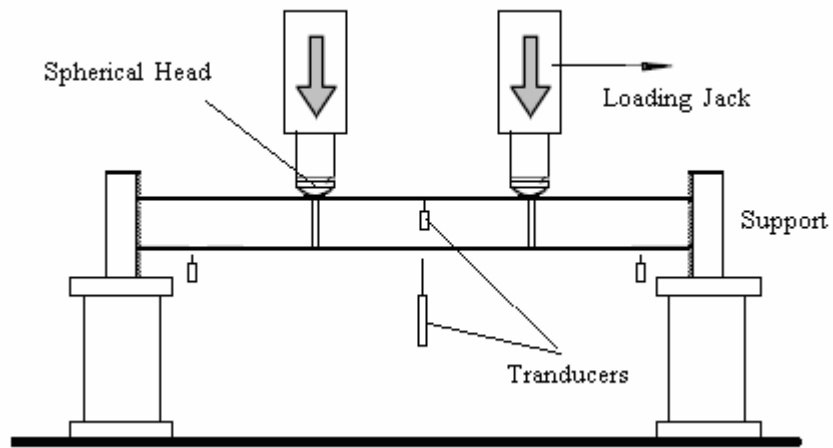


Figure 4.4: Schematic Diagram of Test Set-Up

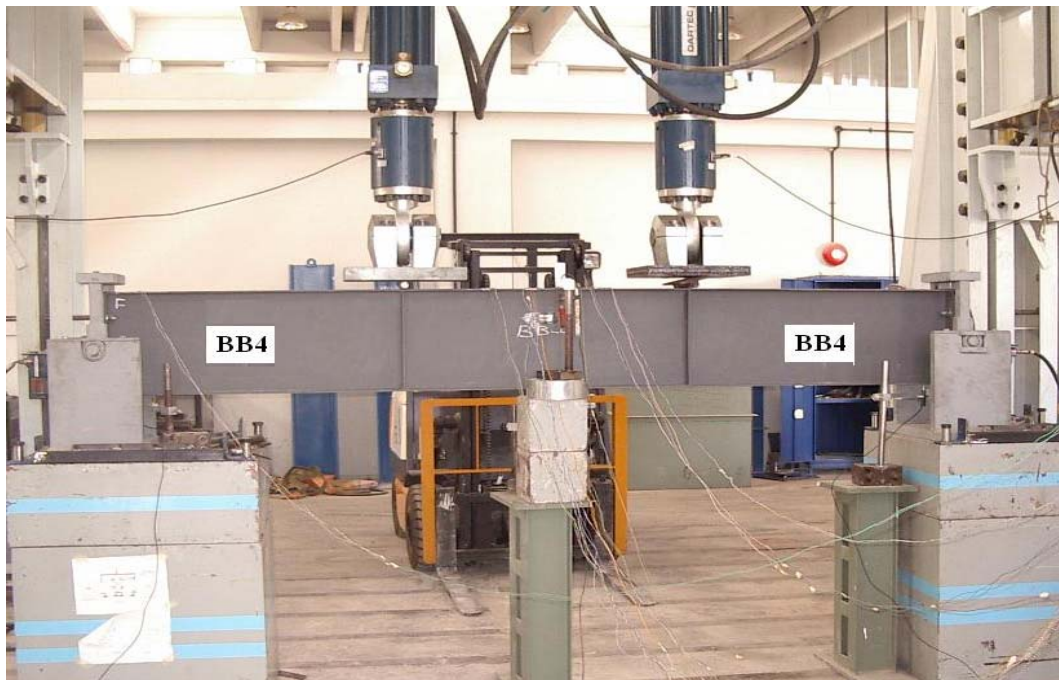


Figure 4.5: Buckling Test Apparatus

4.6.2 Displacement Measuring Instruments

Measurements of the horizontal and vertical deflections of the central section of the selected beams in each group were obtained by using Linear Variable Displacement Transducer LVDTs. An LVDT is composed of a metal barrel out of which a metal piston protrudes. When this piston moves it causes a change in potential which in turn is a measure of displacement. Four LVDTs were used to measure displacement at different positions for each specimen. Three vertical LVDTs were used to measure vertical displacements at supports and mid span respectively. In addition, one horizontal was attached to the top fiber of the compression flange at mid span to measure lateral deflection. The general arrangement of LVDTs as installed on the specimen is shown in Fig.4.5.

4.6.3 Strain Measurement

Electric resistance strain gages type AP-11-S300N-120-EL were bonded to the specimens to measure localized strains. Four strain gages were located at mid span on the top and bottom fiber of the section to verify the bending moment within the span, and two strain gages were bonded to the web to detect the onset of local buckling of the web. An additional indication of the onset of the plate buckling was obtained by the concept of strain reversal using three pairs of electrical resistance strain gages mounted along the unsupported edges on opposite faces of the flange. A polished surface for each strain gage was prepared and cleaned prior to fixing the strain gage to the specimen. The location of the measurements made for strain on the beam web and flanges are shown in Fig.4.6.

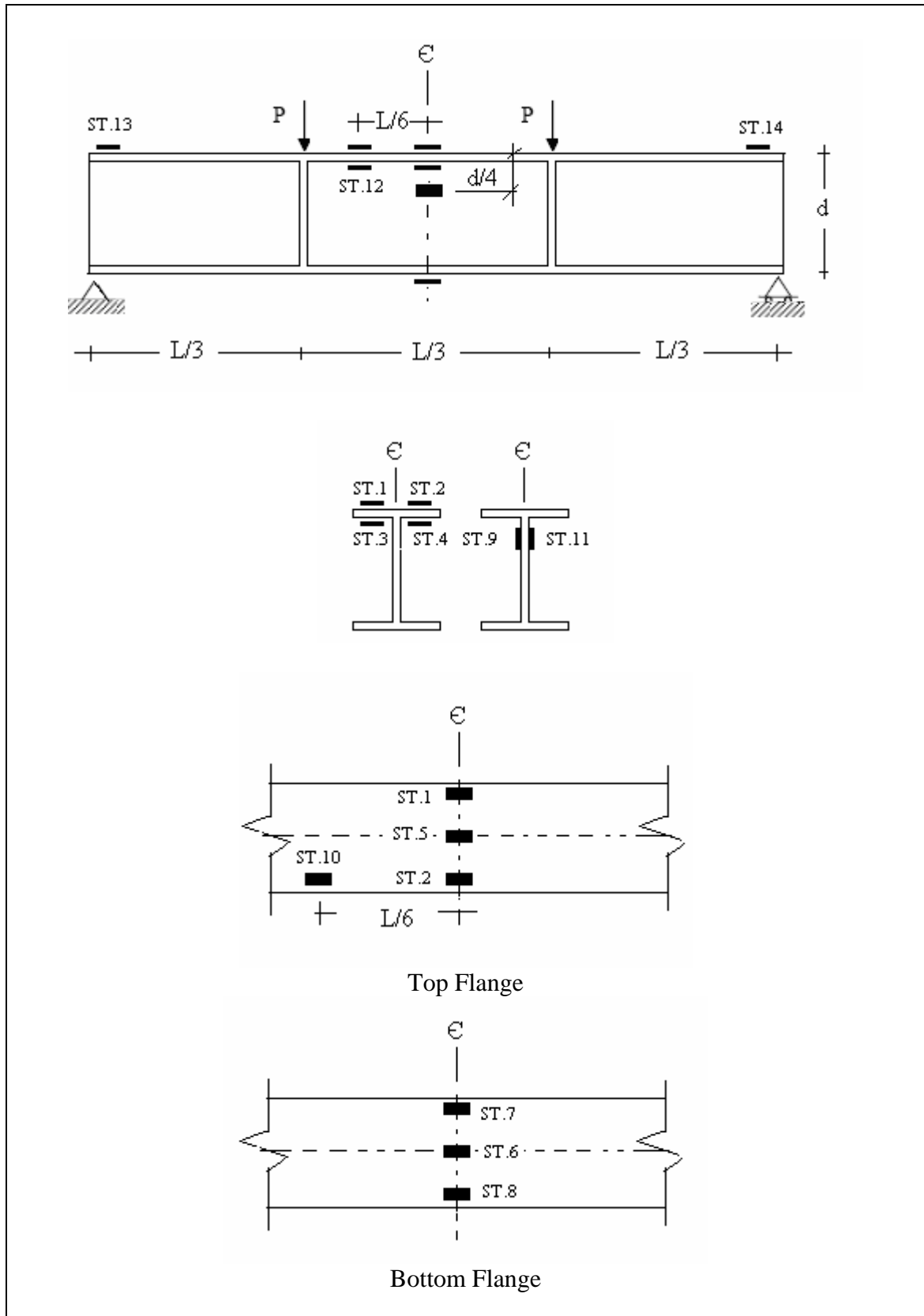


Figure 4.6: Strain Gage Identification Numbers and Locations

4.7 Experimental Procedure

After each beam was prepared with its strain gages. It was placed onto the support and clamped in position by means of set screws threaded into the plate of the support. This had the effect of reducing warping of the end sections of the beams. The displacement transducers were set in place. The hydraulic jacks were carefully located and aligned as any eccentric loading would be undesirable. Both hydraulic jacks are connected to one servo-valve and hence apply equal loads. Since the load was applied using load control, particular care was required to accurately determine the ultimate loads without catastrophic failure. The tests load was applied in increments, the size and rate of application of which depends on the proximity to failure estimated from the development of inelasticity and the growth of buckling deformations. The experiments proceeded with trail loading in the elastic range, up to about one third of the predicted failure load to ensure proper functioning of the instruments. Increments of 10 kN were applied in the early loading stages and were gradually reduced to 0.5 kN as the maximum loads was neared. At every load step in the elastic range, a check of static equilibrium was obtained from the load cell reading, thereby assuring that system was functioning properly. The magnitude of the applied constant bending moment within the span of the specimens was obtained by multiplying the jack load by the distance of the jack from the support ($L/3$). This value was compared with the bending moment calculated using the measured midspan strains (average of top and bottom flange strains). The agreement was good in all cases in the elastic range.

The output from electrical resistance strain gages, LVDTs , cable transducers and load cells, amounting to as many as twenty one channels were recorded automatically at

each step during the test on the data acquisition system at a rate of five readings per second . The failure mode was carefully observed. Buckling was deemed to occur when a load-deflection curve or lateral-deflection curve of one of the flange cross sections reached a horizontal asymptote. Even after each beam reached the ultimate strength point, tests were continued for a period of time to record the gradual unloading path.

CHAPTER 5

EXPERIMENTAL RESULTS

5.1 Introduction

The results of the full-scale beam tests are presented and analyzed in this chapter, as are the results obtained from the residual stress measurements used to predict the behavior of these tests. Nineteen buckling tests were carried out on five groups of built-up I-beams, each group has identical dimensions and span length, but the flange-to-web fillet weld was different. The buckling tests were performed under same loading conditions with two point load applied at the top flange. It is recognized that this test situation represents a more severe loading condition because of the destabilizing effect of the load applied above the shear center.

5.2 Behavior of Specimens and Failure Loads

Different data reveal different aspects of a beam behavior and can provide insight into local, overall or combined effects in a structural system. In this case, in-plane data relates primarily to behavior related to vertical stiffness and reveals little about buckling behavior. Out-of-plane behavior relates primarily to buckling mechanisms and can provide more insight into buckling behavior.

Experimental observations of tested specimens and recorded data are utilized in this section to explain the behavior of the built-up steel beams and to describe different

modes of failure. The buckling modes observed in these tests were characterized in general by changes in cross-sectional shape, arising from interaction between local flange and lateral-torsional buckling. Test observations show that web buckling is noticeable and critical in some specimens where the webs are relatively thin.

In the AISC-LRFD (2005) specifications, the nominal bending strength of I-shaped beams is determined by the lowest value obtained according to the limit states of: Lateral-torsional buckling (LTB); flange local buckling (FLB); and web local buckling (WLB). The nominal bending strength M_n in the inelastic range and a summary of the experimental maximum loads, P_u , of all test beams are summarized in Table 5.1. Also shown are the modes of failure for the test beams, and modes predicted by LRFD.

From the experimental failure loads of beams in the first group, shown in Table 5.1, it can be seen that the beams with fillet weld on one side of the web (FWO) showed a slight increase in strength over those of beams with fillet welds on both sides of the web (FWB). M_u / M_p of beam AB1 is 5% higher than its counterpart AB1A and that of beam AB2 is 3% higher than that of AB2A. The reason for this increase might be due delayed yielding of the compression flange tips in beams with (FWO) because the compressive residual stresses near the flange tips are small.

The failure modes of beams in the first group were predominantly either local or coupled. The local flange failure with a single wavelength was observed for beams with (FWO), as seen in Fig. 5.2 for beam AB1. For beams with (FWB), AB1A and AB2A the local buckling and the lateral buckling are combined to produce a coupled mode of failure with a single wavelength for both local and lateral buckling as shown in Fig 5.1.

Although slight variations in wave lengths with location along the span were sometimes noted in this group, the length of an individual wave remained constant as shown in Fig 5.3 for beams AB1 and AB1A.

A third mode of failure occurred only in beams with (FWB), this was web buckling. This can be explained due to the compression residual stresses in the web which precedes yielding and thereby the reduction in effective cross-sectional stiffness.

The behavior of beams in the second group was influenced by the presence of residual stresses. Beams with (FWB) display higher strength than their counterpart beams with (FWO). When M_u / M_p are compared, beam BB1A is 4% higher than its counterparts BB1 and BB2A is 12% higher than BB2, indicating that tensile residual stresses in the flange imparts an improvement of 8% approximately for beams with (FWB).

While local buckling was dominant in the failure of beams in this group as shown in Figs. 5.4-5.6, lateral buckling was very probably a contributing factor in the failure of these beams especially beams with (FWO). A single wave in the longitudinal direction was observed for each beam in this group.

Buckling of the web plates was observed at a load level of about 120 kN for beams with (FWB) and at a load level higher than 160 kN for beams with (FWO) in the same group. The presence of compression residual stresses in the webs of the beams BB1A and BB2A seems to have had a minor effect on their strength.

Table 5.1 Failure Loads and Failure Modes

Group	Specimens	Experimental			M_u / M_p	AISC LRFD Specification	
		P_u (kN)	M_u (kN.m)	Failure modes		M_n (kN.m)	Failure modes
1	AB1	147.55	98.37	FLB	0.81	95.45	FLB
	AB2	141.46	94.24	FLB	0.77	95.51	FLB
	AB1A	142.97	95.31	Combined	0.77	96.1	FLB
	AB2A	140.70	93.80	Combined	0.75	99.11	FLB
2	BB1	244.62	163.08	Combined	0.79	174.92	FLB
	BB2	245.36	163.57	Combined	0.78	178.34	FLB
	BB1A	259.46	172.97	Combined	0.82	178.32	FLB
	BB2A	275.10	183.40	Combined	0.87	180.19	FLB
3	AB3	95.12	95.12	FLB	0.80	85.20	LTB
	AB3A	92.24	92.24	Combined	0.77	84.87	LTB
	AB4A	90.22	90.22	Combined	0.76	85.89	LTB
4	BB3	163.72	163.72	FLB	0.77	143.46	LTB
	BB4	168.50	168.50	FLB	0.80	141.56	LTB
	BB3A	175.70	175.70	Combined	0.83	142.82	LTB
	BB4A	197.70	197.70	Combined	0.93	142.34	LTB
5	CB3	257.53	257.53	LTB	0.97	185.89	LTB
	CB4	247.16	247.16	LTB	0.94	184.77	LTB
	CB3A	246.04	246.04	LTB	0.92	186.74	LTB
	CB4A	206.44	206.44	LTB	0.77	186.65	LTB



Figure 5.1: Combined Buckling Mode in Beam AB1A.



Figure 5.2: Local Buckling Mode in Beam AB1.

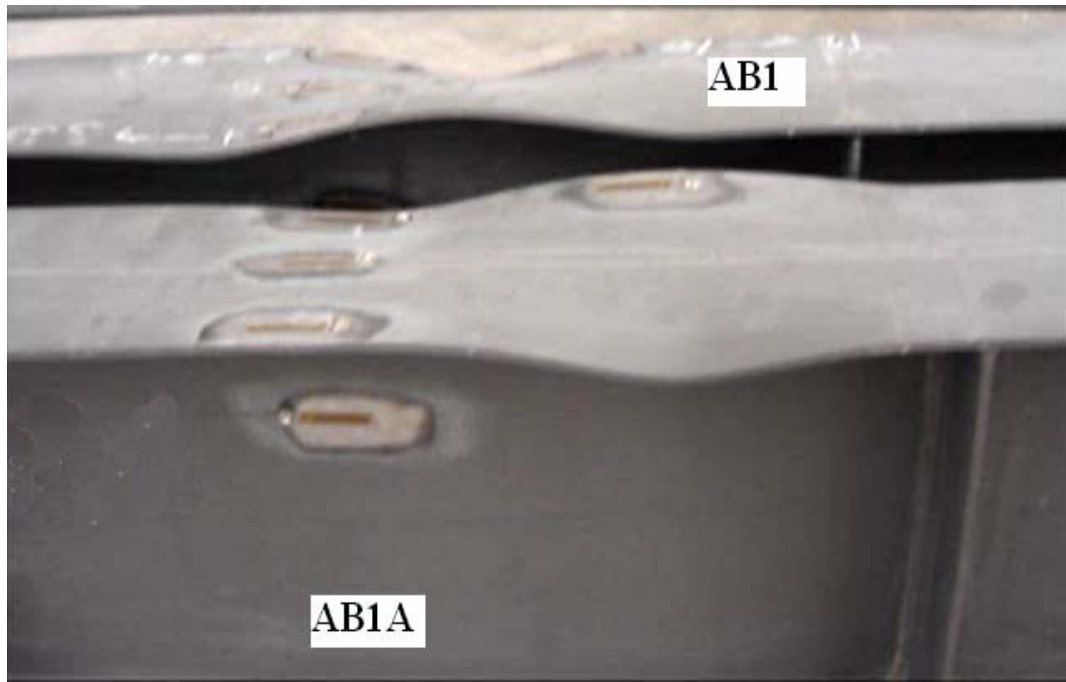


Figure 5.3: Typical Wave shapes for Beams AB1 and AB1A at Collapse dition.



Figure 5.4: Combined Buckling Mode in Beam BB2

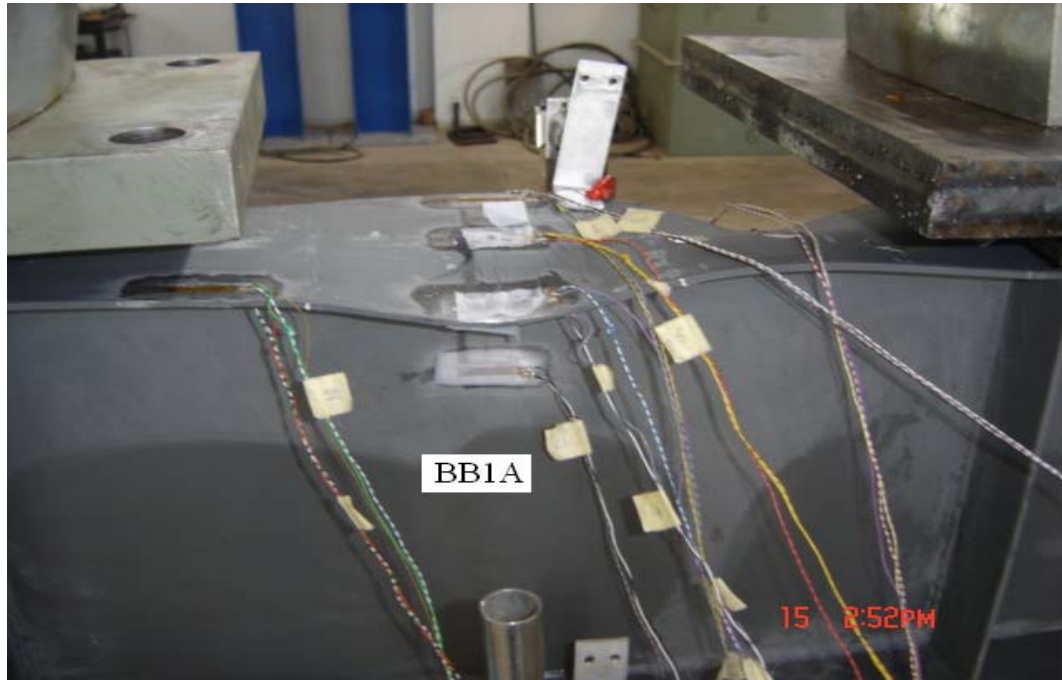


Figure 5.5: Combined Buckling Mode in Beam BB1A



Figure 5.6: Combined Buckling Mode in Beam BB1

The behavior of specimens in the third group was quite abrupt. Local buckling was dominant in the failure of AB3 while beams with (FWB) failed by combined local and lateral-torsional buckling. The buckling mode with one wave occurred only at the middle third of the span as shown in Figs. 5.7- 5.8 for beams AB3 and AB3A respectively. From Table 5.1 it can be seen that M_u / M_p of beam AB3 is 4% and 5% higher than its counterparts AB3A and AB4A respectively.

Beams BB3A and BB4A in the fourth group failed by combined local flange and lateral-torsional buckling. Local buckling failure with one wave was observed for beams with (FWO). The wave shapes of beams BB4A and BB4 at the collapse condition are shown in Figs. 5.9-5.10 respectively. Table 5.1 clearly shows the improvement of lateral buckling capacity of beams with (FWB). The presence of tensile residual stresses in these beams seems to have had a beneficial effect on their strength in comparison with their counterparts with (FWO). M_u / M_p of beam BB3A is 8% higher than that of beam BB3 and that of beam BB4A is 16% higher than that of beam BB4, indicating that tensile residual stresses in compression flange imparts an improvement of 12% on average for beams with (FWB).

Lateral-torsional buckling was the primary mode of failure for the beams in the fifth group. Figs. 5.11-5.12 show the buckling mode of beams CB4A and its counterpart CB4 respectively. Buckling of web plates was not observed on any of the test beams in this group.



Figure 5.7: Local Buckling Mode in Beam AB3



Figure 5.8: Combined Buckling Mode in Beam AB3A



Figure 5.9: Combined Buckling Mode in Beam BB4A

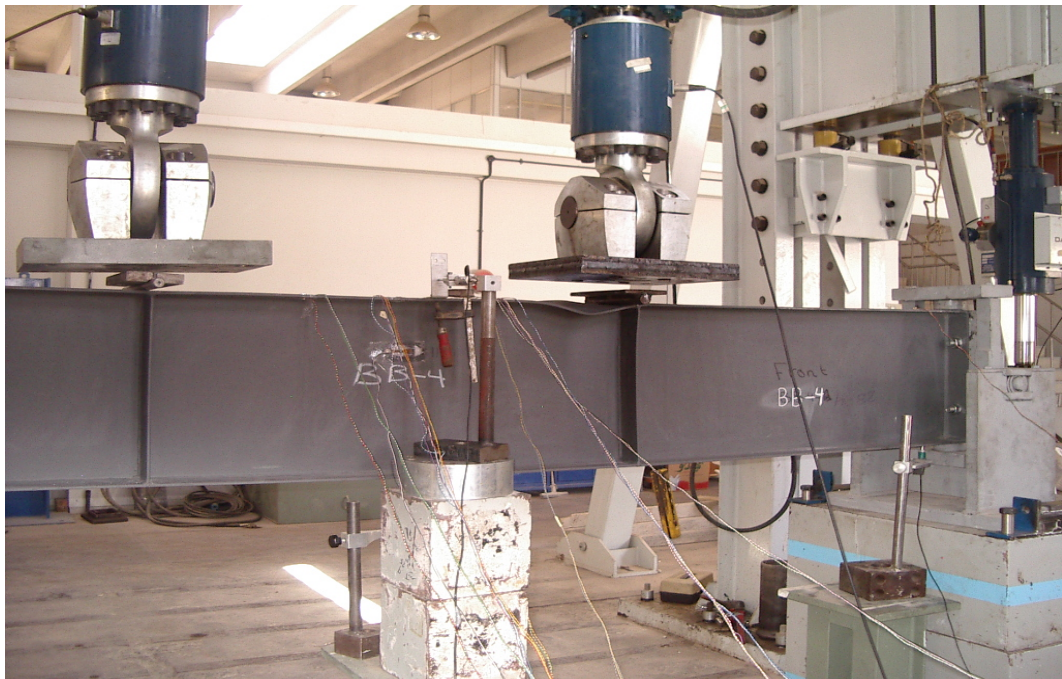


Figure 5.10: Local Buckling Mode in Beam BB4



Figure 5.11: Lateral-Torsional Buckling Mode in Beam CB4A



Figure 5.12: Lateral-Torsional Buckling Mode of Beam CB4

The results in Table 5.1 clearly show the reduction in lateral buckling capacity of beams when fillet welds was used on both sides of the web. If comparisons are performed using M_u / M_p , beam CB3A is 6% lower than CB3 and CB4A is 22% lower than CB4. This is due to the reduction of stiffness in beams with (FWB) due to the extent of yielded zone since the full width of the compression flange does not remain fully yielded due to lateral curvature. In other words lateral curvature eliminated the beneficial effect of tensile residual stresses which delays yielding.

5.3 Support Conditions

The behavior of specimens of large slenderness was significantly influenced by the presence of end-plate connection which reduces warping. It is also apparent that the bolted end-plated connections provide a considerable improvement in buckling loads over simply supported end conditions which are free to warp. For built-up beams with high slenderness the improvement in the buckling moment over the nominal moments predicted by LRFD (2005) as shown in Table 5.1 are 9%, 24% and 29% for the third, fourth and fifth groups respectively. For the first and the second groups specimens with lower slenderness the beneficial effect of end-plate connections is not noticeable. This result conforms to that reported by Bradford and Trahair (1981). For short-length beams where the flange of in-plane stiffness is high, buckling occurs in an antisymmetric mode in which the compressive flange deflects laterally as a near-rigid body while for long beams, this antisymmetric mode requires an excessive amount of strain energy to be stored in the web. Because of this the beam prefers to buckle in symmetric mode in which little strain energy is stored in the web.

5.8 Effect of Residual Stress

The predicted residual stress distributions of residual stress specimens, discussed previously in chapter 3, are characterized by significant tensile stresses at the flange-web junctions ranging from high tensile stress for specimens with (FWB) to small compressive stresses at flange tips for specimens with (FWO). The level of compressive residual stresses in the webs for specimens with (FWO) is less than that for specimens with (FWB).

Based on the mean level of compressive residual stresses given in Table 3.1 of -192 MPa and -92 MPa for specimens AA30 and A30, respectively, the mean level of maximum compressive residual stresses at the tips are $0.51 F_y$ and $0.25 F_y$, respectively. This would result in a value of $0.49 F_y$ and $0.75 F_y$ at the onset of cross-sectional yielding or degradation in lateral stiffness. Due to the delayed yielding of the compression flange tips, the strengths of specimens with (FWO) in the first and third groups are slightly higher than those of specimens with (FWB). Nethercot (1974) suggested that the lateral-torsional buckling can be classified as inelastic only when the level of applied bending stresses equals or exceeds the level required to initiate yielding at the compression flange tips. Even though significant yielding may already have occurred at the tension flange, this has little effect on the effective moment of inertia about the weak axis.

For the second and the fourth group specimens, the predicted tensile residual stresses given in Table 3.1 are 292 MPa and 216 MPa as are for specimens BB40 and B40, respectively, tensile yielding of the bottom flange would be predicted to occur at

$0.22 F_y$ and $0.42 F_y$ respectively. The level of compressive residual stress in the flange is approximately the same for all specimens in the second and the fourth groups. Since compressive yielding will start at approximately the same value of the applied moment, it follows that the improvement in strength of beams with fillet welds on both sides will be higher than their counterpart beams with fillet welds on one side of the web. This is because the tensile residual stresses with a peak value at the flange web junction of $0.78 F_y$ tends to reduce the compressive stresses off the compression flange and therefore to delay the onset of lateral instability of the overall beam.

The beneficial effect of tensile residual stress was diminished in specimens of the fifth group. This might be due to the reversal of strain and stress on the outer side of the compression flange. In other words, loss of moment resistance in this group occurs because in the yielded region the full width of the compression flange does not remain fully yielded in compression due to lateral curvature. Consequently, tensile residual stresses do not have a large influence on the maximum buckling strength.

5.5 Load-Strain Behavior and Strain Distribution

The measured flange strains reflect the effect of bending about both strong and weak axes as well as the effect of local buckling of the flange. The measured web strains reflect the effects of bending due to web distortion. To investigate all of these effects, a total of seven strain gauges were mounted longitudinally on the top flange and three in the bottom flange at every strain gage station and, as well, a strain gage was mounted on each side of the web, as shown and identified in Fig. 4.6.

In Figs. 5.13-5.16, for specimens in the first group are plotted the test load versus flange strains of the outer (1 and 2) and inner (3 and 4) strain gage pairs on the top flange and outer pairs of gages (7 and 8) on the bottom flange, respectively, of the station located at 1 m from end supports. The general behavior of these curves is the same. At relatively small loads, strains due to the strong axis bending dominate. The inner and outer top flange strains increase linearly with load and are about the same in compression and of opposite sign to bottom flange strains in tension. As soon as beam begins to buckle laterally, the strains on the same flange but on opposite sides of the webs begin to diverge as lateral bending takes place. For beams with (FWB), AB1A and AB2A, readings of the two strain gages (2 and 4) on the side of buckling direction decrease due to tensile strain from out-of-plane bending, while readings of the two strain gauges (1 and 3) on the opposite side increase in compression.

When plate bending arising from local buckling takes place, a discrepancy between the strains on both surfaces appears, and finally, strain reversal at the convex side of the plate bending can be observed. The diverging strain readings in beams AB1A and AB2A (1 and 3), (2 and 4) and (10 and 12) with one gage in tension and the other gage in compression indicates that local buckling occurred before their ultimate loads are reached.

Reading of the strain gages mounted in the bottom flange, gauge 7 and 8, tends to develop tensile strains. Strain gage 8 and strain gauge 2 on the top flange are on the same side of the web. As buckling was approached both showed tensile straining,

indicating that the lateral bending effect, in this case, was more pronounced than warping.

The load versus quarter-height web strains obtained from gauges 9 and 11, 1 m from the end supports for specimen AB1A and AB2A are given in Fig. 5.14 and 5.16 respectively. The diverging strain readings with one gage on tension and the other gage in compression indicates that out of plane bending of the web or web local buckling begins at a load of 80 kN and 90 kN respectively. In all cases, the load versus strain relationship reaches a horizontal asymptote at the maximum load, indicating that buckling is imminent.

Load-versus-strain curves are shown in Figs. 5.17-5.20 for the beams in the second group. The longitudinal strains on both surfaces of top flange tips near the mid span are plotted in these figures. The diverging of strain readings in this group indicates that the web buckling occurs in all beams. Fig. 5.19 shows that the warping in this beam with (FWO) has more effect than lateral buckling from the beginning until buckling loads was approached, strain gage 8 on the bottom flange and strain gage 2, on the top flange are on the same side of the web. As buckling was approached, strain gage 7, showed compression straining, indicating that warping is more pronounced than lateral bending.

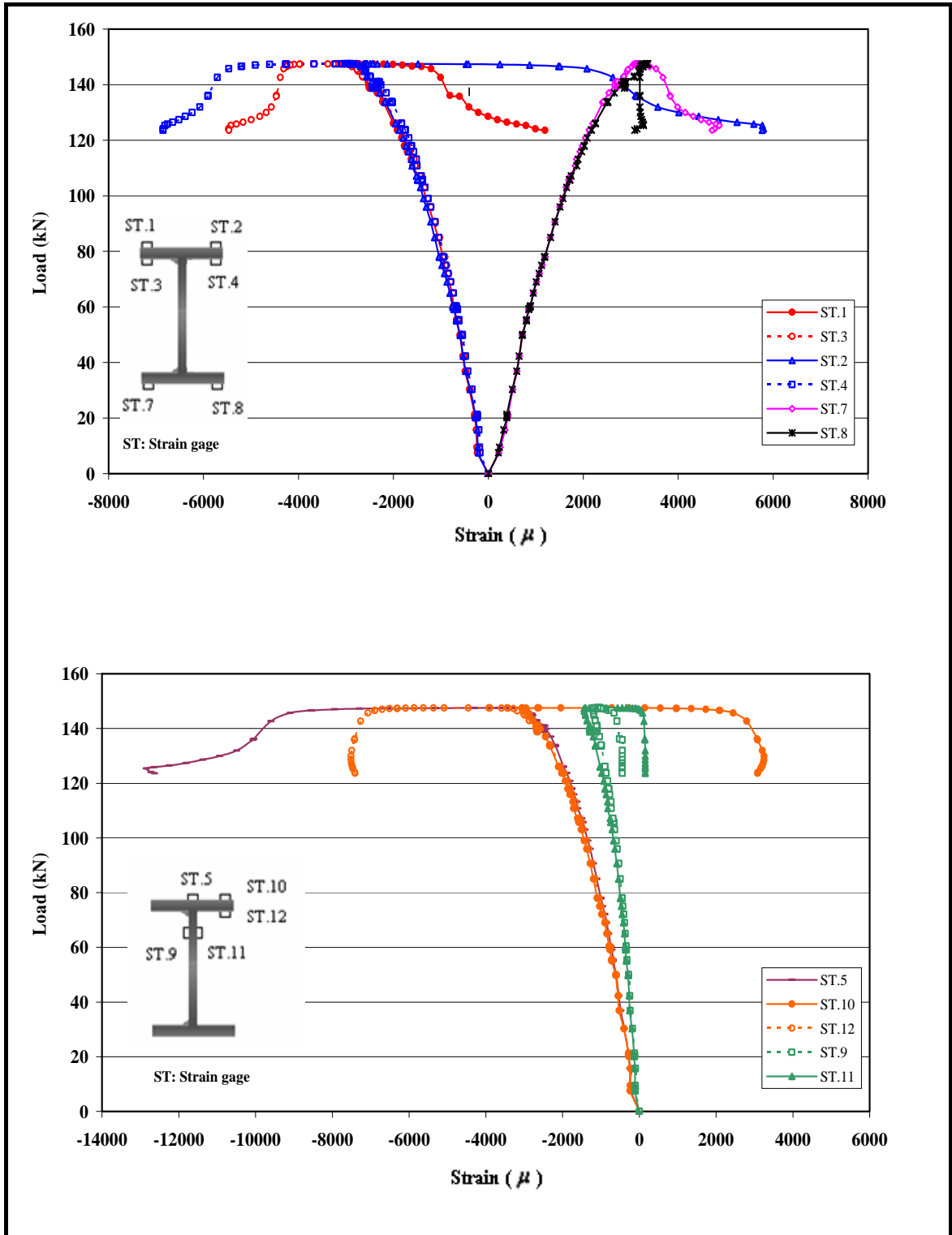


Figure 5.13: Load-Strain Curves for Beam AB1

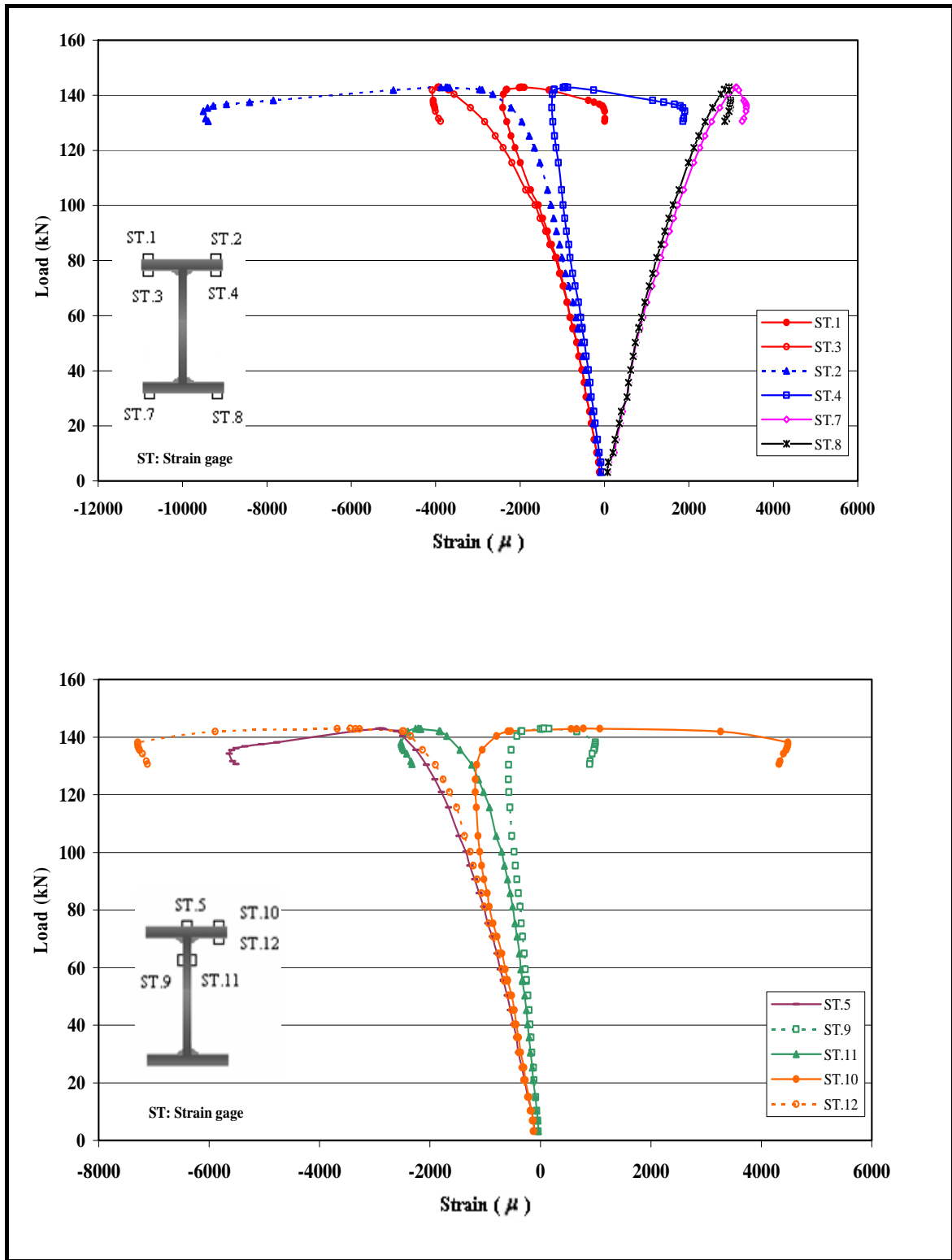


Figure 5.14: Load-Strain Curves for Beam AB1A

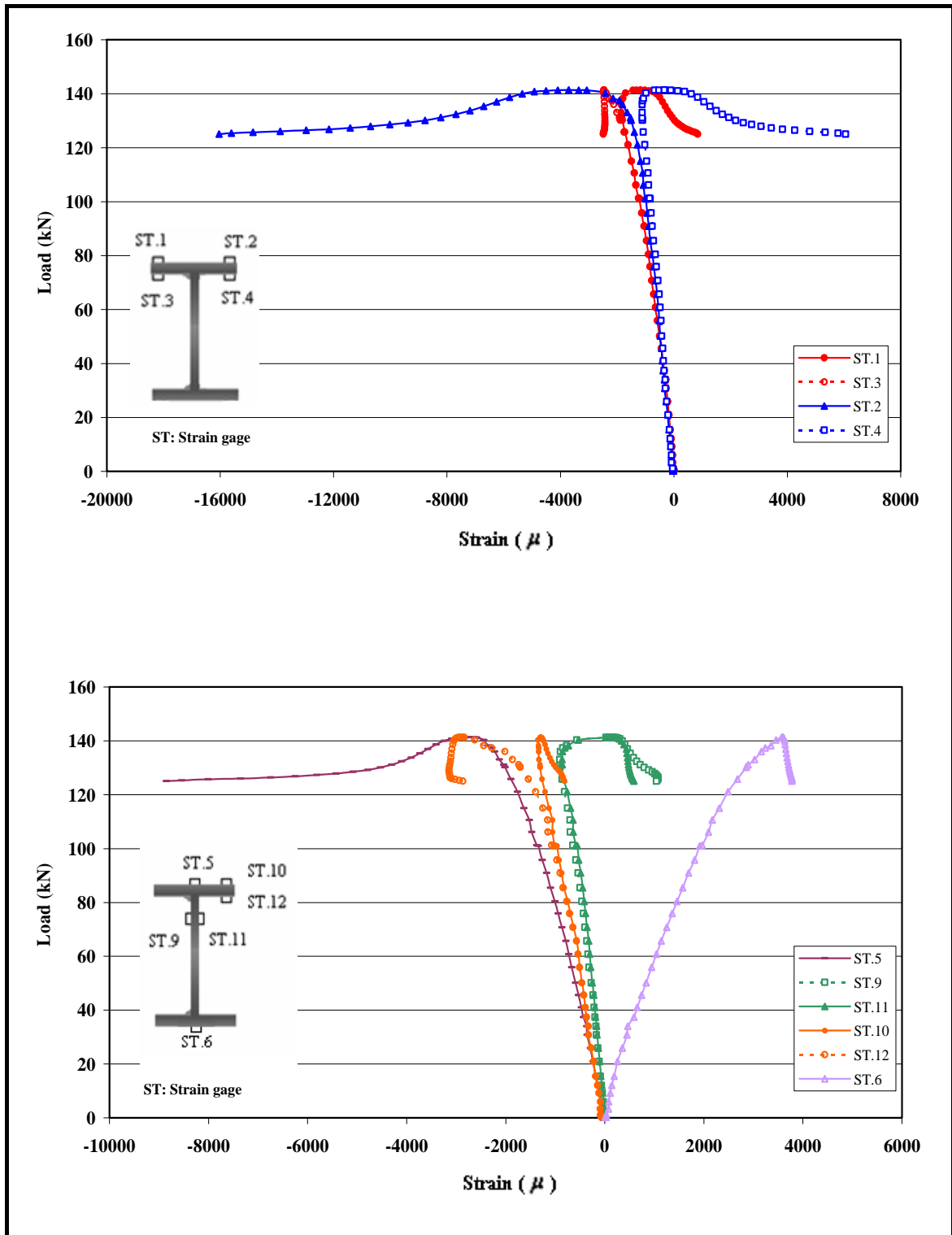


Figure 5.15: Load-Strain Curves for Beam AB2

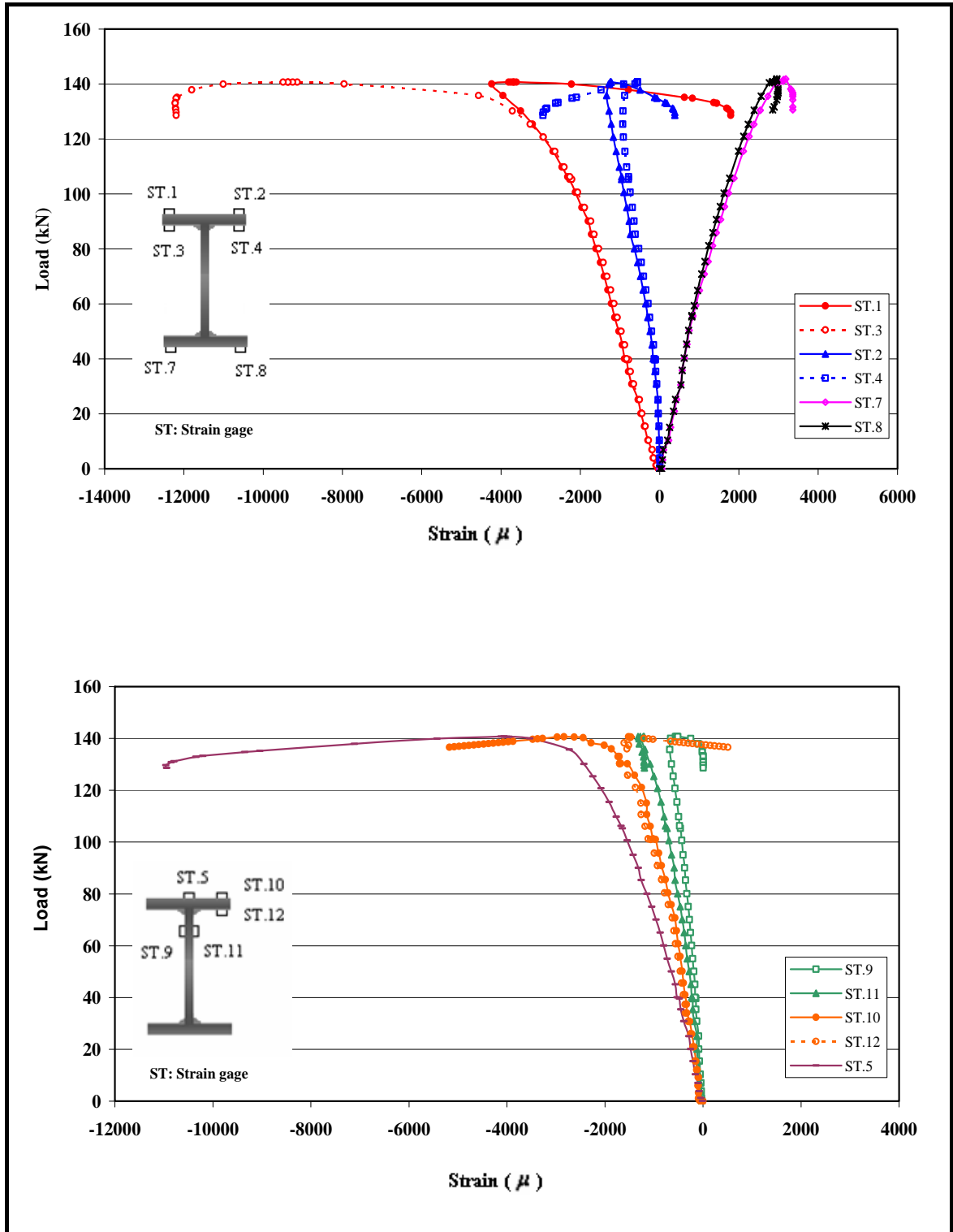


Figure 5.16: Load-Strain Curves for Beam AB2A

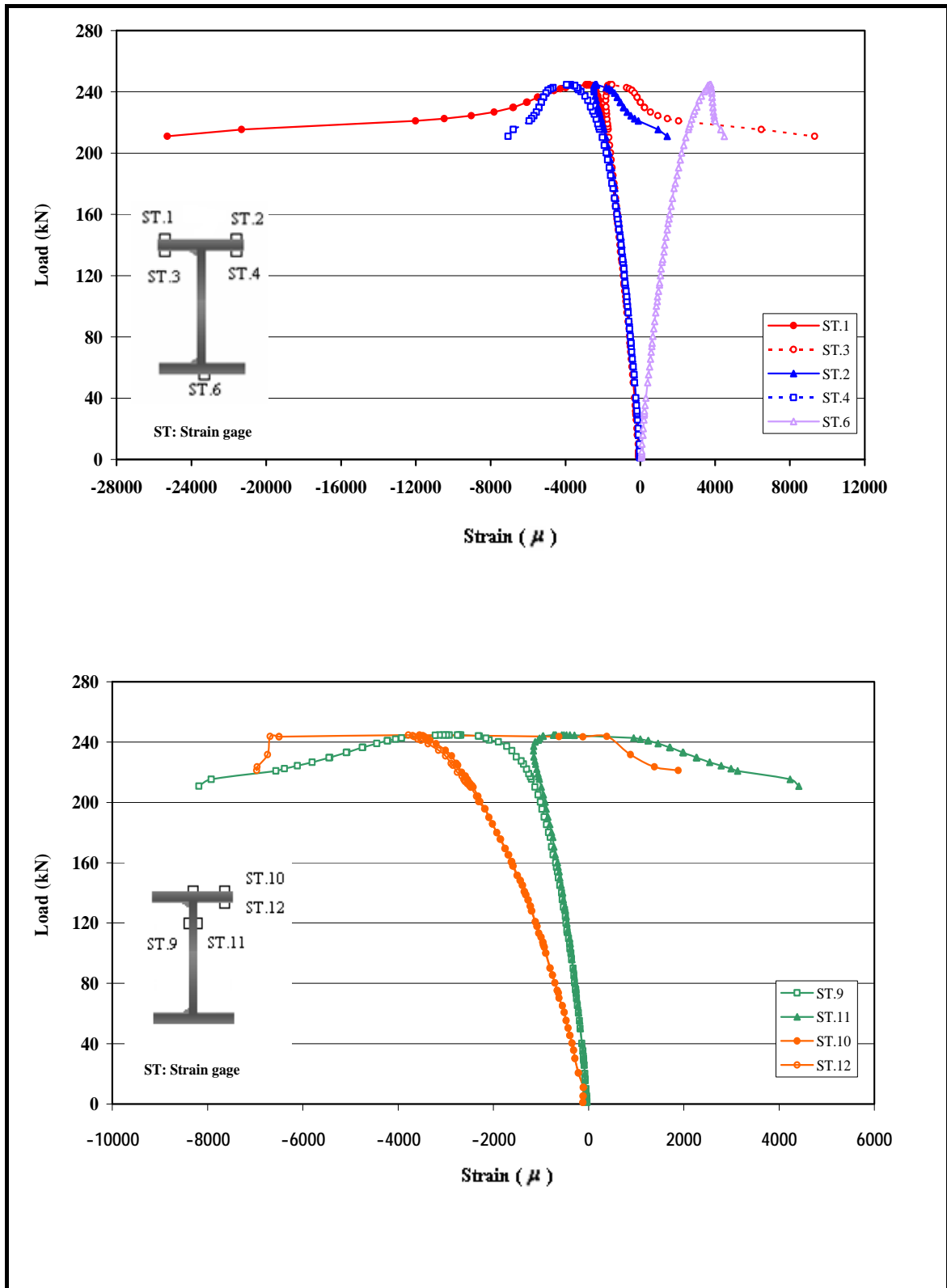


Figure 5.17: Load-Strain Curves for Beam BB1

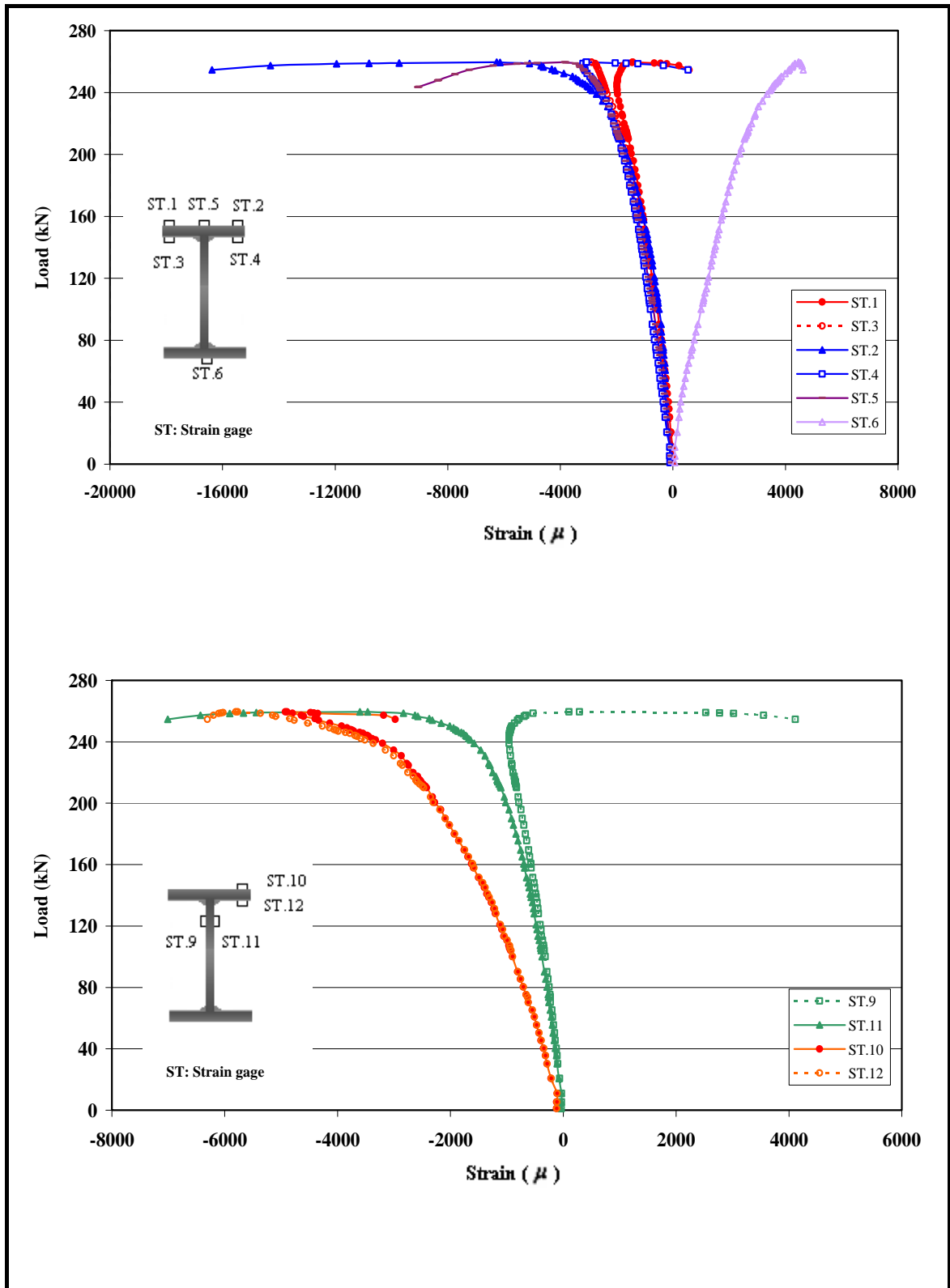


Figure 5.18: Load-Strain Curves for Buckling of Beam BB1A

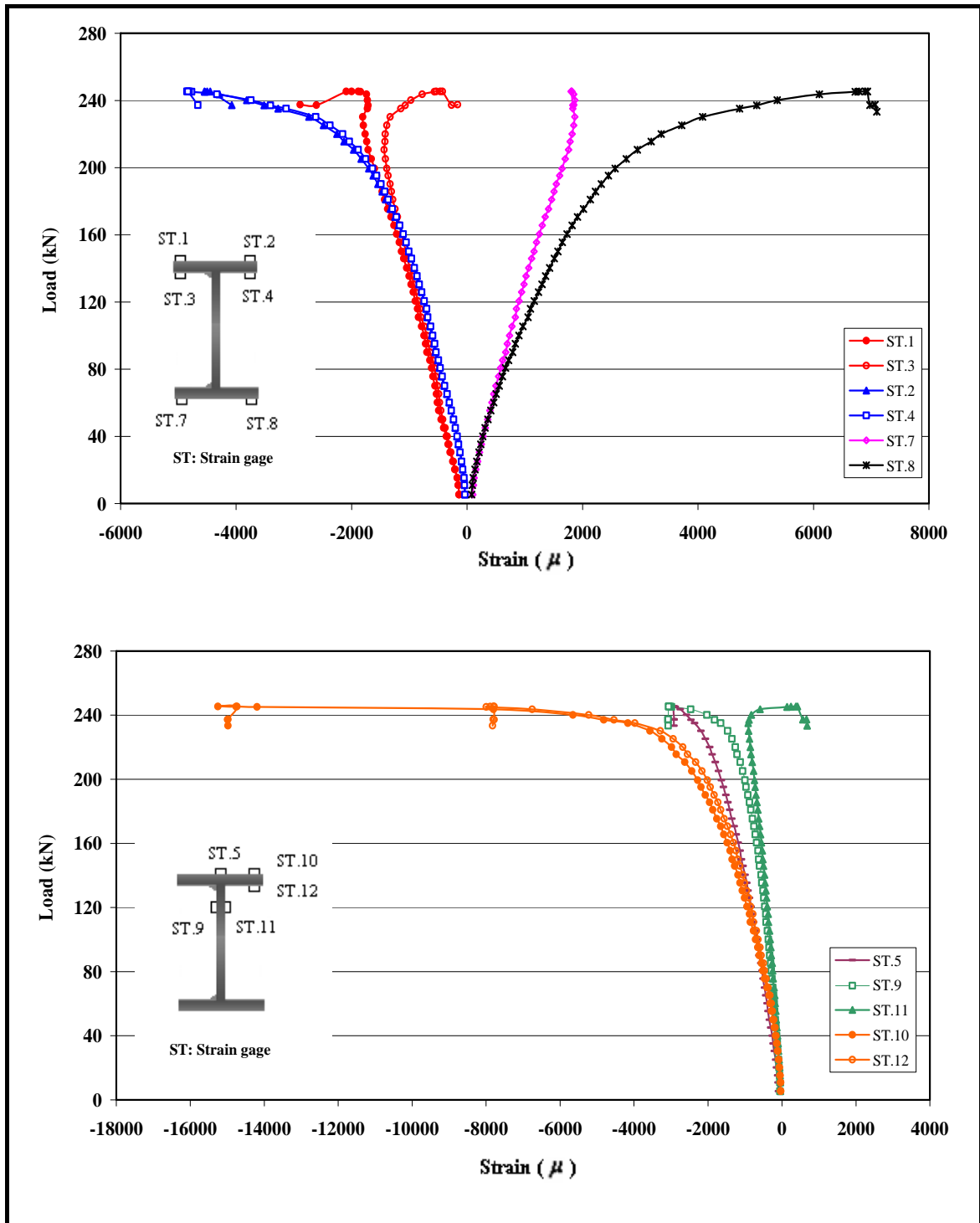


Figure 5.19: Load-Strain Curves for Buckling of Beam BB2

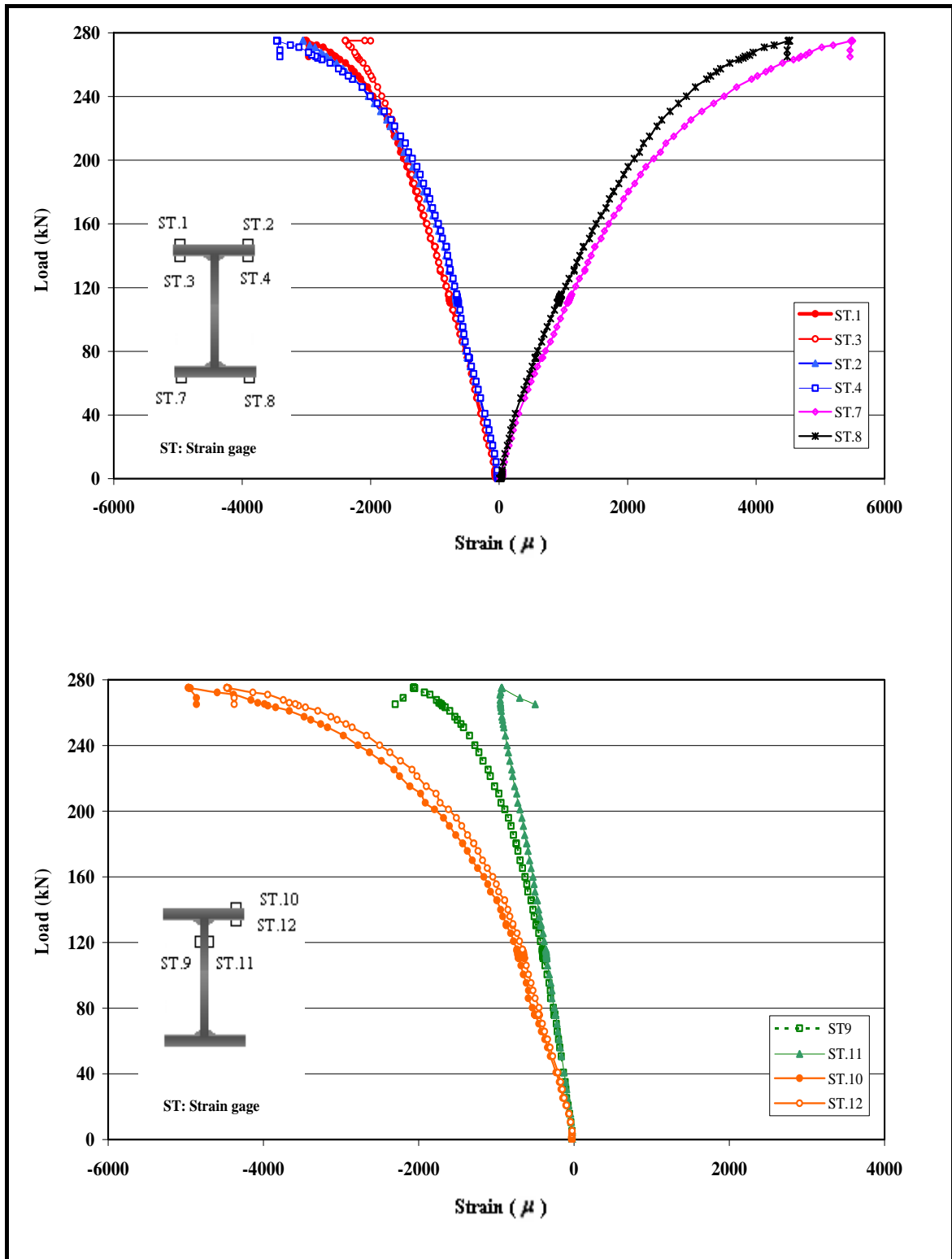


Figure 5.20: Load-Strain Curves for Buckling of Beam BB2A

Typical strain responses along the two edge of the top flange are plotted in Figs. 5.21 and Fig. 5.22 for AB3 and AB3A specimens in the third group. The load strain relationships are approximately linear until the load reached 79 kN and 70 kN for beams AB3 and AB3A respectively. The interactive behavior of local and lateral-buckling was observed only for beams with (FWB).

In Figs. 5.23-5.26, for the fourth group specimens are plotted the test loads versus strains of the outer and inner strain gages on the top flange, of station located at half way between end supports. For beams with (FWB), the strains on the same flange but on opposite sides of the webs (2 and 4) and (1 and 3) begin to diverge as lateral bending take place. Buckling of web plates was not observed on any of the test beams in this group while local buckling was dominant in beams with (FWO). Strain gage 8 and 7 on the bottom flange both showed tensile straining, indicating the lateral bending effect was more pronounced than warping.

Figs. 5.27–5.30 show the plot of the load versus compression flange strain for the specimens of the fifth group. The strains (1 and 3) on the side of buckling direction decrease due to the tensile strain from out-of-plane bending. After passing the ultimate loads, these strains change to tension. Therefore local buckling of the flange and the web did not appear on any of the test beams in this group. Warping was observed in beam CB4A as shown in Fig. 5.30 due to excessive yielding of bottom flange.

5.6 Load-Deflection Behavior

Load-versus-horizontal and vertical deflection curves are shown in Figs. 5.31-5.48 for all beams in the five groups. By monitoring the load deflection behavior during the test, deformation control could be invoked as the buckling load was approached. Buckling was considered to occur when the load-deflection curves reached a horizontal asymptote. The general behaviors of these curves are approximately the same. From an examination of load-deflection curves of beam AB1, see Fig. 5.31, it can be seen that the response is linear-elastic until the load reached 40 kN where upon it jumps on to another linear response curve of only slightly lower relative stiffness. The behavior proceeds smoothly until buckling occurs and the load deflection curves reached a horizontal asymptote.

The post buckling behavior of beam AB1 is characterized by the development of large deformation accompanied by a slight drop in the loading capacity. Fig. 5.40 shows an example of load-vertical deflection curves for beam AB3A in the third group. As would be expected, the vertical deflection is in a good agreement with calculated values based on the linear elastic theory. Beyond a load of 40 kN where yielding commenced at the tension flange-web junction due to the presence of residual stresses, the vertical deflections increase more rapidly than the elastic theory predict.

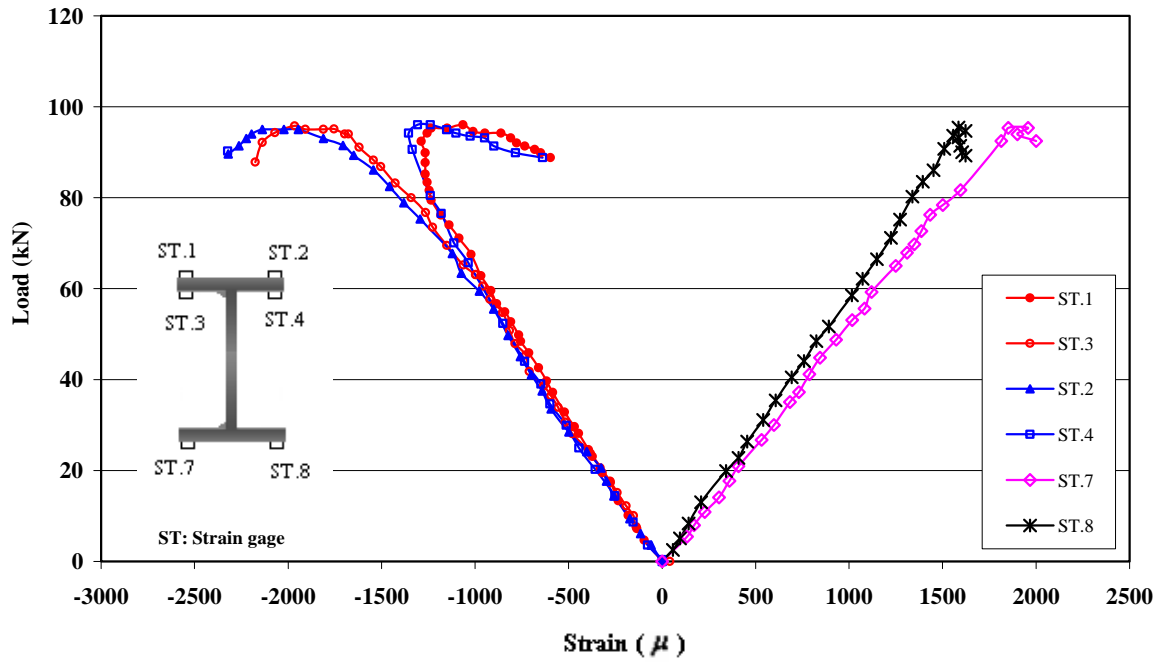


Figure 5.21: Load-Strain Curves for Buckling of Beam AB3

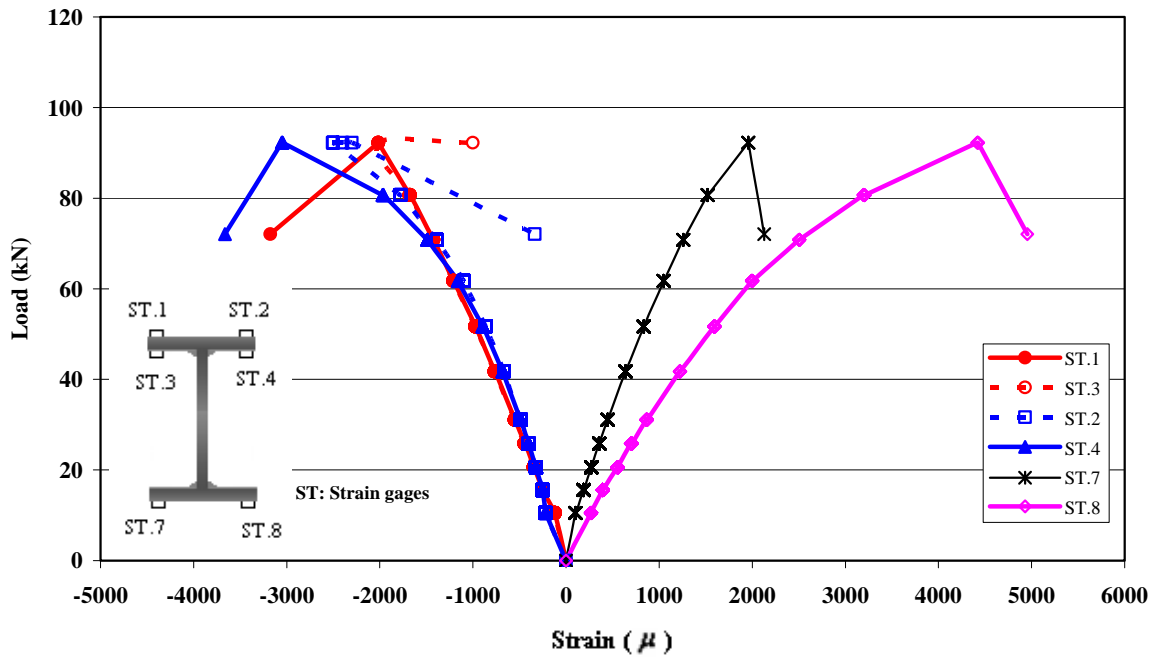


Figure 5.22: Load-Strain Curves for Buckling of Beam AB3A

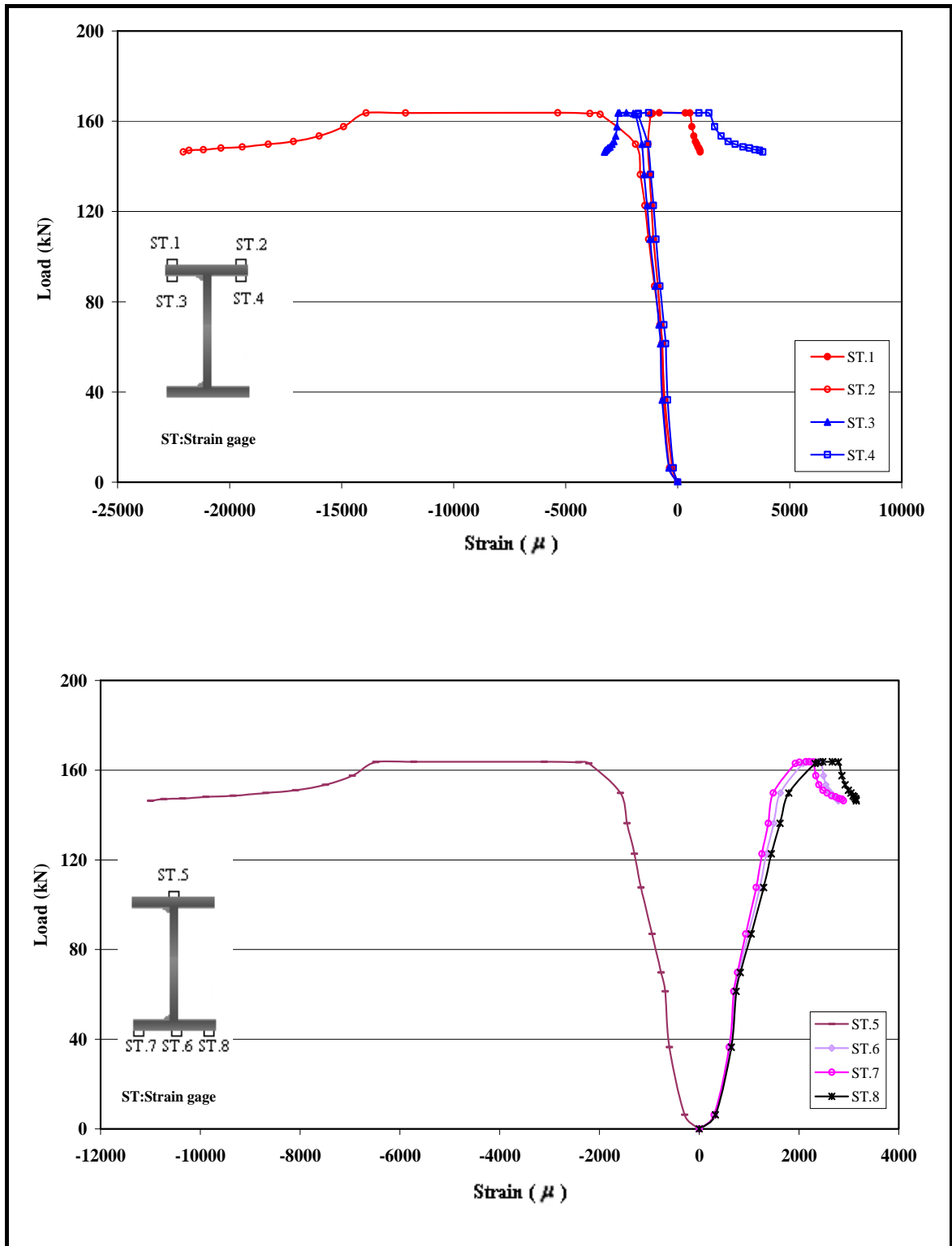


Figure 5.23: Load-Strain Curves for Buckling of Beam BB3

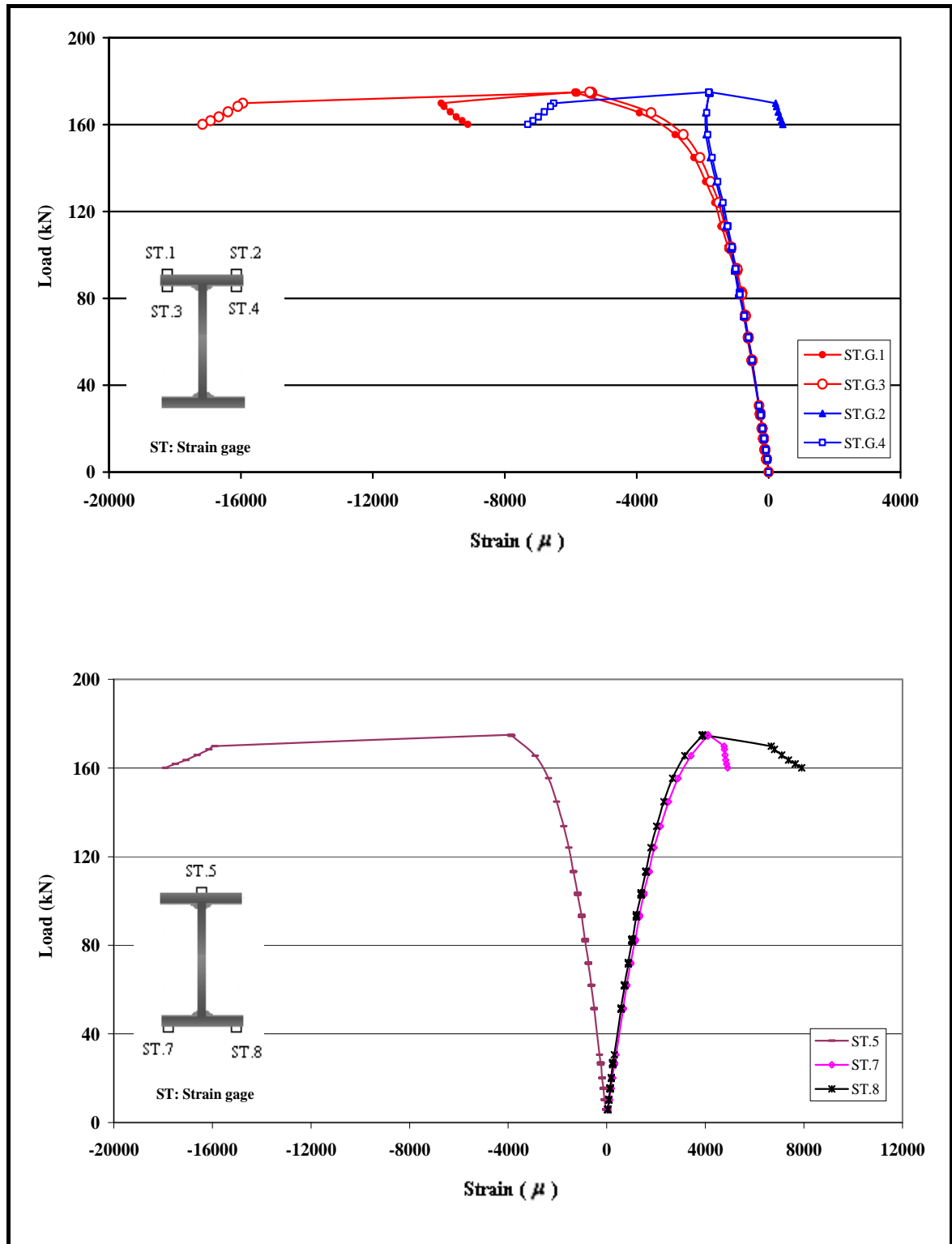


Figure 5.24: Load-Strain Curves for Buckling of Beam BB3A

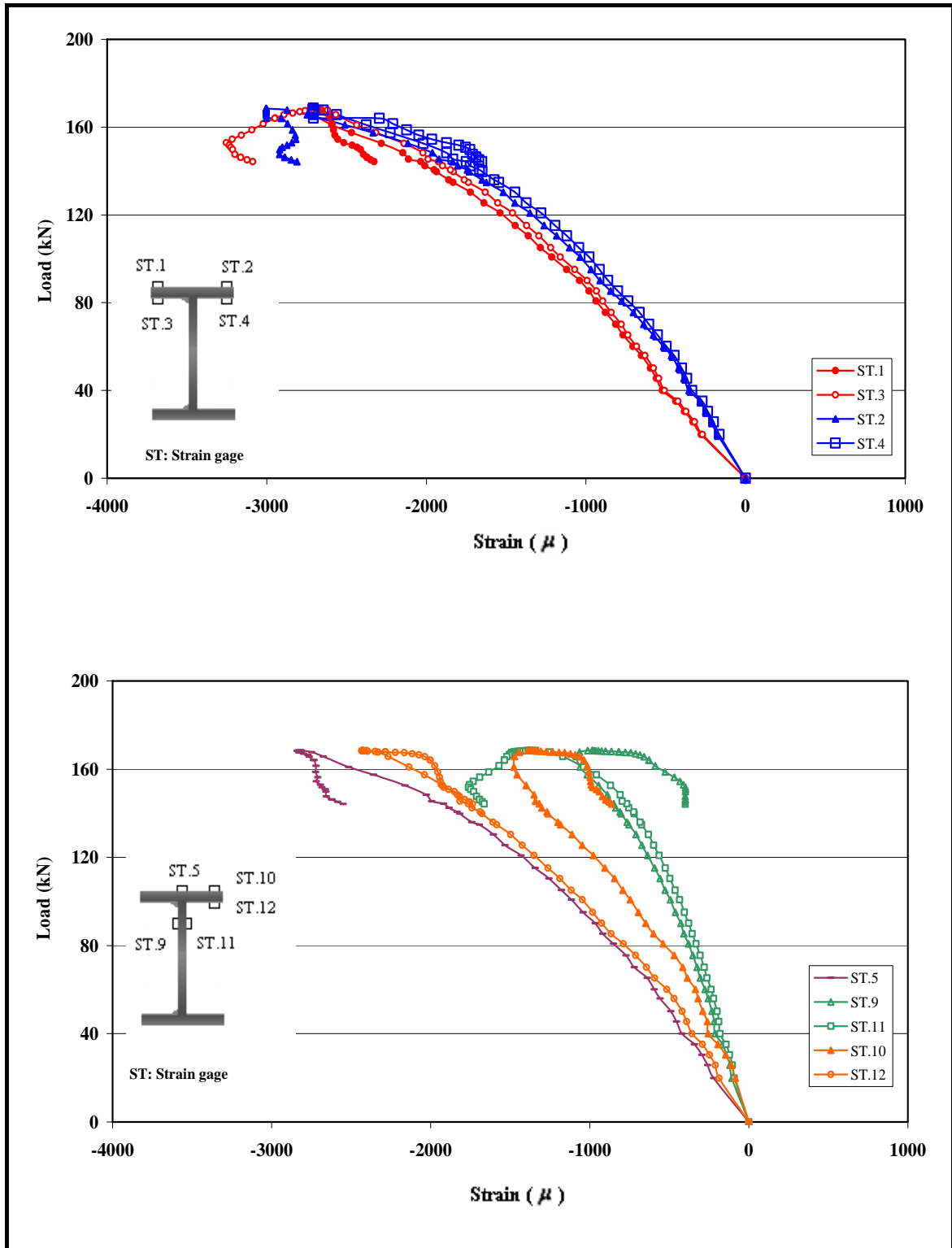


Figure 5.25: Load-Strain Curves for Buckling of Beam BB4

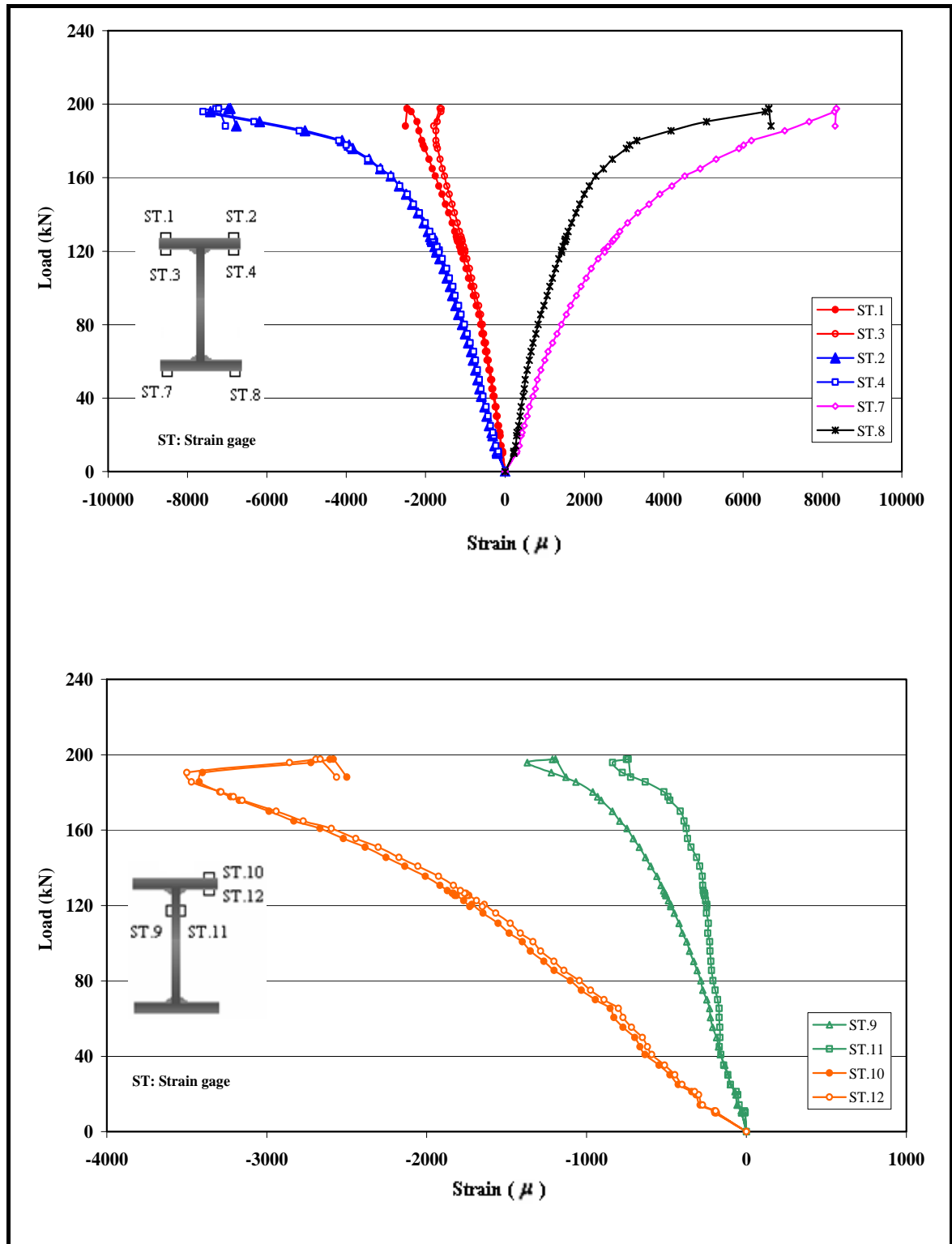


Figure 5.26: Load-Strain Curves for Buckling of Beam BB4A

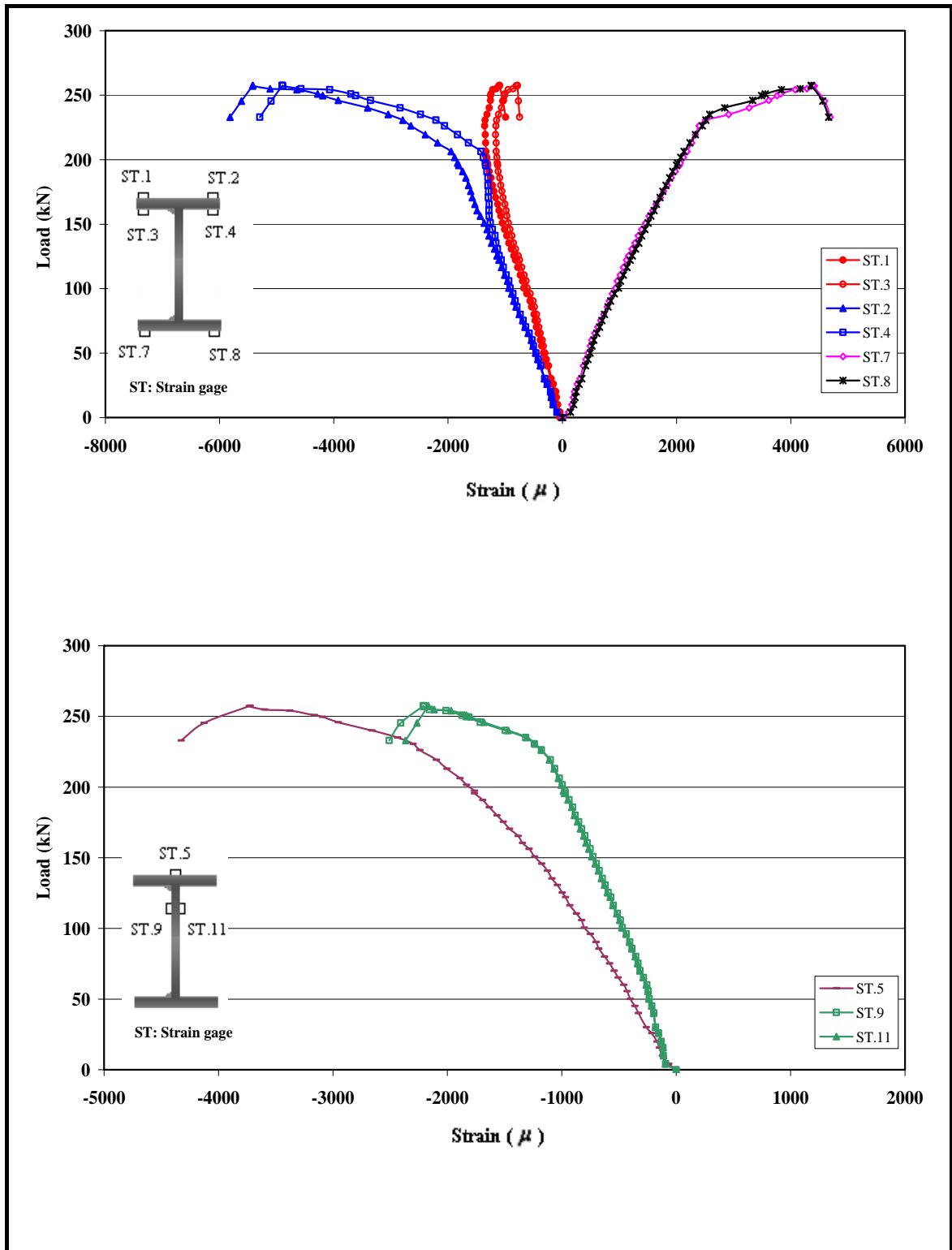


Figure 5.27: Load-Strain Curves for Buckling of Beam CB3

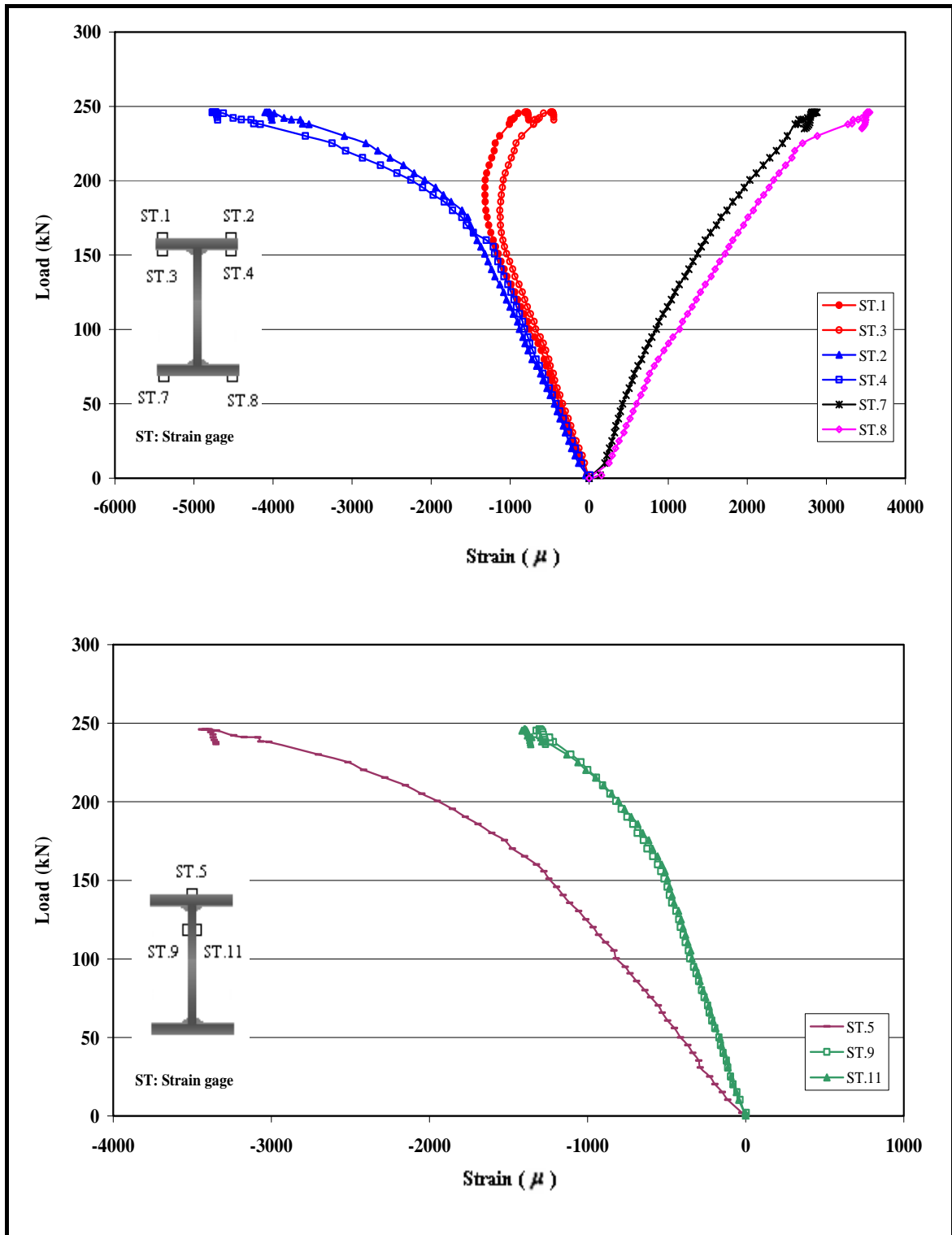


Figure 5.28: Load-Strain Curves for Buckling of Beam CB3A

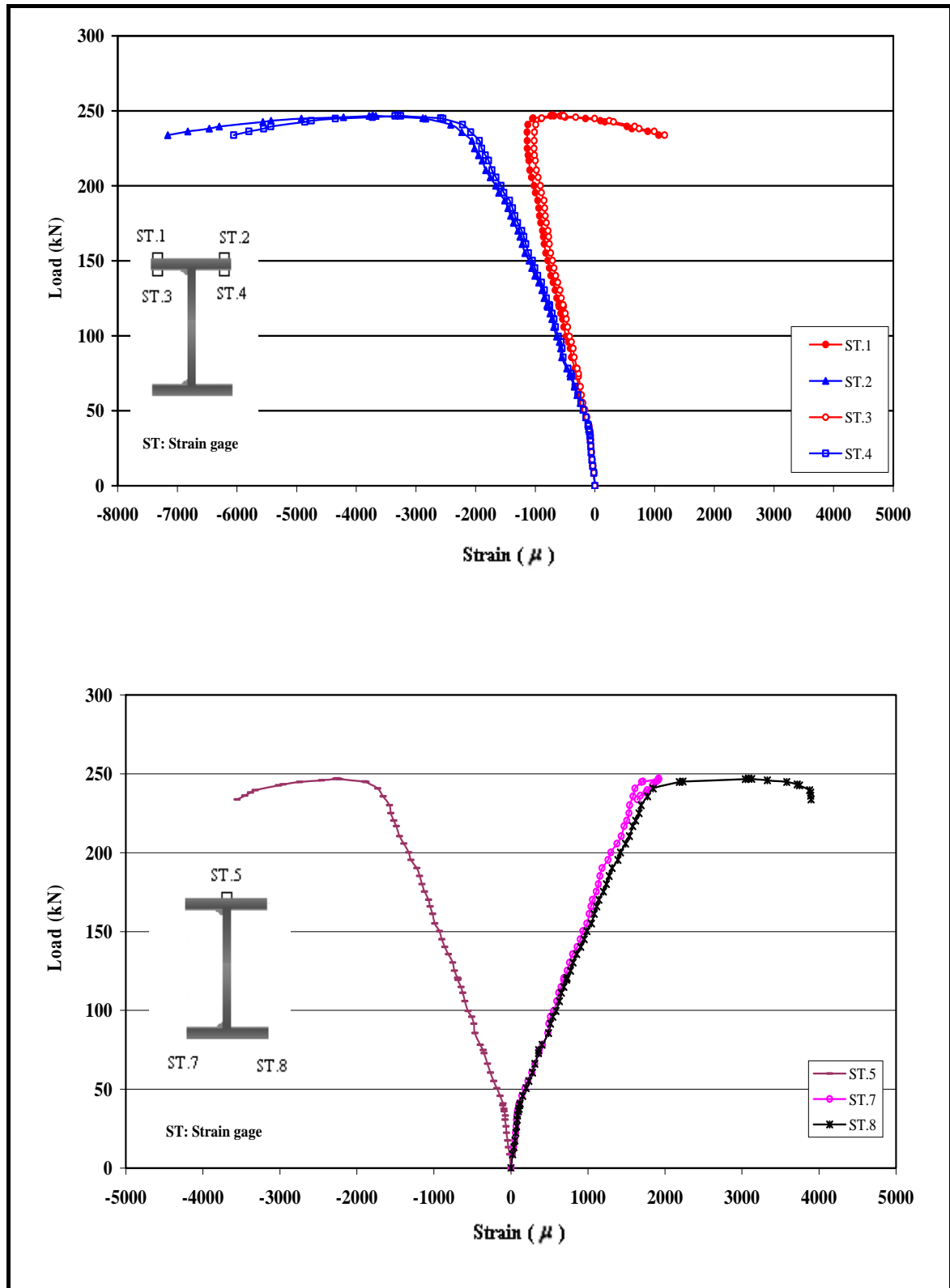


Figure 5.29: Load-Strain Curves for Buckling of Beam CB4

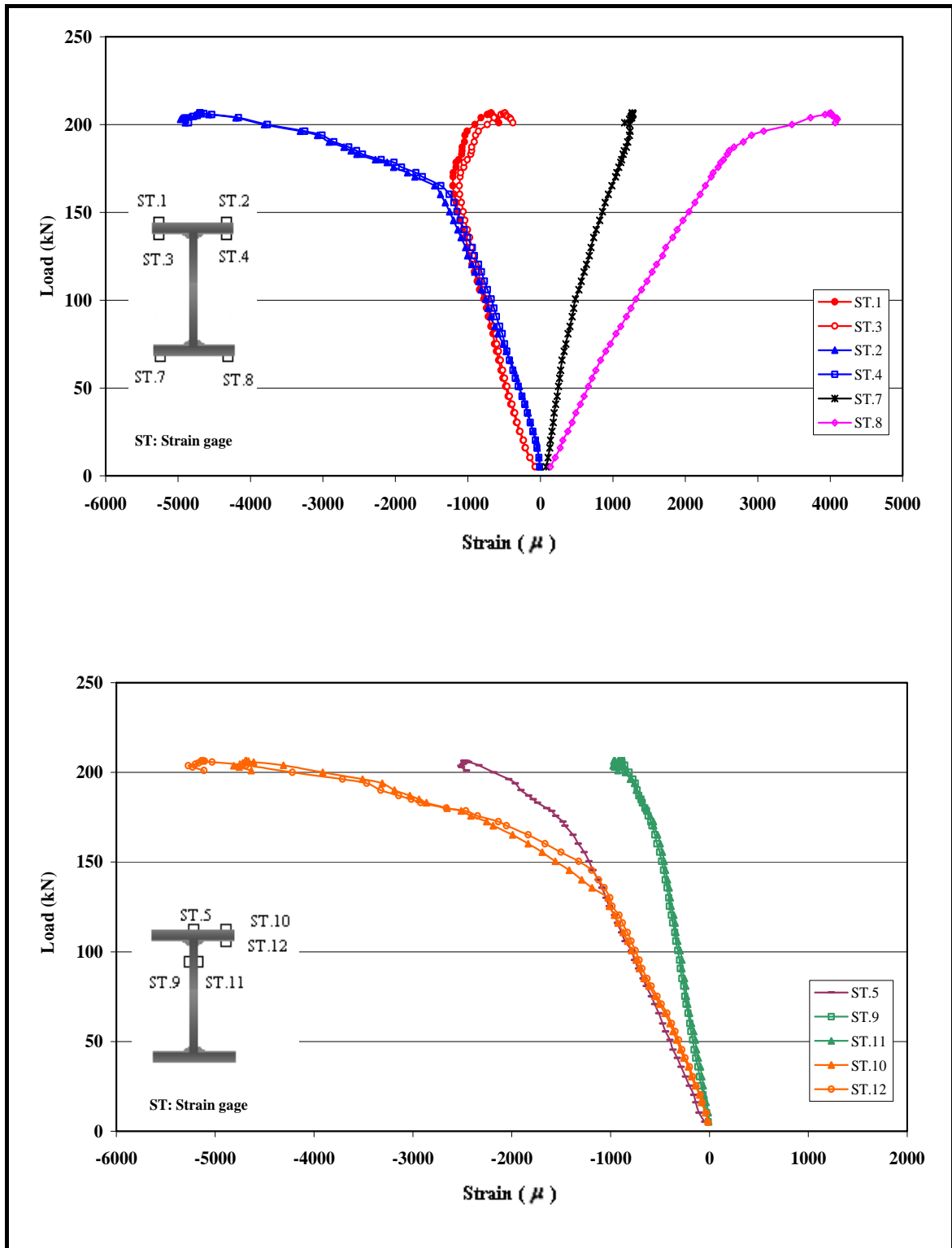


Figure 5.30: Load-Strain Curves for Buckling of Beam CB4A

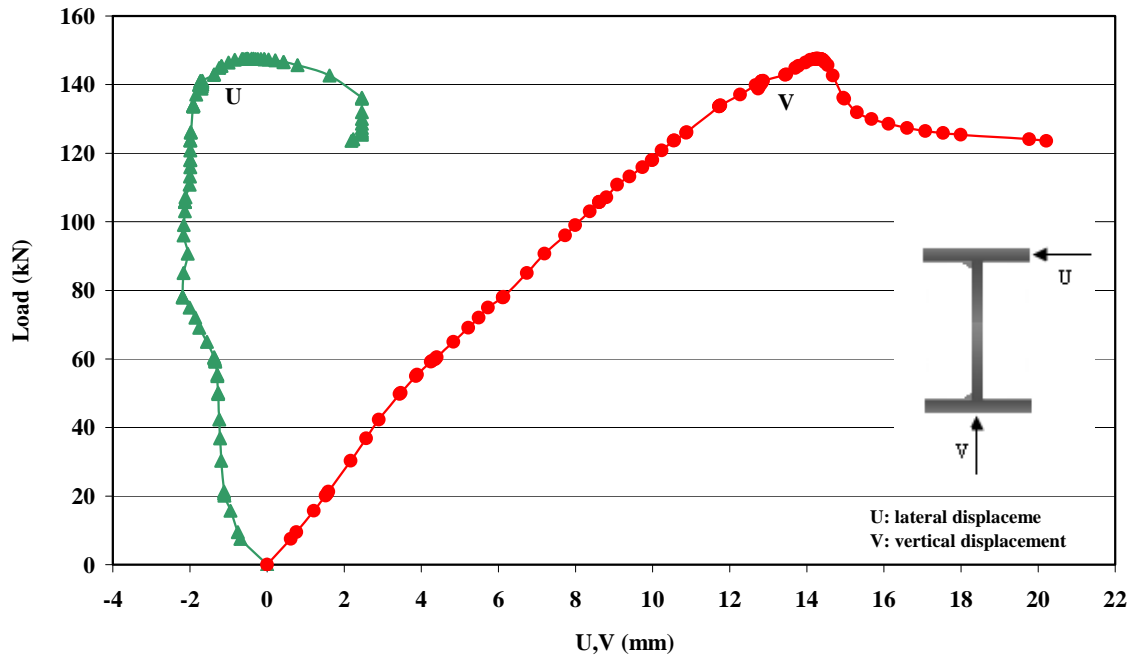


Figure 5.31: Load-Deflection Curves for Beam AB1

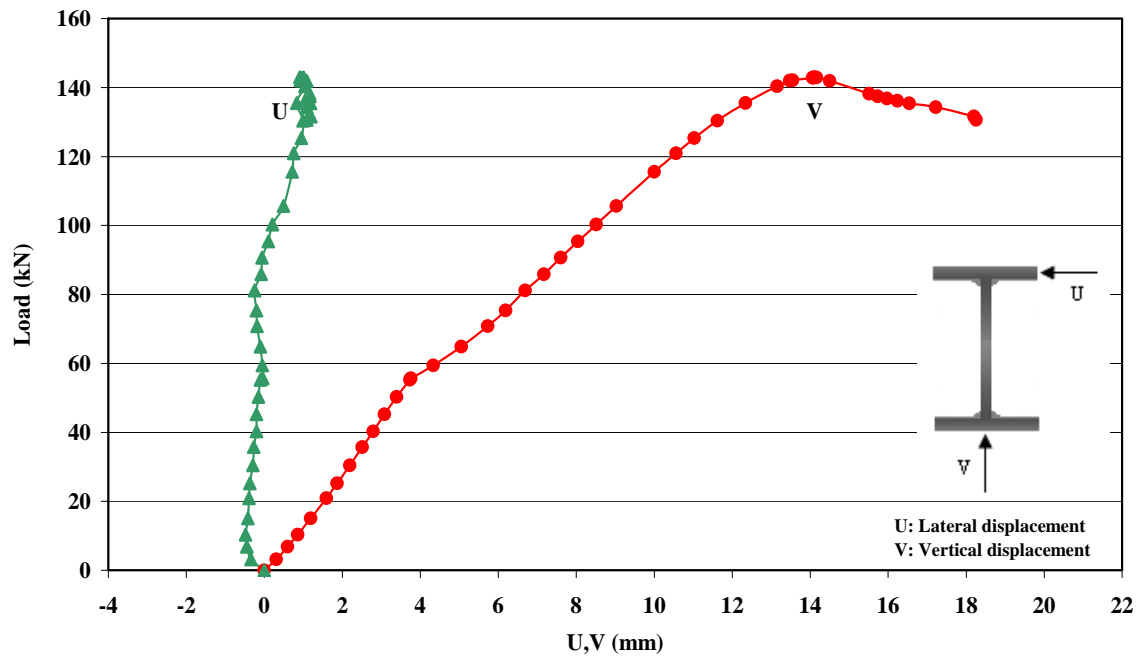


Figure 5.32: Load-Deflection Curves for Beam AB1A

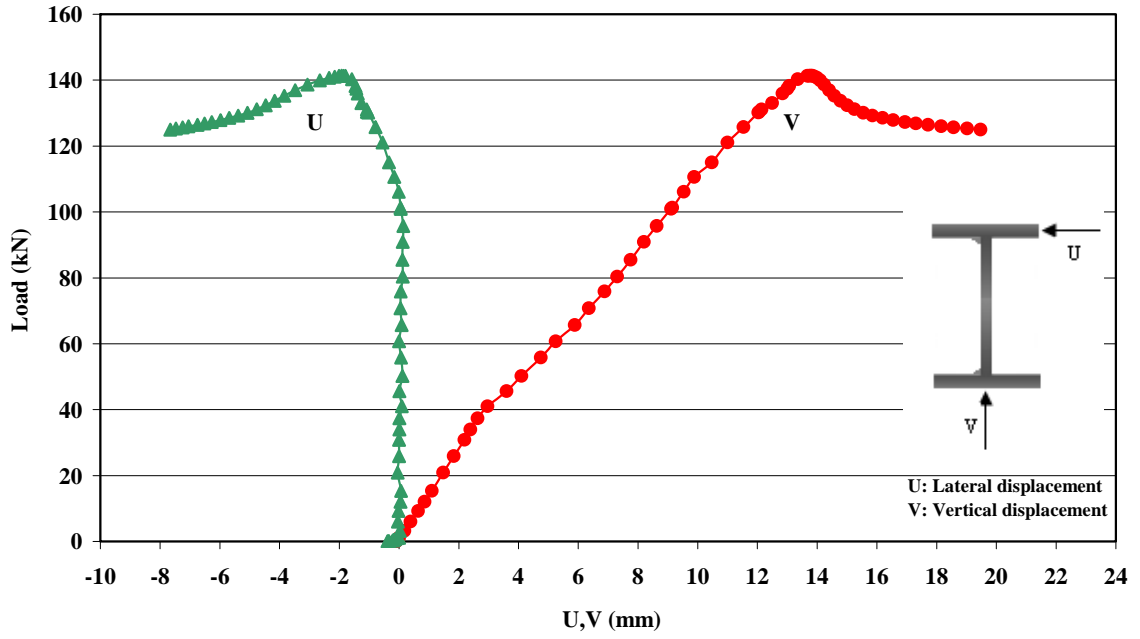


Figure 5.33: Load-Deflection Curves for Beam AB2

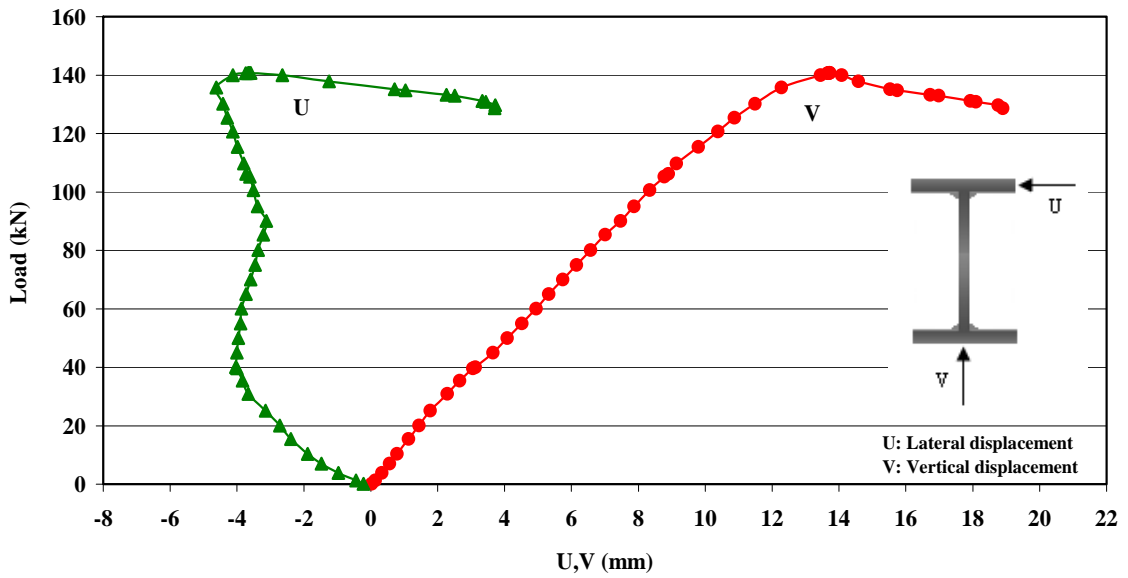


Figure 5.34: Load-Deflection Curves for Beam AB2A

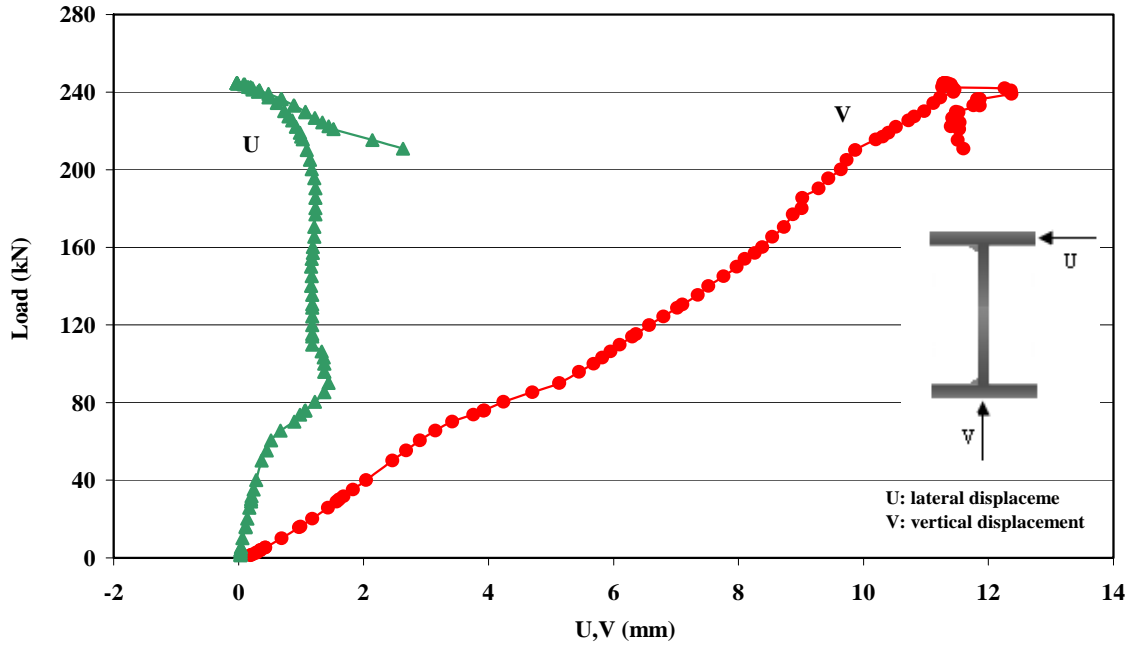


Figure 5.35: Load-Deflection Curves for Beam BB1

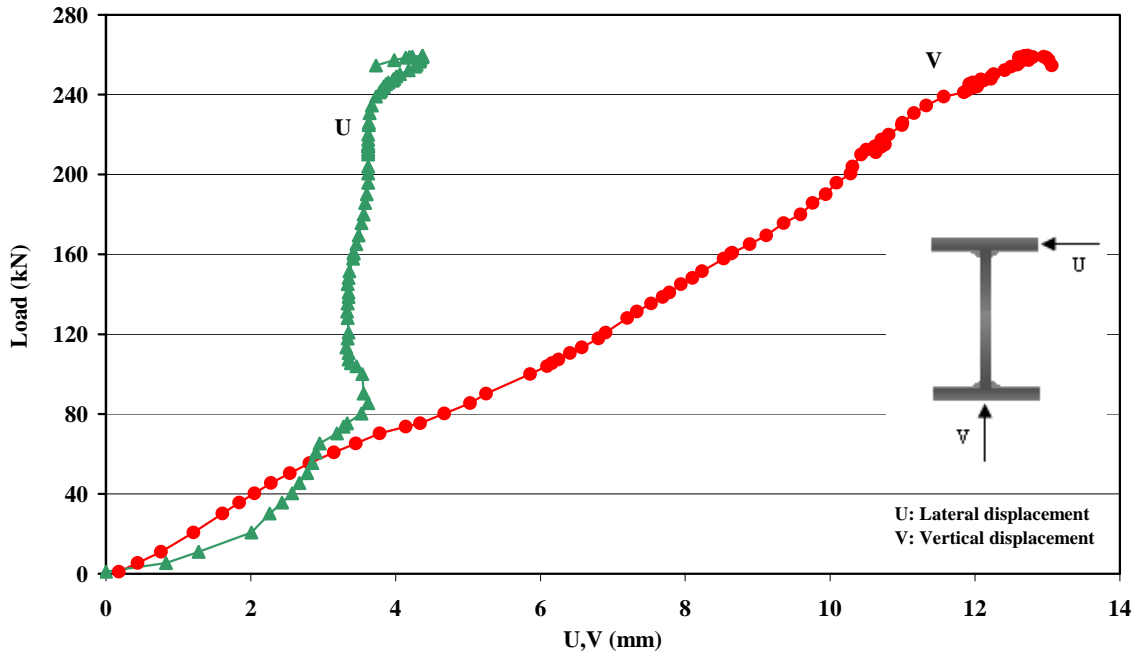


Figure 5.36: Load-Deflection Curves for Beam BB1A

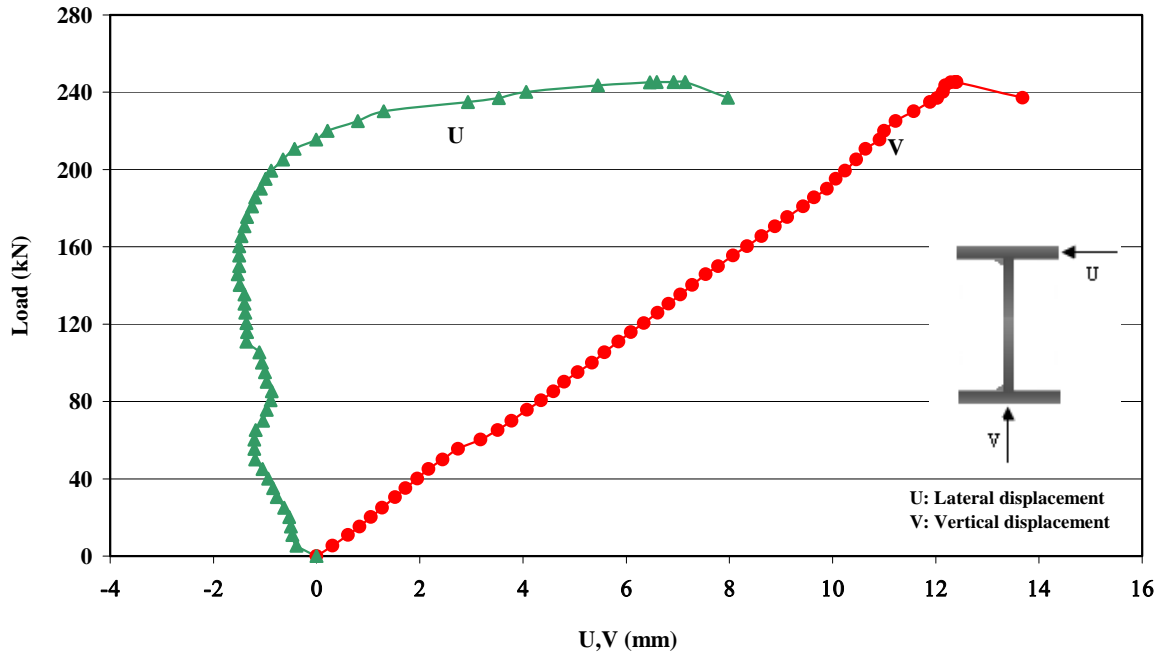


Figure 5.37: Load-Deflection Curves for Beam BB2

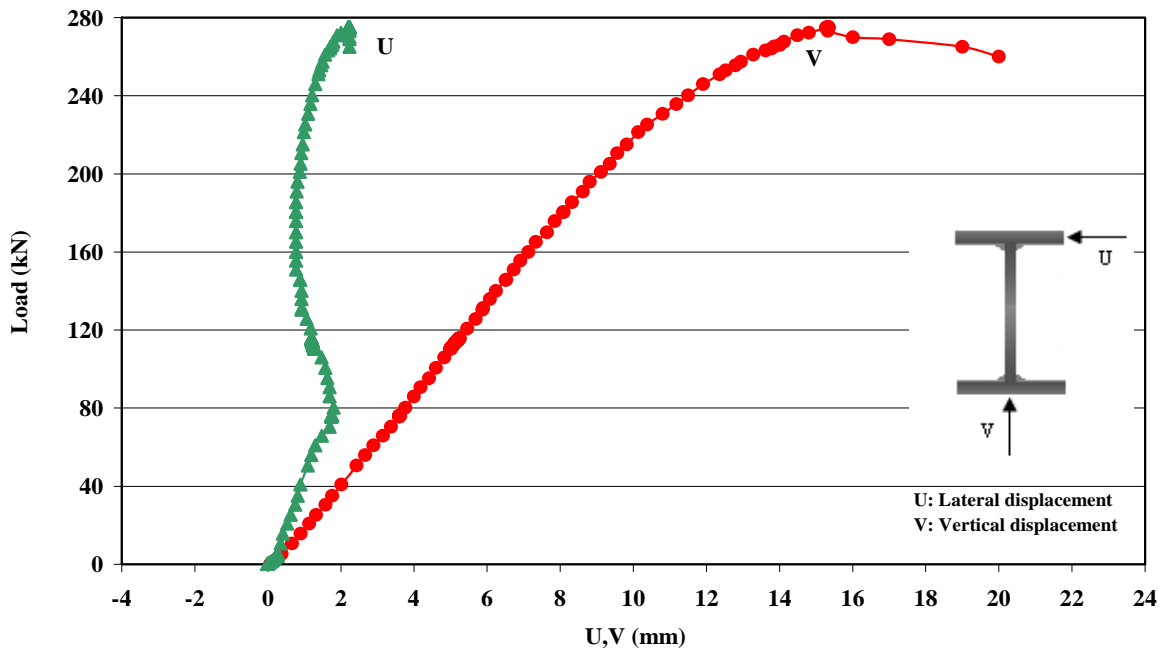


Figure 5.38: Load-Deflection Curves for Beam BB2A

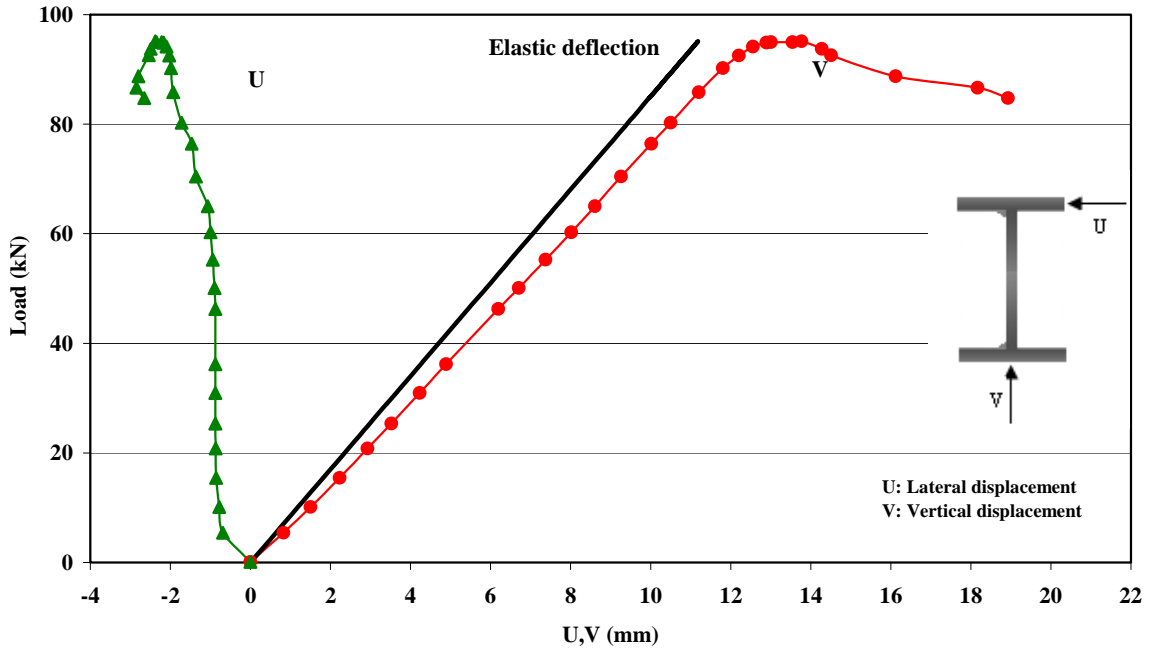


Figure 5.39: Load-Deflection Curves for Beam AB3

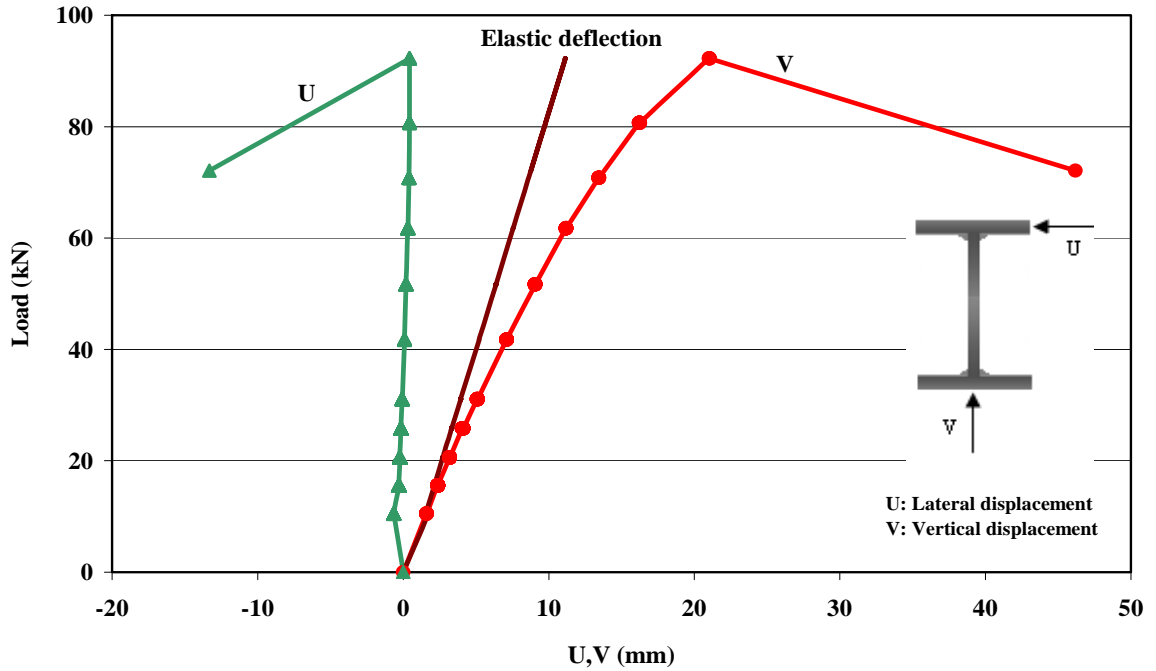


Figure 5.40: Load-Deflection Curves for Beam AB3A

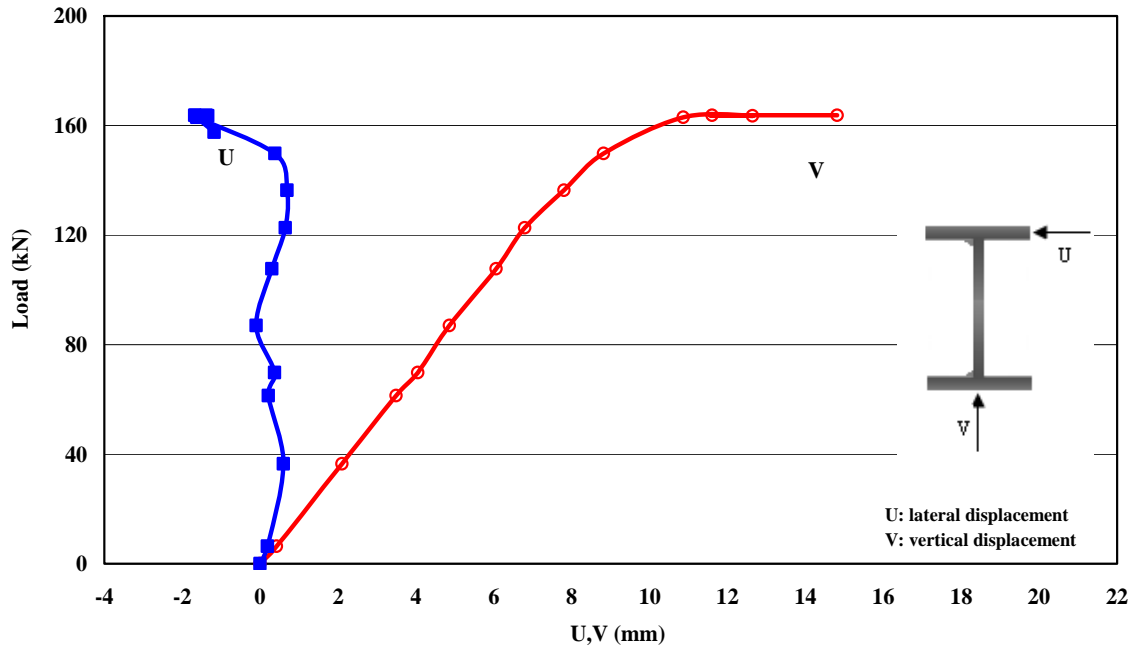


Figure 5.41: Load-Deflection Curves for Beam BB3

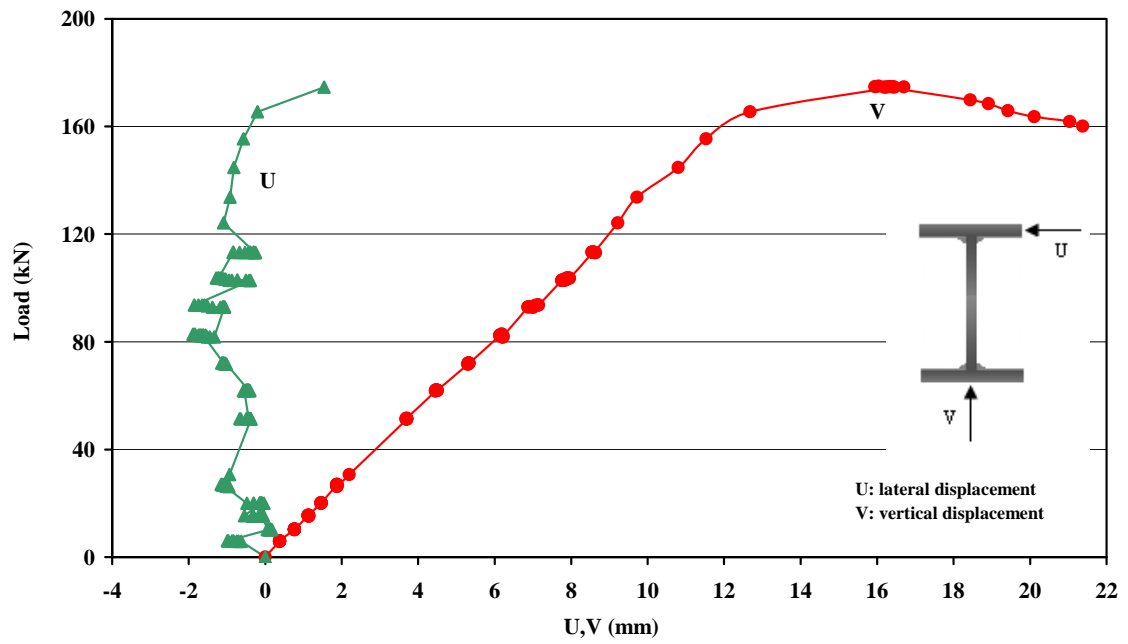


Figure 5.42: Load-Deflection Curves for Beam BB3A

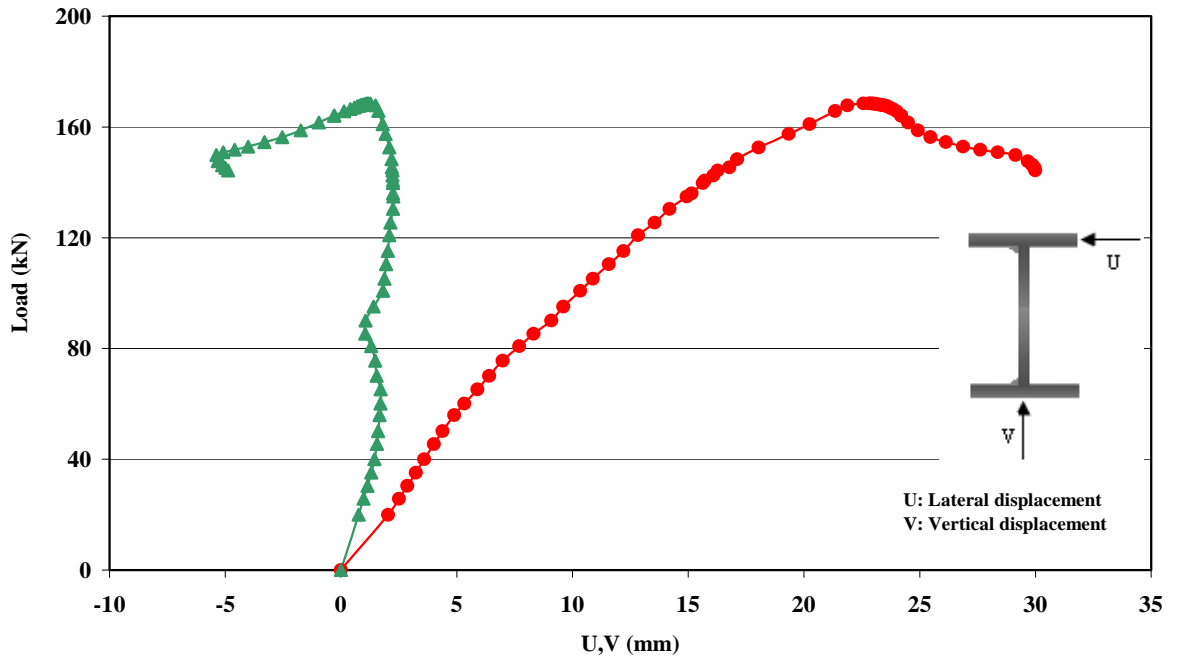


Figure 5.43: Load-Deflection Curves for Beam BB4

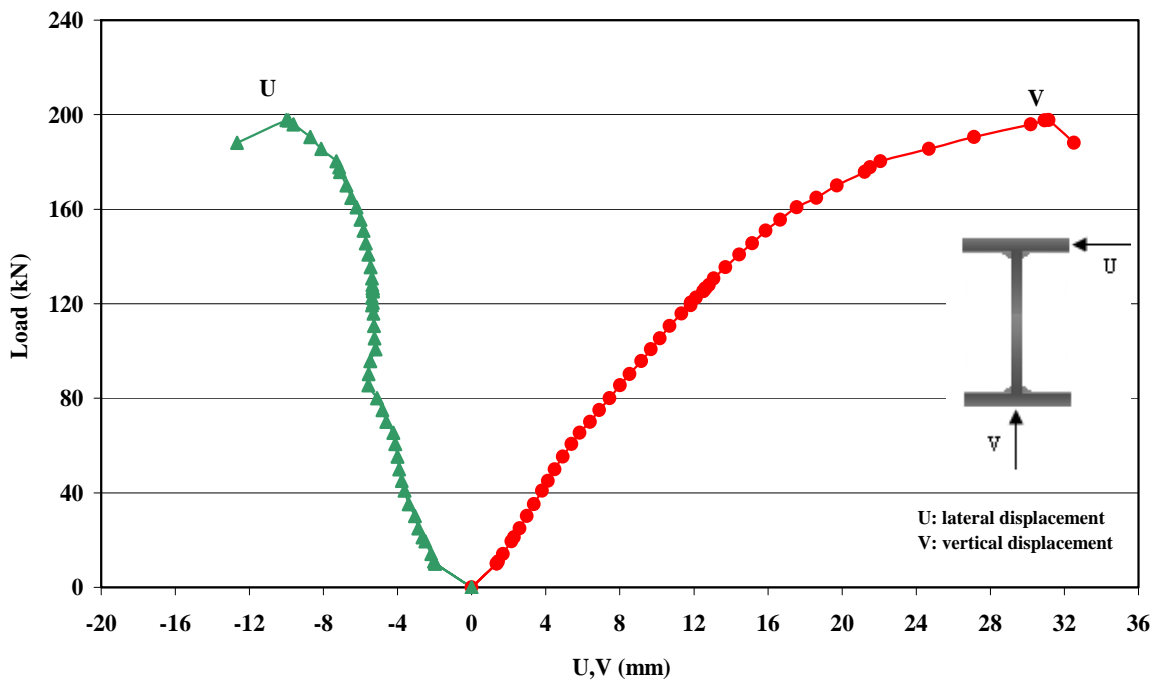


Figure 5.44: Load-Deflection Curves for Beam BB4A

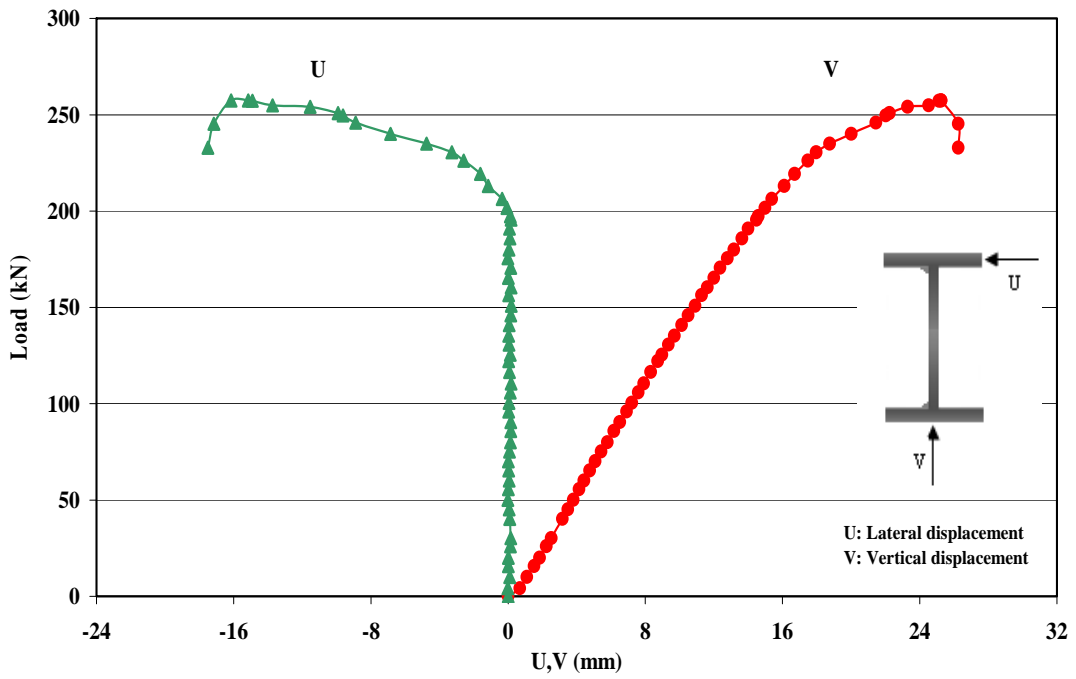


Figure 5.45: Load-Deflection Curves for Beam CB3

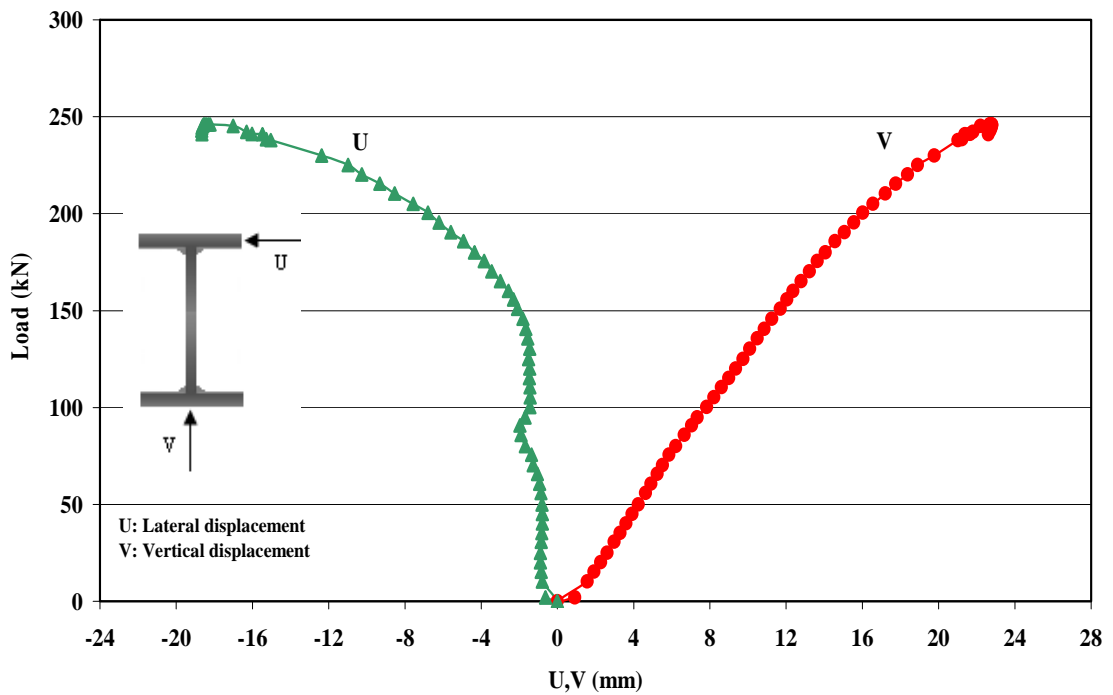


Figure 5.46: Load-Deflection Curves for Beam CB3A

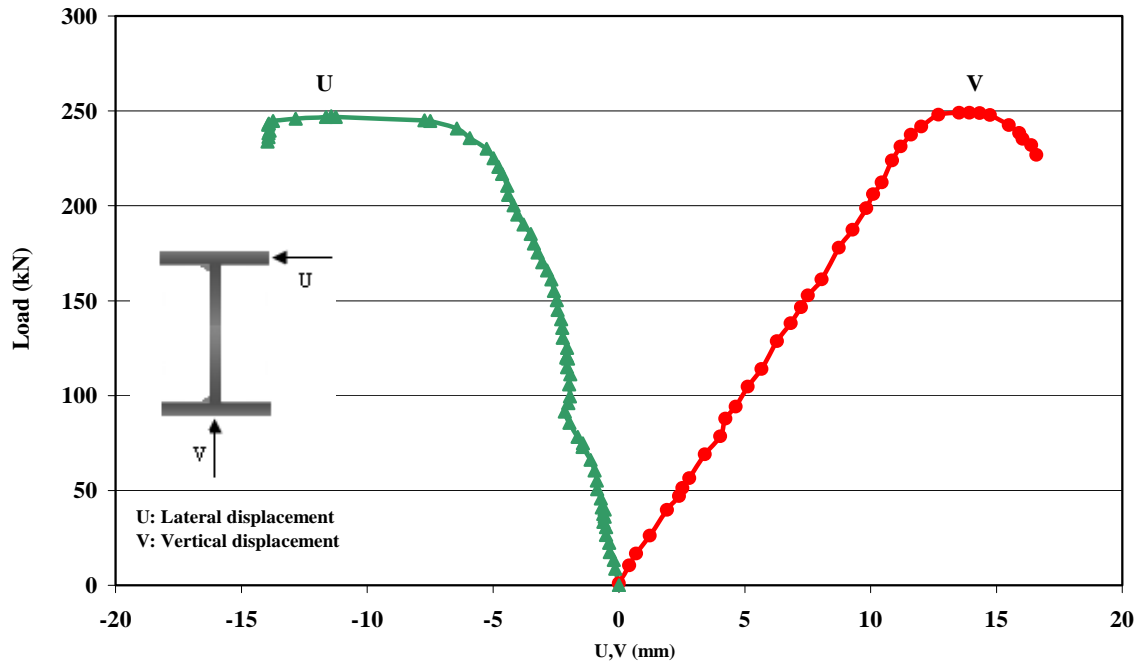


Figure 5.47: Load-Deflection Curves for Beam CB4

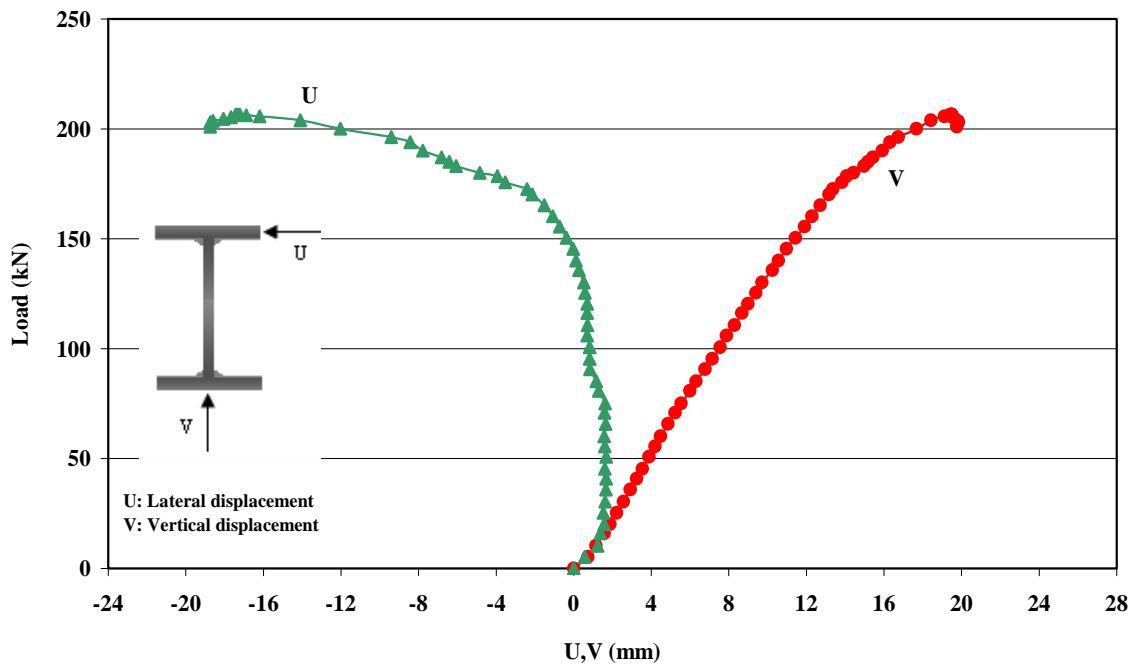


Figure 5.48: Load-Deflection Curves for Beam CB4A

5.7 Evaluation of Test Results

Based on the recorded data and observation during testing which were described in the previous chapter, the ultimate bending moments, $M_u = P_u L/3$, obtained from all the tests are summarized in Table 5.2. The non dimensional ultimate strength, M_u / M_y and M_u / M_p , and the modified slenderness ratio, $\bar{\lambda} = \sqrt{M_p / M_e}$ are also given. M_p is the full plastic moment calculated using the main yield stress and the measured cross sectional dimensions of each specimens. The theoretical critical moment for the elastic lateral buckling M_e was computed from Timoshenko and Gere (1961).

5.7.1 Comparison with Available Test Data of welded Beams

Fig. 5.49 shows the ultimate strength of the nineteen test beams in which M_u / M_p is used for ordinate, and the modified slenderness ratio, $\bar{\lambda} = \sqrt{M_p / M_e}$, is used for the abscissa.

It may be observed from Fig. 5.49, in which are plotted the available test data for welded beams (Fukumoto and Itoh, 1981) and (Kubu and Fukumoto, 1988) and when in Fig. 5.49 all such test points are enclosed by a convex chain-line boundary, fourteen of the test points from the present test groups lie inside this chain, highlighting the strong influence of the present test variables. Also this demonstrates that the plotted results of the test groups are very close to the previous results of specimens which are comparable.

The other five specimens with large $\bar{\lambda}$ are significantly stronger than welded beams from previous tests of equal slenderness; the strength capacity is of the order 11-17 %.

Table 5.2 Summary of Test Result

Group #	Specimen	M_u kN.m	M_u / M_y	M_u / M_p	$\bar{\lambda} = \sqrt{M_p / M_e}$
1	AB1	98.37	0.90	0.81	0.73
	AB2	94.24	0.86	0.77	0.73
	AB1A	95.31	0.86	0.77	0.74
	AB2A	93.80	0.83	0.75	0.74
2	BB1	163.08	0.90	0.79	0.78
	BB2	163.57	0.89	0.78	0.78
	BB1A	172.97	0.94	0.82	0.78
	BB2A	183.40	0.99	0.87	0.78
3	AB3	95.12	0.88	0.80	1.09
	AB3A	92.24	0.86	0.77	1.10
	AB4A	91.22	0.84	0.76	1.09
4	BB3	163.72	0.88	0.77	1.15
	BB4	168.50	0.92	0.80	1.15
	BB3A	175.70	0.94	0.83	1.15
	BB4A	197.70	1.06	0.93	1.16
5	CB3	257.53	1.09	0.97	1.11
	CB4	247.16	1.05	0.94	1.11
	CB3A	246.04	1.03	0.92	1.11
	CB4A	206.44	0.87	0.77	1.12

5.7.2 Comparison with Available Test Data of Rolled Beams

Fukumoto and Kubo (1977) carried out an extensive survey of literature on the lateral buckling tests that had been conducted at various institutions. In Fig. 5.50 the present test results for the five groups are compared with the past 128 test points for rolled sections. The clear trend for the test results in the first and second groups indicate that built-up beams are weaker than rolled beams of equal slenderness for levels of slenderness in the range of $\bar{\lambda} \leq 0.8$. It may be due to the variation in the compressive residual stresses and initial lateral crookedness. In the range of large $\bar{\lambda}$, the test results show higher ultimate strength than rolled beams. It may be explained by the difference in support conditions.

5.7.3 Comparison with Current Standards

The M_u / M_p versus the modified slenderness curves are plotted in Fig. 5.51 together with the test values. It can be seen from Fig. 5.51 that the predicted lateral strengths from the LRFD specification (2005) are upper than the test values for small values of $\bar{\lambda}$ and lower than the test values for large values of $\bar{\lambda}$. The predictions in CSA-S16-01 (2001), which are based on the upper bound of the test values of I-section beams, are lower than the test values. The predictions of Eurocode 3 (2005) Part 1.1 are lower than the test values for large values of $\bar{\lambda}$. The Australian standard AS4100 (1998) gave the most conservative predictions and provided good lower bound estimates to the failure loads of the built-up beams, because it is based on the lower bounds of the test

values I-section beams. The design rules in different standards for lateral-torsional buckling of beams are based on test results of beams restrained at their supports against torsion but not against warping. In current study especially for the fourth and the fifth groups, an improvement in buckling strength was observed due to the bolted end connections which reduce warping.

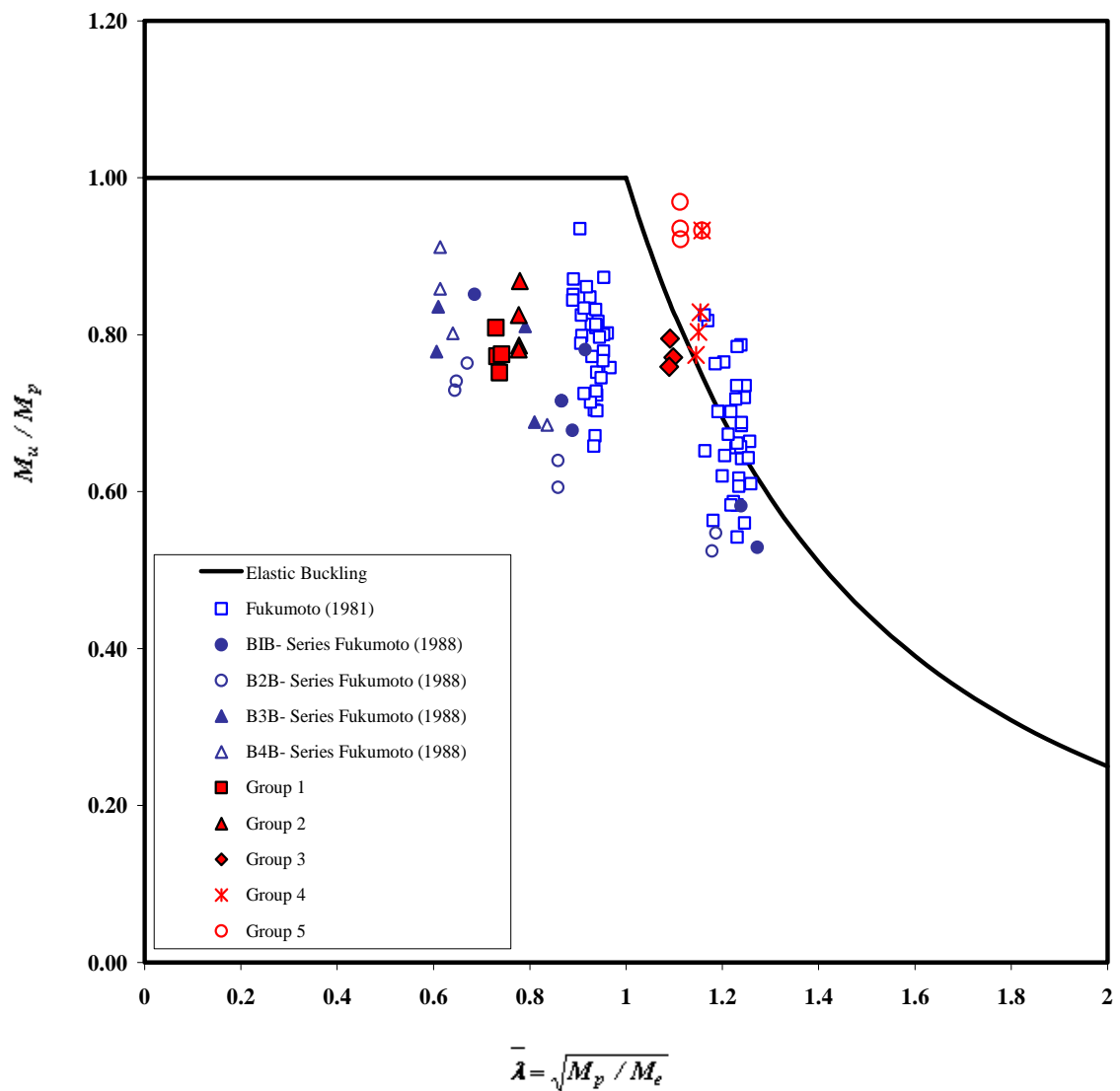


Figure 5.49: Comparison of Test Results with Available Test Data for Welded Beams

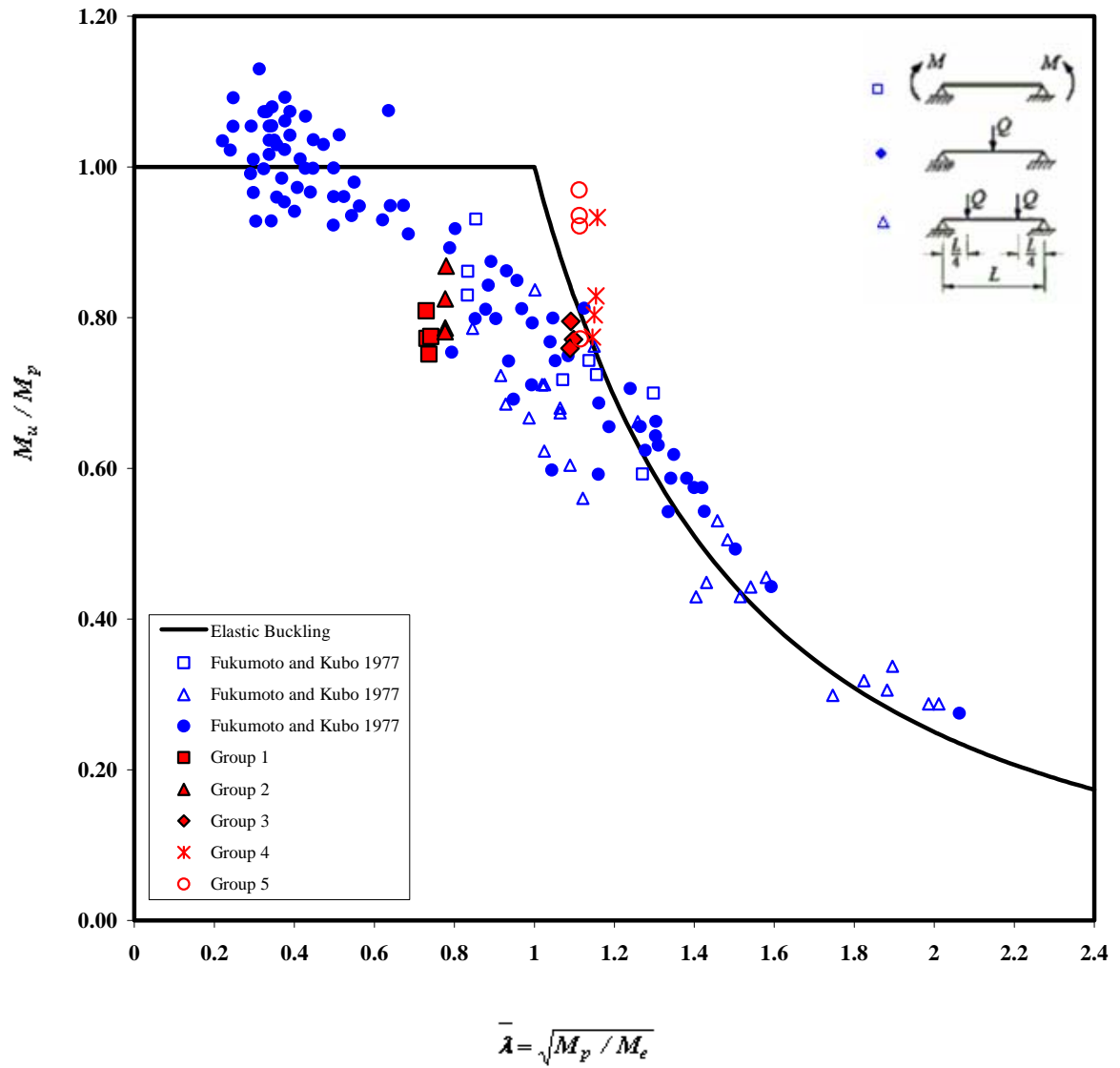


Figure 5.50: Comparison of Test Results with Available Test Data for Hot Rolled Beams

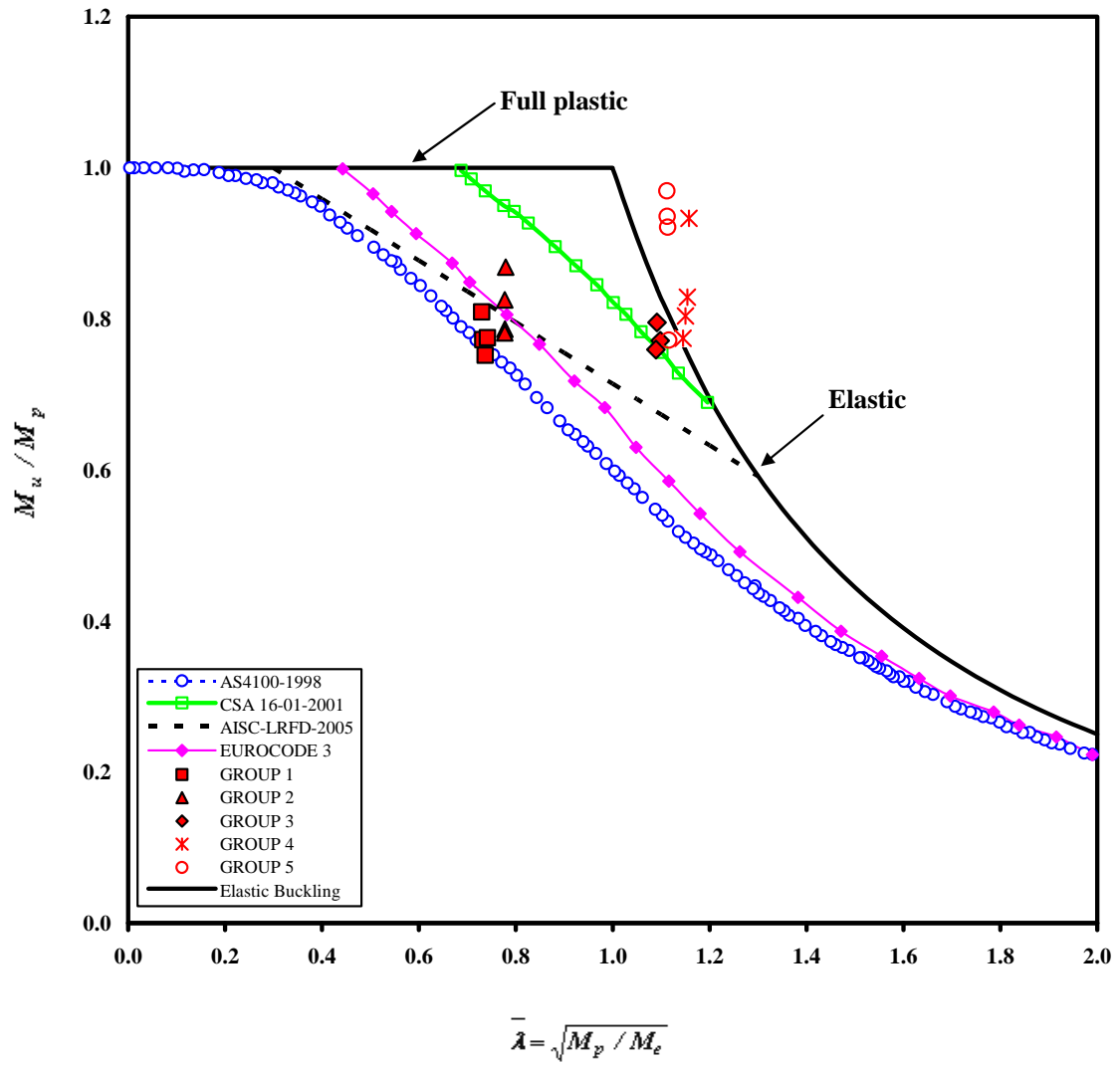


Figure 5.51: Comparison of Test Results with Current Standards

CHAPTER 6

CONCLUSIONS AND RECOMONDATIONS

6.1 Summary

The primary cornerstone of metal building construction is to minimize the building costs, the goal is usually achieved through optimization of steel weight and the fabrication process by adopting the built-up I-shaped web-tapered primary framing members with bolted end-plate connections and the cold-formed secondary structural members. Since no design procedure for metal building systems exists in the current codes, the industry takes advantage of all allowed code exceptions and options that frequently result in lighter and more economical structures.

It is a common practice in metal building industry to connect both flanges to web at one time using fillet weld on one side of the thickness of the web. This method of fabrication is not explicitly explained in current codes. Moreover, limited information about this subject causes ambiguity among practicing engineers.

An experimental program was devised and constructed in collaboration with Jordan University of Science and Technology (JUST), to study the lateral buckling behavior of simply supported built-up I-beams with fillet welds: 1) on one side of the web; 2) on both sides of the web. Nineteen buckling tests were carried out on five groups of built-up I-beams with two symmetrical concentrated loads applied vertically at third point of the compression flange. Specially designed supports which allowed the end cross sections of each test beam to rotate about the major and minor axes, but restrained them

against twisting about the longitudinal axis, were fabricated. Thirteen tension tests were carried out on specimens prepared from the original plates to determine the mechanical properties of steel. Residual stresses in the flange and the web are measured for four specimens using the Hole-Drilling method. The data is acquired by using certain instruments as Linear Variable Displacement Transducers (LVDTs) and electronic strain gages to measure the deflections and strains at different position on the tested beams.

6.2 Conclusions

Regarding the experimental results and observations the following conclusions can be drawn.

1. The usual types of buckling of steel members assumed in design code are lateral-torsional and local buckling modes. In lateral-torsional buckling, the cross sections of the member translate and twist as rigid bodies. On the other hand local buckling is characterized by localized distortions of the cross-section over a short wavelength. the experimental results revealed that the interaction between local and lateral buckling can be a significant feature of the general instability problem.
2. For relatively large $\bar{\lambda}$, about 1.1, when flange thickness to web thickness ratio (t_f/t_w) equal 1.2 (for the second and the fourth groups) the combined failure mode of local flange buckling and lateral-torsional buckling was obtained for beams with fillet weld on both sides of the web, while the beam with fillet weld on one side of the web failed only by local flange-buckling. In the range of

intermediate $\bar{\lambda}$, about .78, local flange-buckling and local web-buckling were the primary modes of failure.

3. For large and intermediate $\bar{\lambda}$, when the ratio of thicknesses of the flange to the web, $t_f / t_w = 1.25$ (for the first and the third groups), The combined failure mode of local flange and lateral-torsional buckling was observed for beams with fillet weld on both sides of the web, while beams with fillet weld on one side of the web failed only due to local buckling of the flange.
4. For relative large $\bar{\lambda}$, about 1.1, when t_f / t_w equal 1.33 (for the fifth group), lateral torsional-buckling was the primary mode of failure.
5. The presence of residual stresses seems to have had only a decrease effect when t_f / t_w increases.
6. The ultimate strength of built-up sections with fillet welds on both sides of the web is not always greater than their counterpart beams with fillet weld on one side of the web.
7. The bolted end-plate connection at the beams ends may induces end-restraining moments in the that oppose the warping deformation and modify the lateral buckling resistance of the beam especially for high slenderness ratios, $\bar{\lambda} \geq 1.1$.

8. The predicted residual stresses type of pattern for built-up I-sections with fillet welds on one side of the web is characterized by very high tensile stresses near the web flange welds balanced by compression elsewhere. A significant portion of the web is in residual compression.
9. The design curves for various codes vary markedly. The design loads predicted by the AS4100 (1998) provided good lower bound estimated to failure loads of the tested beams.
10. The test results reaffirm that built-up beams should be fabricated with controlled level of initial crookedness.

6.3 Recommendations

Based on the experimental results presented in the previous section the following may be recommended:

1. The main goal of this research is to study the problem of inelastic buckling of I-beams under monotonic loading. The problem was studied using experimental approaches. The need for further research which must be done to fully understand the phenomena of inelastic buckling of thin-walled structure still exist. Therefore, the response and buckling of common structural shapes under cyclic loading still need to be addressed on a case-by-case basis.

2. The effect of end-warping restrains on the lateral-buckling resistances of beams have been studied extensively. However, no method is provided for the calculation of end-warping restraint stiffness in the design codes.
3. This test was carried out on small size of built-up beams. It is recommended to perform experiments on full size tapered frames under both monotonic and cyclic loads.

REFERENCES

- American Institute of Steel Construction (2005). **Load and Resistance Factor Design Specification for Structural Steel Buildings**.
- ASTM Standard E837**, (2001). Standard Test Method for Determining Residual stresses by the Hole-Drilling Strain Gage Method.
- American Welding Society (2000), **Structural Welding Code-Steel**, American National Standards Institute/ American Welding Society (ANSI/AWS), D1.1-2000.
- Bradford, M. A., and Trahair, N. S. (1981). Distorsional buckling of I-beams. **Journal of Structural Division**, ASCE, 107(2), 335-370.
- Bradford, M. A., and Hancock, G. J. (1984). Elastic interaction of local and lateral buckling in beams. **Thin-Walled Structure**, 2(1), 1-25.
- Bradford, M. A. (1987). Inelastic local buckling of fabricated I-beams. **Journal of Constructional Steel Research**, 7, 317-334.
- Canadian Standard Association (2001). Steel Structure for Building (**Limit State Design**). CAN/CSA-16-01, Rexdale, Ontario, Canada.
- Chen, W.F. and Lui, E.M (1987). **Structural Stability-Theory and Implementation** .Elsevier Applied Science, New York, USA.
- Cherry, S. (1960). The stability of beams with buckled compression flanges. **Structural Engineer**, 38(9), 277-285.
- Eurocode 3 (2005). **Design of Steel Structures**: Part 1.1- General Rules and Rules for Buildings. DD ENV, 1993-1.1.
- Fukumoto, Y., and Kubo, M. (1971). Inelastic lateral buckling strength of mono-symmetric I-beams. **Transaction of the Japanese Society of Civil Engineering**, 161-162.
- Fukumoto, Y., and Kubo, M. (1977). A survey of tests on lateral buckling strength of beams. European Convention for Constructional Steel Work, Preliminary Report, **Second International Colloquium on Stability of Steel Structures**, Liege, Belgium, pp. 233-240.
- Fukumoto, Y., Itoh, Y., and Kobo, M. (1980). Strength variation of laterally unsupported beams. **Journal of Structural Division**, ASCE, 106(ST1), 165-181.
- Fukumoto, Y., Itoh, Y. (1981). Statistical study of experiments on welded beams. **Journal of Structural Division**, ASCE, 107(ST1), 89-103.

Fukumoto, Y., Itoh, Y., and Hattori R. (1982). Lateral buckling tests on welded continuous beams. **Journal of Structural Division**, ASCE, 108(ST10), 2245-2262.

Galambos, T. V. (1963). Inelastic lateral buckling of beams. **Journal of Structural Division**, ASCE, 89(ST5), 217-242.

Galambos, T.V. (1998). **Guide to Stability Criteria for Metal Structure**, 5th Ed., John. New York: Wiley and Sons.

Graham, P., and Richard, B. (1971). Elastic lateral buckling of steel beams. **Journal of Structural Division**, ASCE, 96(ST9), 1919-1932.

Kelsey, R.A. (1956). Measuring non-uniform residual stresses by the Hole-Drilling method. Proc., **SESA XIV**, 14(1), 181-194.

Kemp, A. R. (1986). Factors affecting the rotation capacity of plastically designed members. **The Structural Engineer**, 64B(2), 8-35.

Kitipornchai, A.M., Nicholes, S., and Trahair, M. (1975). Inelastic buckling of simply supported steel I-beams. ASCE, **Journal of Structural Division**, ASCE, 101(ST7), 1333-1347.

Kubo, M., Itoh, Y., and Fukumoto, Y. (1988). Lateral-torsional buckling of thin-walled I-beams. **Journal of Structural Engineering**, ASCE, 114(4), 841-855.

Lay, M.G. and Galambos, T. (1965). Inelastic Steel Beams under Uniform Moment. Proc. ASCE, **Journal of Structural Division**, ASCE, 91(ST6), 67-93.

Lee, G. and Galambos, T. (1962). Post-Buckling strength of side-flange Beams. Proc. ASCE, **Journal of the Eng. Mech. Div.**, 88(EM 1), 59-75.

Lim N. H., Park N.H., Kang Y. J. and Sung I. H. (2003). Elastic buckling I-beam under linear moment gradient. **International Journal of Solid and Structures**, 40, 5635-5647.

Mathar, J. (1934). Determination of initial stress by measuring the deformation around drilled holes, **Trans. ASME**, 56(4), 249–254.

Nethercot, D.A. and Rocky K. C. (1971). A unified approach to the elastic lateral buckling of beams . **The Structural Engineer**, 49(7), 321-329.

Nethercot, D.A. and (1974). Residual stresses and their influence upon the lateral buckling of rolled steel beams. **The Structural Engineer**, vol. 52.

Nethercot, D. A., and Trahair, N. S. (1976). Inelastic lateral buckling of determinate beams. **Journal of Structural Division**, ASCE, 102(ST4), 701-717.

Nethercot, D. A. (1983). **Elastic Lateral Buckling of Beams**. Applied Science Publishers, Essex, England.

Ojalvo, M., and Chambers, R. S. (1977). Effects of warping restraints on I-beam buckling. **Journal of Structural Division**, ASCE, 103(ST12), 2351-2360.

Park J. S., Stallings J. M. and Kang Y. J. (2004). Lateral-torsional buckling of prismatic beams with continuous top-flange bracing. **Journal of Constructional Steel Research**, 60, 147-160.

Powell, G., Klingner, R. (1970). Elastic lateral buckling of steel beams. **Journal of Structural Division**, ASCE, 96(ST9), 1919-1932.

Schajer, G.S. (1981). Application of finite element calculations to residual stress measurements. **Journal of Engineering Materials and Technology**, Transaction, ASME, 103, 157-163.

Schajer, G.S. (1988). Measurement of non-uniform residual stresses using the Hole Drilling Method. **Journal of Engineering Materials and Technology**, 110(4): Part I, 338-343; Part II, 344-349.

Soete and Vancrombrugge (1954). Determination of Residual Stresses Below the surface in residual stresses in metals and metal construction, in: **W.R.Osgood (Ed.)**, Reinhold Publishers, New York. 17 –28.

Standard Association of Australia. (SAA). (1998). Steel Structures. **Australian Standard AS4100**, Sydney, Australia.

Suryoatmono B. and Ho D., (2002). The moment gradient factor on lateral-torsional buckling of wide flange steel section. **Journal of Constructional Steel Research**, 58, 1247-1264.

Technical Notes TN-503-2 (2000). Measurement of residual stresses by the hole-drilling strain-gage method.

Timoshenko, S. P., and Gere, J. M. (1961). **Theory of Elastic Stability**. McGraw-Hill, New York.

Trahair N.S.(1993). **Flexural-Torsional Buckling of Structures**, Chapman and Hall, London.

Trahair, N.S. and Hancock, G.J. (2002). Member strength by inelastic lateral buckling. **Research Report R824**, Department of Civil Engineering, University of Sydney.

Vacharajittiphan, P., Woolcock, S.T., Trahair, N.S (1974). Effect of in-plane deformation on lateral buckling. **Journal of Structural Mechanics**, 3(I), 29-60.

Yoshido, H., and Maegawa, K. (1984). Lateral instability of I-beams with imperfection. **Journal of Structural Engineering**, ASCE, 110(8), 1875-1892.

APPENDICES

Appendix A

Residual Stress Measurements

Tables A.1-A.12 show the measured relieved strains via incremental hole-drilling to a depth of 2 mm and the stresses versus the dimensionless hole depth, Z/D are shown in Figs. A.1-A.12.

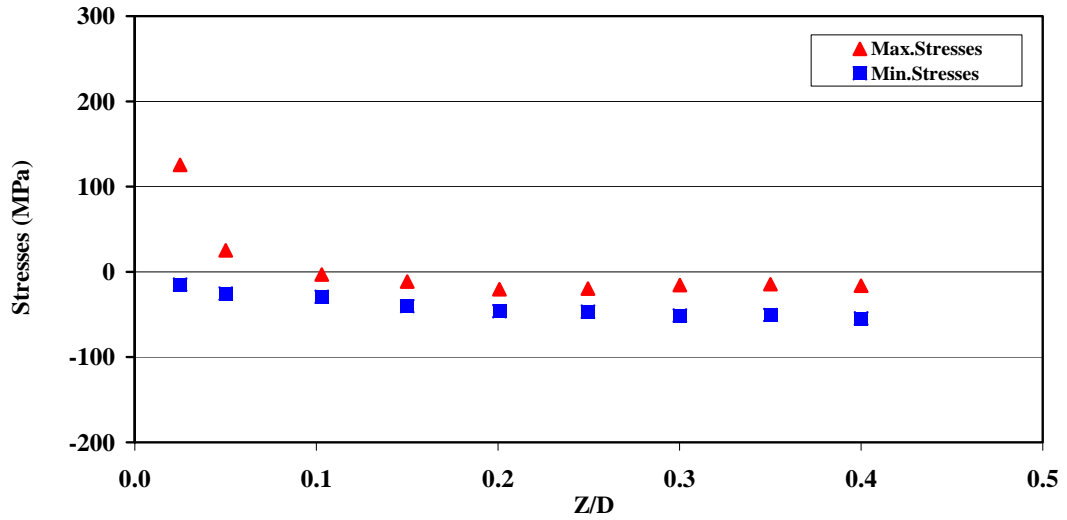


Figure A.1: Maximum and Minimum Stresses for Specimen AA30 at Point 1

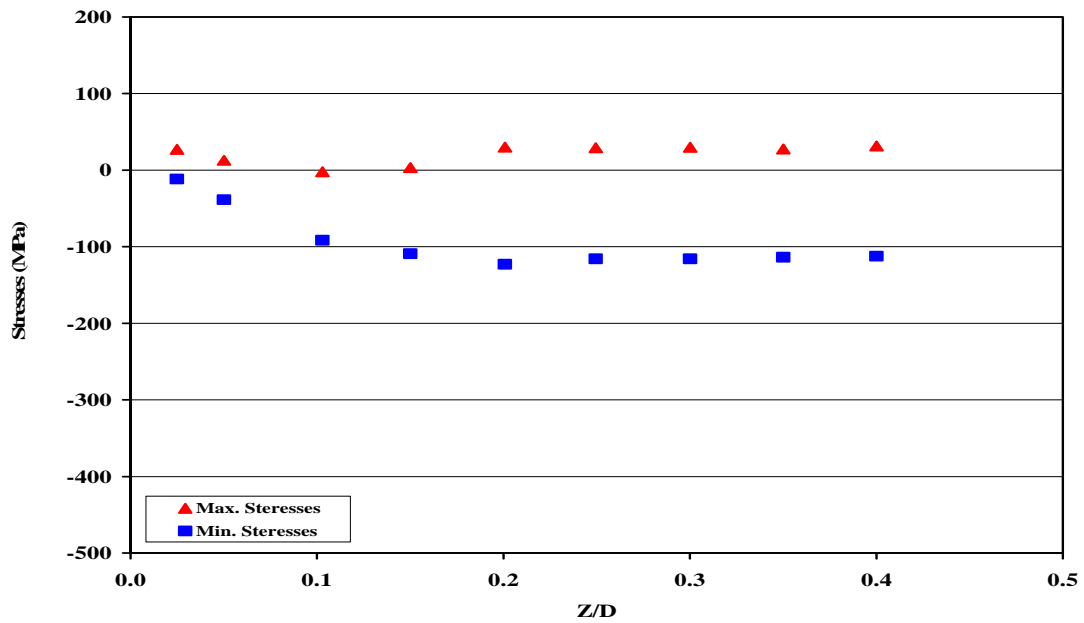


Figure A.2: Maximum and Minimum Stresses for Specimen AA30 at Point 2

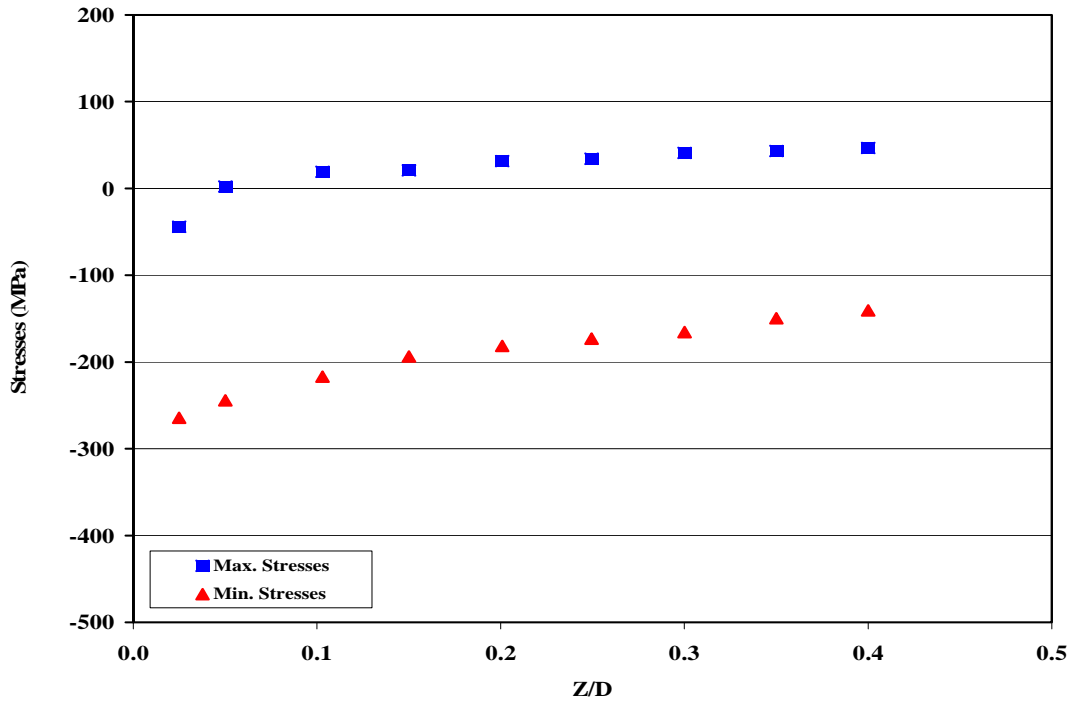


Figure A.3: Maximum and Minimum Stresses for Specimen AA30 at Point3

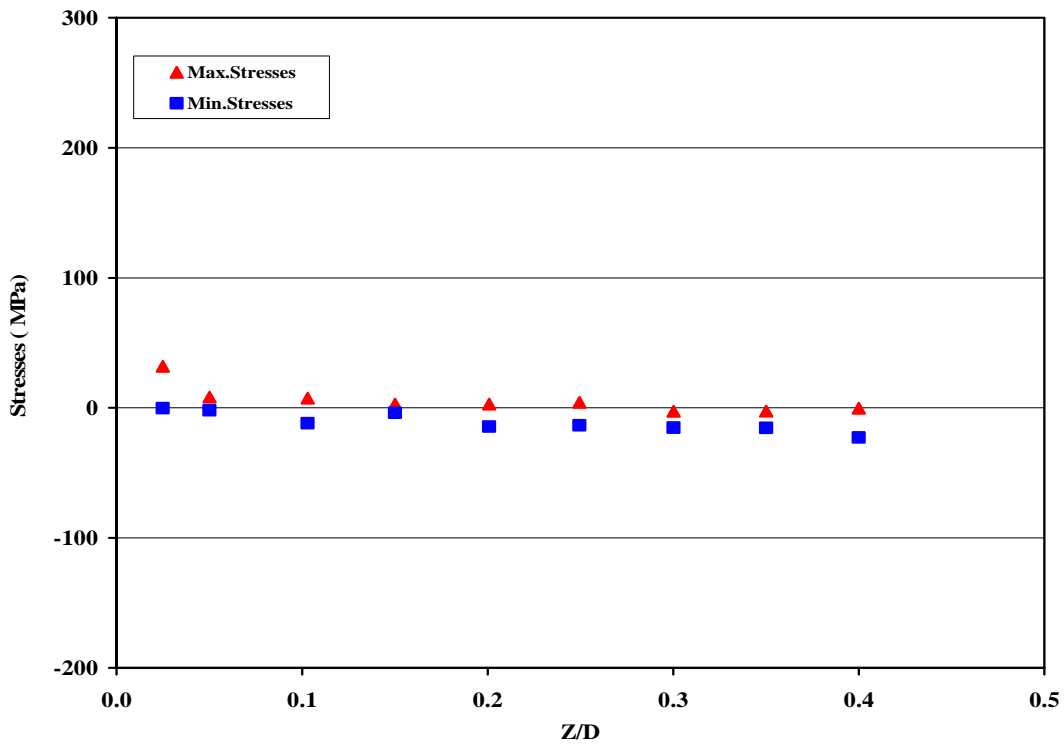


Figure A.4: Maximum and Minimum Stresses for Specimen A30 at Point 1

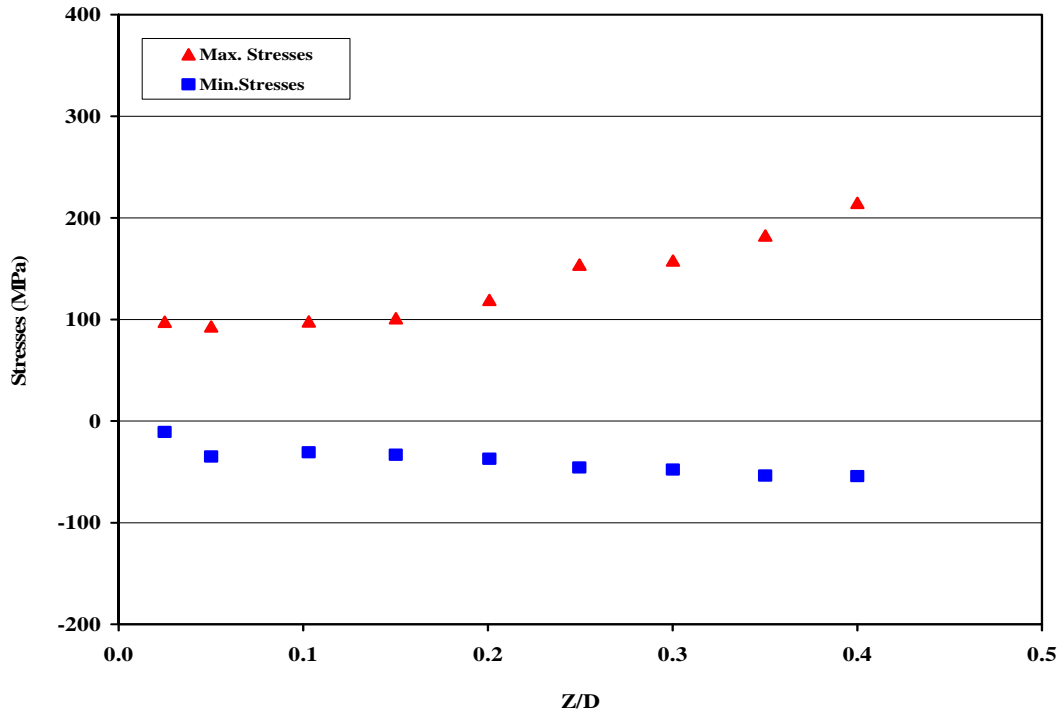


Figure A.5: Maximum and Minimum Stresses for Specimen A30 at Point 2

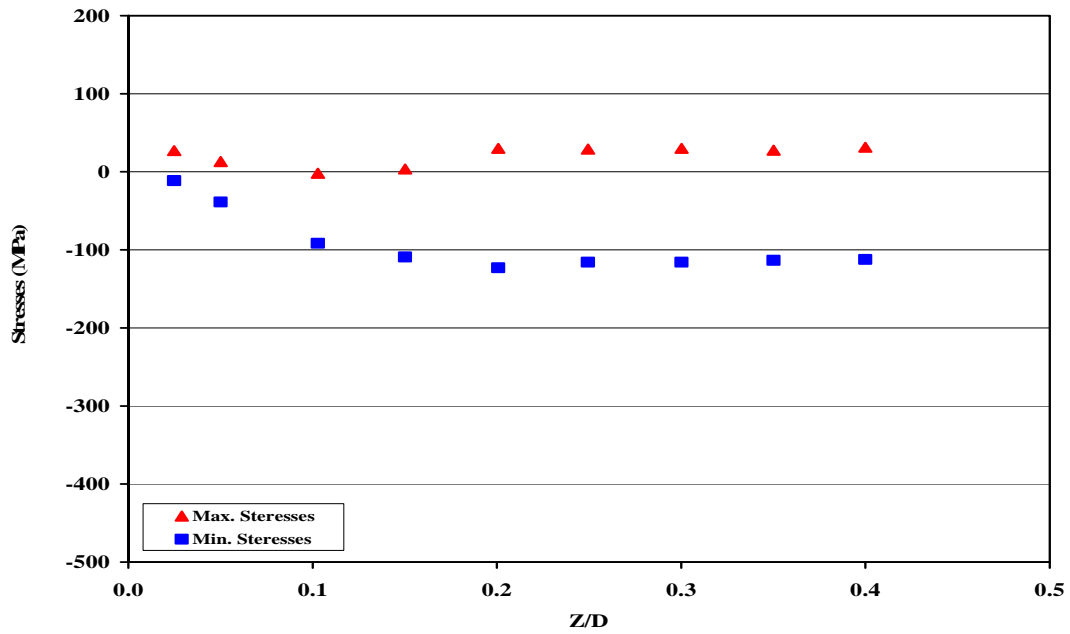


Figure A.6: Maximum and Minimum Stresses for Specimen A30 at Point 3

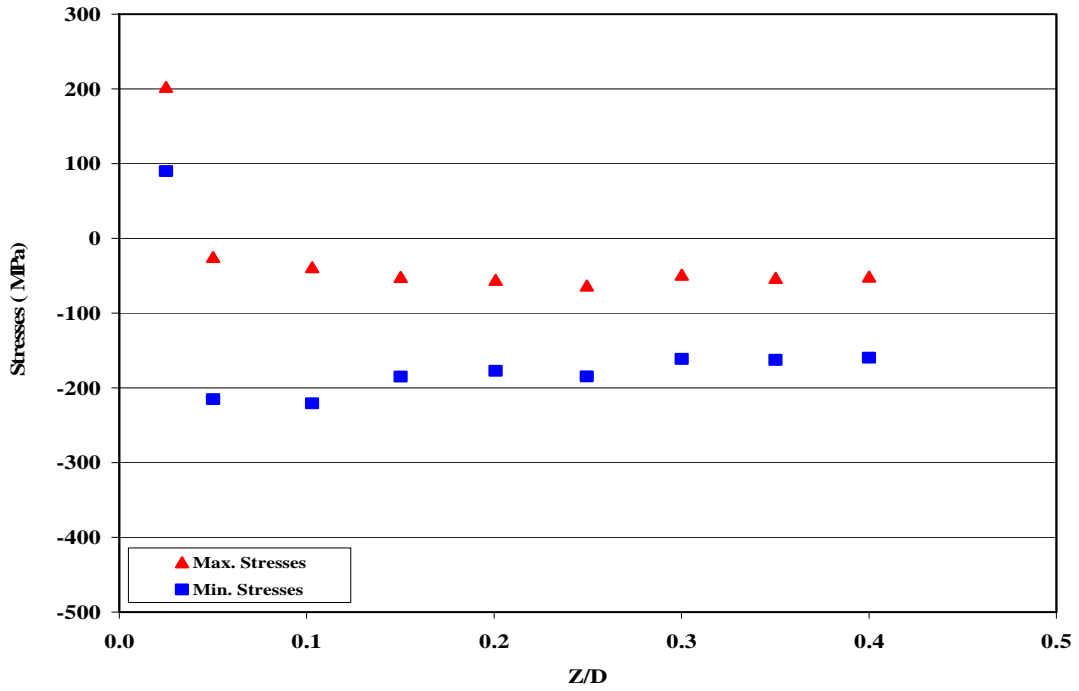


Figure A.7: Maximum and Minimum Stresses for Specimen BB40 at Point 1

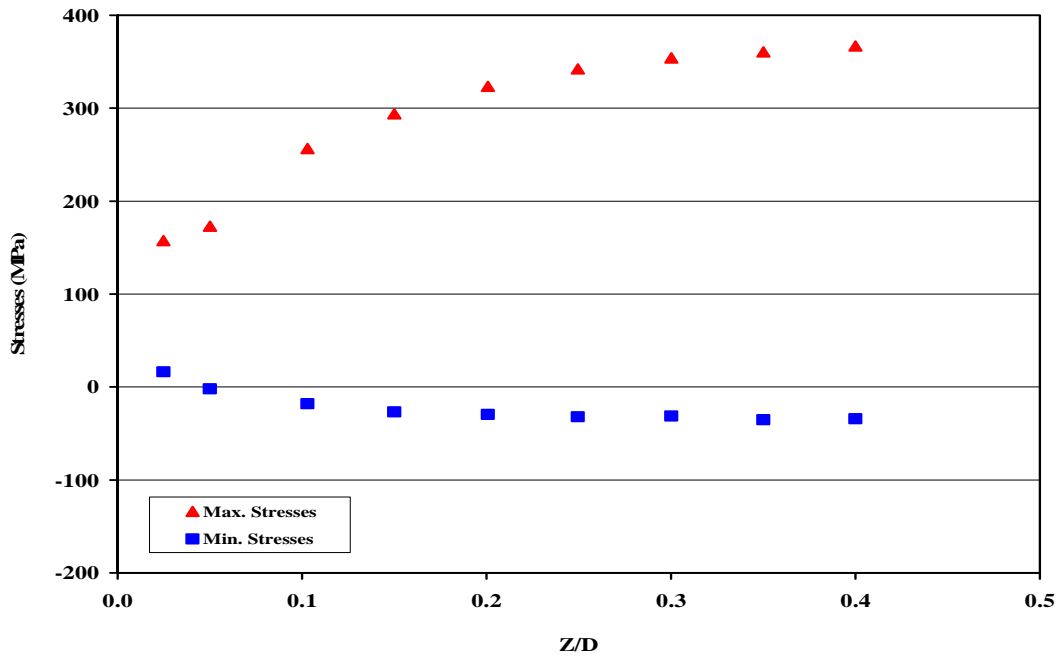


Figure A.8: Maximum and Minimum Stresses for Specimen BB40 at Point 2

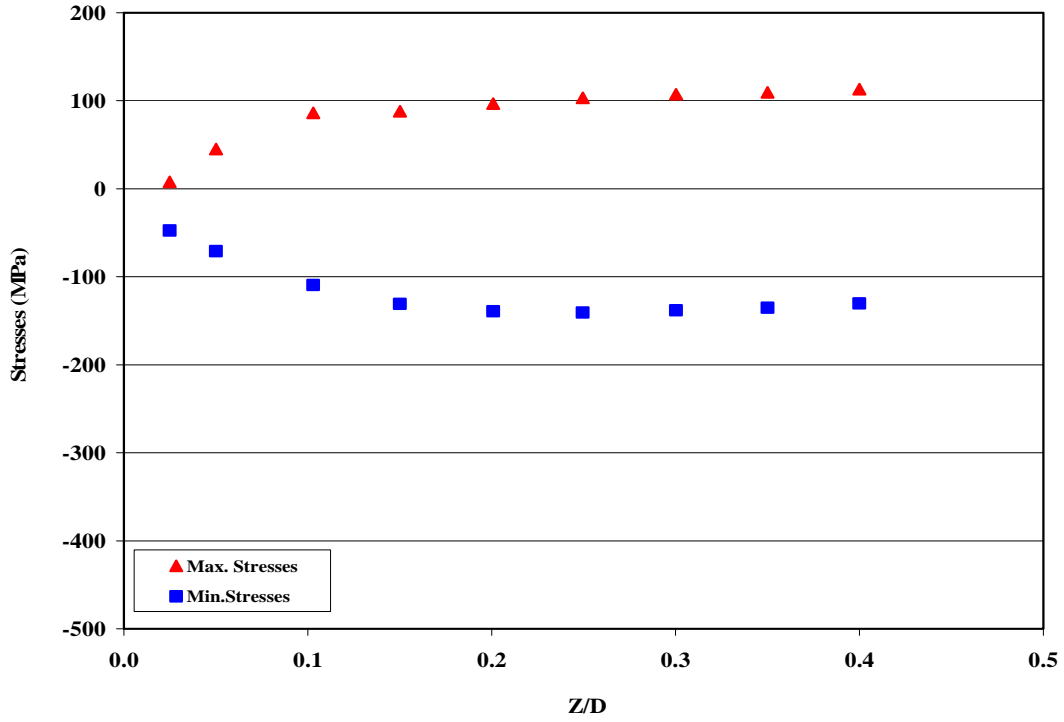


Figure A.9: Maximum and Minimum Stresses for Specimen BB40 at Point 3

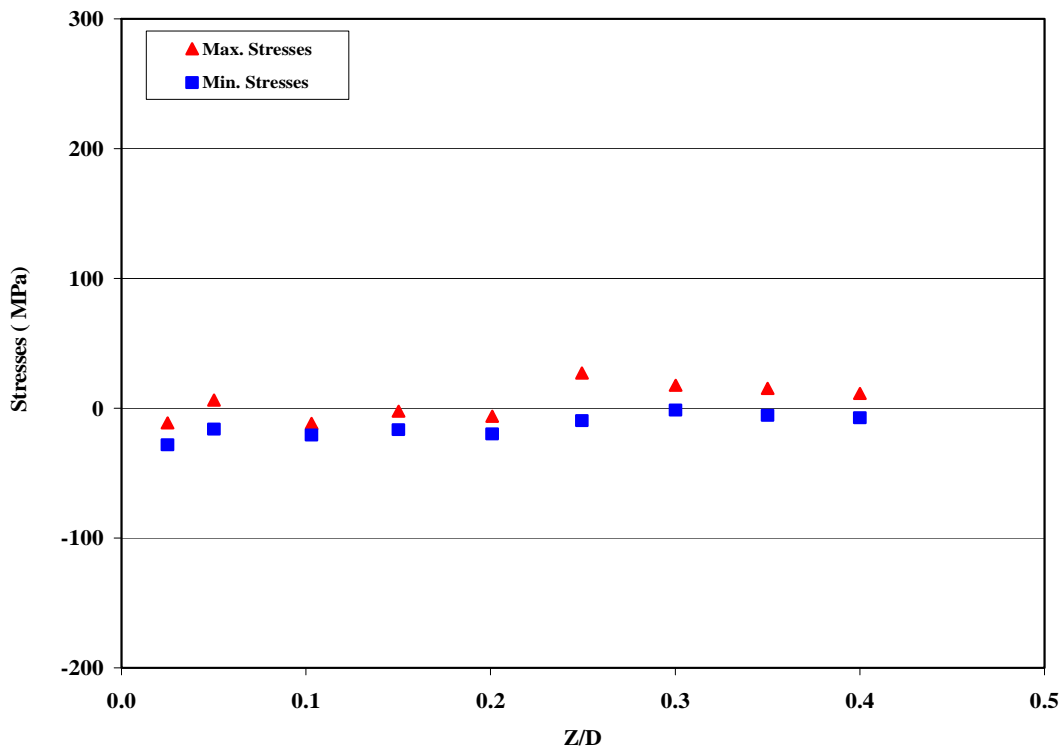


Figure A.10: Maximum and Minimum Stresses for Specimen B40 at Point 1

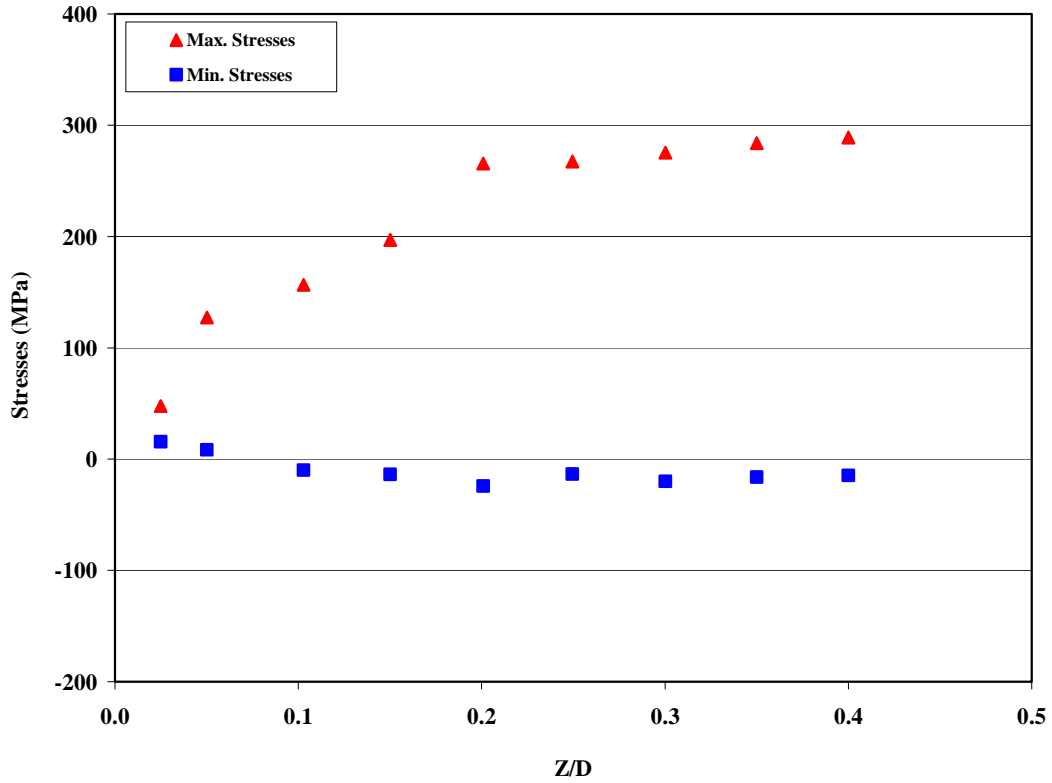


Figure A.11: Maximum and Minimum Stresses for Specimen B40 at Point 2

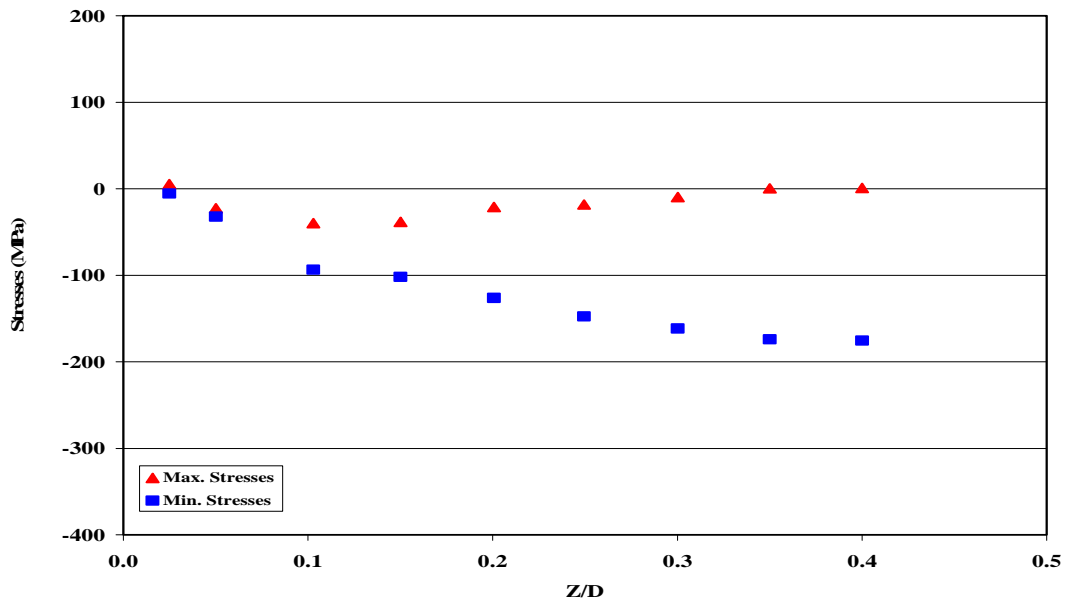


Figure A.12: Maximum and Minimum Stresses for Specimen B40 at Point 3

Table A.1 Measurement of Residual Stress by the Hole-Drilling Method

Specimen AA30 at Point 1

Z/D	Measured Strain	$\varepsilon_3 + \varepsilon_1$	$\varepsilon_3 - \varepsilon_1$	$\varepsilon_3 + \varepsilon_1 - 2\varepsilon_2$	Coefficients		Equivalent Uniform Stresses	
	μ_ε	%	%	%	\bar{a}	\bar{b}	σ_{\min} (MPa)	σ_{\max} (MPa)
0.025	-14	-14	14	-22	0.020	0.038	-15	125
	4	-16%	-23%	33%				
	0							
0.050	-2	0	4	-22	0.049	0.090	-25	25
	11	0%	-6%	33%				
	2							
0.103	9	22	4	-26	0.108	0.206	-29	-3
	24	26%	-6%	39%				
	13							
0.150	26	49	-3	-43	0.151	0.305	-40	-11
	46	57%	5%	65%				
	23							
0.201	43	74	-12	-46	0.177	0.377	-46	-20
	60	86%	19%	70%				
	31							
0.250	51	80	-22	-52	0.19	0.425	-47	-20
	66	93%	52%	72%				
	29							
0.300	58	82	-34	-72	0.195	0.454	-51	-15
	77	95%	55%	109%				
	24							
0.350	61	80	-42	-72	0.195	0.472	-50	-14
	76	93%	68%	109%				
	19							
0.400	74	86	-62	-66	0.192	0.482	-54	-16
	76	100%	100%	100%				
	12							

Table A.2 Measurement of Residual Stress by the Hole-Drilling Method

Specimen AA30 at Point 2

Z/D	Measured Strain	$\varepsilon_3 + \varepsilon_1$	$\varepsilon_3 - \varepsilon_1$	$\varepsilon_3 + \varepsilon_1 - 2\varepsilon_2$	Coefficients		Equivalent Uniform Stresses	
	μ_ε	%	%	%	\bar{a}	\bar{b}	σ_{\min} (MPa)	σ_{\max} (MPa)
0.025	-14	6	34	26	0.020	0.038	-139	91
	-10	-5%	4%	6%				
	20							
0.050	-41	6	88	58	0.049	0.090	-129	110
	-26	-5%	11%	14%				
	47							
0.103	-132	-12	252	148	0.108	0.206	-136	153
	-80	10%	31%	37%				
	120							
0.150	-241	-50	432	242	0.151	0.305	-139	192
	-146	43%	52%	60%				
	191							
0.201	-319	-82	556	292	0.177	0.377	-133	207
	-187	70%	68%	72%				
	237							
0.250	-381	-107	655	323	0.19	0.425	-131	220
	-215	91%	80%	80%				
	274							
0.300	-419	-119	719	349	0.195	0.454	-131	228
	-234	102%	87%	86%				
	300							
0.350	-454	-131	777	375	0.195	0.472	-133	240
	-253	112%	94%	93%				
	323							
0.400	-470	-117	823	405	0.192	0.482	-146	242
	-261	100%	100%	100%				
	353							

Table A.3 Measurement of Residual Stress by the Hole-Drilling Method

Specimen AA30 at Point 3

Z/D	Measured Strain	$\varepsilon_3 + \varepsilon_1$	$\varepsilon_3 - \varepsilon_1$	$\varepsilon_3 + \varepsilon_1 - 2\varepsilon_2$	Coefficients		Equivalent Uniform Stresses	
	μ_ε				%	%	%	\bar{a}
0.025	34	39	-29	29	0.020	0.038	-264	-44
	5	34%	7%	14%				
	5							
0.050	85	75	-95	53	0.049	0.090	-244	2
	11	66%	24%	25%				
	-10							
0.103	167	135	-199	131	0.108	0.206	-217	19
	2	118%	51%	62%				
	-32							
0.150	215	165	-265	181	0.151	0.305	-194	21
	-8	145%	68%	85%				
	-50							
0.201	246	168	-324	224	0.177	0.377	-182	32
	-28	147%	84%	106%				
	-78							
0.250	257	167	-347	257	0.19	0.425	-173	34
	-45	146%	89%	121%				
	-90							
0.300	265	154	-376	264	0.195	0.454	-166	41
	-55	135%	97%	125%				
	-111							
0.350	262	131	-393	211	0.195	0.472	-150	43
	-40	115%	101%	100%				
	-131							
0.400	251	114	-388	212	0.192	0.482	-141	47
	-49	100%	100%	%100				
	-137							

Table A.4 Measurement of Residual Stress by the Hole-Drilling Method

Specimen A30 at Point 1

Z/D	Measured Strain	$\varepsilon_3 + \varepsilon_1$	$\varepsilon_3 - \varepsilon_1$	$\varepsilon_3 + \varepsilon_1 - 2\varepsilon_2$	Coefficients		Equivalent Uniform Stresses	
	μ_ε	%	%	%	\bar{a}	\bar{b}	σ_{\min} (MPa)	σ_{\max} (MPa)
0.025	-2	-4	0	-6	0.020	0.038	0	32
	1	-14%	0%	-12%				
	-2							
0.050	0	-2	-2	-4	0.049	0.090	-2	8
	1	-7%	20%	-8%				
	-2							
0.103	4	3	-5	19	0.108	0.206	-12	8
	-8	11%	50%	37%				
	-1							
0.150	3	1	-5	9	0.151	0.305	-4	3
	-4	4%	50%	17%				
	-2							
0.201	10	13	-7	31	0.177	0.377	-14	3
	-9	46%	70%	60%				
	3							
0.250	7	11	-3	37	0.19	0.425	-13	4
	-13	39%	30%	71%				
	4							
0.300	16	22	-10	26	0.195	0.454	-15	-3
	-2	79%	100%	50%				
	6							
0.350	16	22	-10	28	0.195	0.472	-15	-2
	-3	79%	100%	54%				
	6							
0.400	19	28	-10	52	0.192	0.482	-23	0
	-12	100%	100%	100%				
	-9							

Table A.5 Measurement of Residual Stress by the Hole-Drilling Method

Specimen A30 at Point 2

Z/D	Measured Strain				Coefficients		Equivalent Uniform Stresses	
	μ_ε	$\varepsilon_3 + \varepsilon_1$ %	$\varepsilon_3 - \varepsilon_1$ %	$\varepsilon_3 + \varepsilon_1 - 2\varepsilon_2$ %	\bar{a}	\bar{b}	σ_{\min} (MPa)	σ_{\max} (MPa)
0.025	-14	-11	17	-11	0.020	0.038	-11	98
	0	6%	3%	-20%				
	3							
0.050	-37	-18	56	-8	0.049	0.090	-35	93
	-5	9%	9%	-15%				
	19							
0.103	-88	-46	130	4	0.108	0.206	-31	98
	-25	24%	21%	7%				
	42							
0.150	-133	-65	201	7	0.151	0.305	-33	101
	-36	33%	32%	13%				
	68							
0.201	-190	-92	288	24	0.177	0.377	-37	119
	-58	47%	45%	44%				
	98							
0.250	-272	-130	414	46	0.19	0.425	-46	154
	-88	67%	65%	84%				
	142							
0.300	-296	-136	456	44	0.195	0.454	-48	158
	-90	70%	72%	80%				
	160							
0.350	-352	-159	545	39	0.195	0.472	-54	183
	-99	82%	86%	71%				
	193							
0.400	-414	-195	633	55	0.192	0.482	-54	215
	-125	100%	100%	100%				
	219							

Table A.6 Measurement of Residual Stress by the Hole-Drilling Method

Specimen A30 at Point 3

Z/D	Measured Strain	$\varepsilon_3 + \varepsilon_1$	$\varepsilon_3 - \varepsilon_1$	$\varepsilon_3 + \varepsilon_1 - 2\varepsilon_2$	Coefficients		Equivalent Uniform Stresses	
	μ_ε				%	%	%	\bar{a}
0.025	1	-2	-4	6	0.020	0.038	-11	27
	-4	-2%	1%	-3%				
	-3							
0.050	11	8	-14	18	0.049	0.090	-39	13
	-5	8%	5%	-10%				
	-3							
0.103	65	64	-66	62	0.108	0.206	-92	-2
	1	65%	23%	-34%				
	-1							
0.150	113	101	-125	113	0.151	0.305	-109	3
	-6	103%	43%	-63%				
	-12							
0.201	154	104	-204	-196	0.177	0.377	-123	30
	150	106%	71%	109%				
	-50							
0.250	172	104	-240	-184	0.19	0.425	-116	29
	144	106%	83%	102%				
	-68							
0.300	183	106	-260	-194	0.195	0.454	-116	30
	150	108%	90%	108%				
	-77							
0.350	190	106	-274	-178	0.195	0.472	-114	28
	142	108%	95%	99%				
	-84							
0.400	193	98	-288	-180	0.192	0.482	-112	32
	139	100%	100%	100%				
	-95							

Table A.7 Measurement of Residual Stress by the Hole-Drilling Method

Specimen BB40 at Point 1

Z/D	Measured Strain				Coefficients		Equivalent Uniform Stresses	
	μ_ε	$\varepsilon_3 + \varepsilon_1$ %	$\varepsilon_3 - \varepsilon_1$ %	$\varepsilon_3 + \varepsilon_1 - 2\varepsilon_2$ %	\bar{a}	\bar{b}	σ_{\min} (MPa)	σ_{\max} (MPa)
0.025	-23	-37	9	-19	0.020	0.038	90	203
	-9	-14%	-6%	-9%				
	-14							
0.050	70	74.5	-65.5	52.5	0.049	0.090	-215	-25
	11	29%	43%	25%				
	4.5							
0.103	156	177	-135	125	0.108	0.206	-221	-38
	26	69%	89%	61%				
	21							
0.150	184	226	-142	140	0.151	0.305	-185	-52
	43	88%	93%	68%				
	42							
0.201	204	260.5	-147.5	170.5	0.177	0.377	-177	-55
	45	102%	97%	83%				
	56.5							
0.250	215	298	-132	216	0.19	0.425	-185	-63
	41	116%	87%	105%				
	83							
0.300	206	259	-153	199	0.195	0.454	-161	-49
	30	101%	101%	97%				
	53							
0.350	210	266	-154	202	0.195	0.472	-163	-53
	32	104%	101%	98%				
	56							
0.400	204	256	-152	206	0.192	0.482	-160	-51
	25	100%	100%	100%				
	52							

Table A.8 Measurement of Residual Stress by the Hole-Drilling Method

Specimen BB40 at Point 2

Z/D	Measured Strain	$\varepsilon_3 + \varepsilon_1$	$\varepsilon_3 - \varepsilon_1$	$\varepsilon_3 + \varepsilon_1 - 2\varepsilon_2$	Coefficients		Equivalent Uniform Stresses	
	μ_ε	%	%	%	\bar{a}	\bar{b}	σ_{\min} (MPa)	σ_{\max} (MPa)
0.025	2	-22	-26	4	0.020	0.038	16	158
	-13	5%	3%	2%				
	-24							
0.050	12	-53	-77	5	0.049	0.090	-2	173
	-29	13%	8%	2%				
	-65							
0.103	55	-163	-273	49	0.108	0.206	-18	257
	-106	40%	30%	22%				
	-218							
0.150	108	-255	-471	89	0.151	0.305	-27	294
	-172	63%	51%	39%				
	-363							
0.201	156	-329	-641	121	0.177	0.377	-30	323
	-225	81%	70%	54%				
	-485							
0.250	195	-373	-763	161	0.19	0.425	-32	342
	-267	92%	83%	71%				
	-568							
0.300	220	-398	-838	182	0.195	0.454	-31	354
	-290	99%	91%	81%				
	-618							
0.350	245	-401	-891	211	0.195	0.472	-35	360
	-306	99%	97%	93%				
	-646							
0.400	258	-404	-920	226	0.192	0.482	-34	367
	-315	100%	100%	100%				
	-662							

Table A.9 Measurement of Residual Stress by the Hole-Drilling Method

Specimen BB40 at Point 3

Z/D	Measured Strain	$\varepsilon_3 + \varepsilon_1$	$\varepsilon_3 - \varepsilon_1$	$\varepsilon_3 + \varepsilon_1 - 2\varepsilon_2$	Coefficients		Equivalent Uniform Stresses	
	μ_ε				%	%	%	\bar{a}
0.025	0	5	5	-9	0.020	0.038	-47	8
	7	24%	2%	2%				
	5							
0.050	-9	8	26	-44	0.049	0.090	-71	45
	26	38%	9%	9%				
	17							
0.103	-35	16	86	-178	0.108	0.206	-110	86
	97	76%	30%	36%				
	51							
0.150	-62	41	165	-283	0.151	0.305	-131	88
	162	195%	57%	57%				
	103							
0.201	-88	48	224	-374	0.177	0.377	-139	97
	211	229%	78%	75%				
	136							
0.250	-107	45	259	-437	0.19	0.425	-141	103
	241	214%	90%	88%				
	152							
0.300	-119	38	276	-472	0.195	0.454	-138	107
	255	181%	96%	95%				
	157							
0.350	-127	32	286	-488	0.195	0.472	-135	109
	260	152%	99%	98%				
	159							
0.400	-134	21	289	-497	0.192	0.482	-130	113
	259	100%	100%	100%				
	155							

Table A.10 Measurement of Residual Stress by the Hole-Drilling Method

Specimen B40 at Point 1

Z/D	Measured Strain	$\varepsilon_3 + \varepsilon_1$	$\varepsilon_3 - \varepsilon_1$	$\varepsilon_3 + \varepsilon_1 - 2\varepsilon_2$	Coefficients		Equivalent Uniform Stresses	
	μ_ε				%	%	%	\bar{a}
0.025	3	5	-1	3	0.020	0.038	-36	-28
	1	-100%	3%	12%				
	2							
0.050	5	3	-7	-7	0.049	0.090	23	-16
	5	-60%	19%	-28%				
	-2							
0.103	7	22	8	-4	0.108	0.206	-13	-21
	13	-440%	-22%	-16%				
	15							
0.150	2	18	14	-16	0.151	0.305	-24	-17
	17	-360%	-38%	-64%				
	16							
0.201	5	29	19	-17	0.177	0.377	-21	-20
	23	-580%	-51%	-68%				
	24							
0.250	6	-21	-33	-69	0.19	0.425	32	-10
	24	420%	89%	-276%				
	-27							
0.300	6	-20	-32	28	0.195	0.454	-21	-1
	-24	400%	86%	112%				
	-26							
0.350	12	-12	-36	32	0.195	0.472	-21	-6
	-22	240%	97%	128%				
	-24							
0.400	16	-5	-37	25	0.192	0.482	-17	-7
	-15	100%	100%	100%				
	-21							

Table A.11 Measurement of Residual Stress by the Hole-Drilling Method

Specimen B40 at Point 2

Z/D	Measured Strain	$\varepsilon_3 + \varepsilon_1$	$\varepsilon_3 - \varepsilon_1$	$\varepsilon_3 + \varepsilon_1 - 2\varepsilon_2$	Coefficients		Equivalent Uniform Stresses	
	μ_ε				%	%	%	\bar{a}
0.025	-1	-8	-6	0	0.020	0.038	16	48
	-4	2%	1%	0%				
	-7							
0.050	5	-42	-52	-6	0.049	0.090	8	127
	-18	13%	7%	-40%				
	-47							
0.103	34	-100	-168	-8	0.108	0.206	-10	156
	-46	30%	23%	-53%				
	-134							
0.150	70	-175	-315	-7	0.151	0.305	-14	197
	-84	53%	44%	-47%				
	-245							
0.201	130	-270	-530	78	0.177	0.377	-24	266
	-174	81%	74%	520%				
	-400							
0.250	140	-305	-585	17	0.19	0.425	-14	267
	-161	92%	82%	113%				
	-445							
0.300	171	-315	-657	19	0.195	0.454	-20	275
	-167	95%	92%	127%				
	-486							
0.350	182	-330	-694	16	0.195	0.472	-16	284
	-173	99%	97%	107%				
	-512							
0.400	192	-333	-717	15	0.192	0.482	-15	289
	-174	100%	100%	100%				
	-525							

Table A. 12 Measurement of Residual Stress by the Hole-Drilling Method**Specimen B40 at Point 3**

Z/D	Measured Strain	$\varepsilon_3 + \varepsilon_1$	$\varepsilon_3 - \varepsilon_1$	$\varepsilon_3 + \varepsilon_1 - 2\varepsilon_2$	Coefficients		Equivalent Uniform Stresses	
	μ_ε				%	%	%	\bar{a}
0.025	-1	0	2		0.020	0.038	-5	5
	0	0%	1%	0%				
	1							
0.050	7	17	3	-3	0.049	0.090	-32	-23
	10	8%	1%	-1%				
	10							
0.103	34	91	23	-49	0.108	0.206	-93	-40
	70	43%	7%	-22%				
	57							
0.150	20	134	94	14	0.151	0.305	-102	-38
	60	63%	27%	6%				
	114							
0.201	-9	165	183	65	0.177	0.377	-126	-21
	50	78%	52%	90%				
	174							
0.250	-22	199	243	117	0.19	0.425	-148	-18
	41	94%	69%	52%				
	221							
0.300	-44	211	299	157	0.195	0.454	-161	-10
	27	100%	85%	69%				
	255							
0.350	-64	214	342	214	0.195	0.472	-174	0
	0	101%	98%	95%				
	278							
0.400	-69	212	350	226	0.192	0.482	-175	1
	-7	100%	100%	100%				
	281							

Appendix B

Tension Tests

The stress-strain curves for the ten coupons are shown in Figs. B.1-B.10. Poisson's ratio was calculated for three coupons by taking the negative ratio of the transverse strain to its corresponding axial strain. Figs. B.11-B.13 show the axial and transverse strains for these coupons.

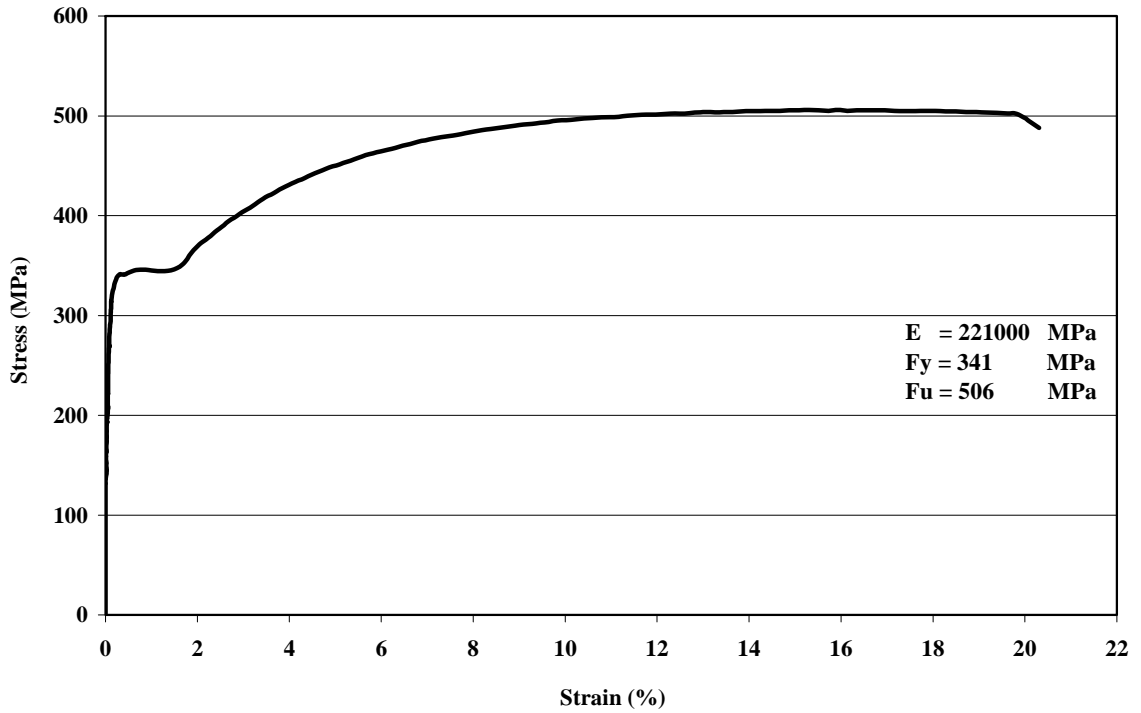


Figure B.1: Stress-Strain Curve for Specimen CP4-T1

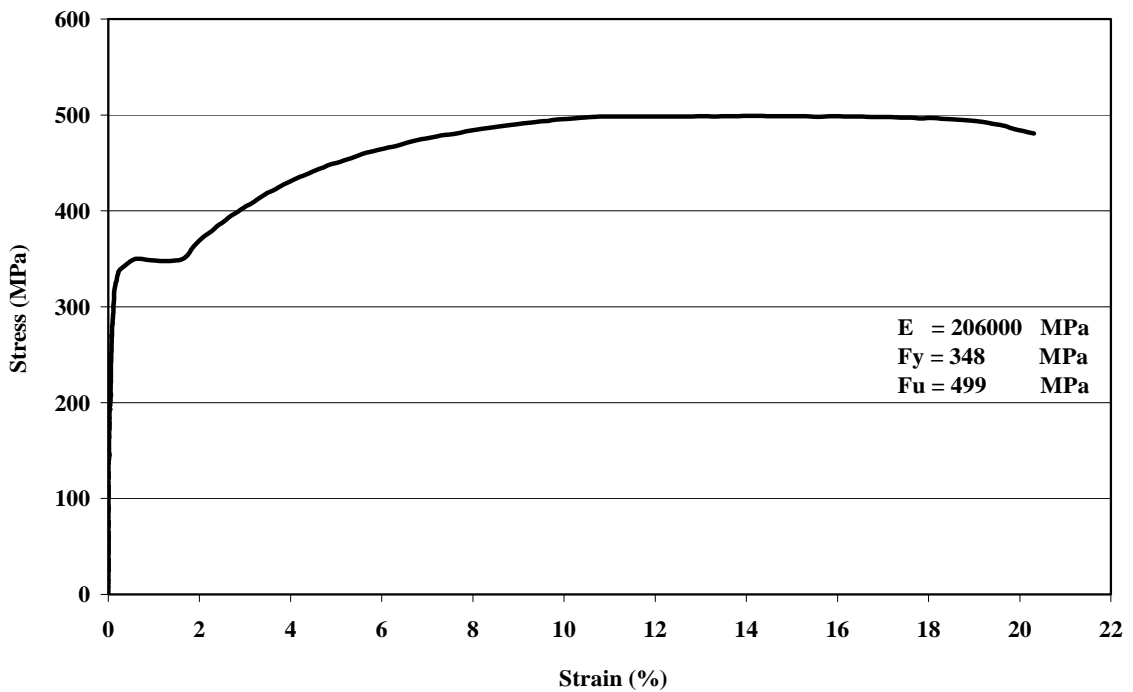


Figure B.2: Stress-Strain Curve for Specimen CP4-T2

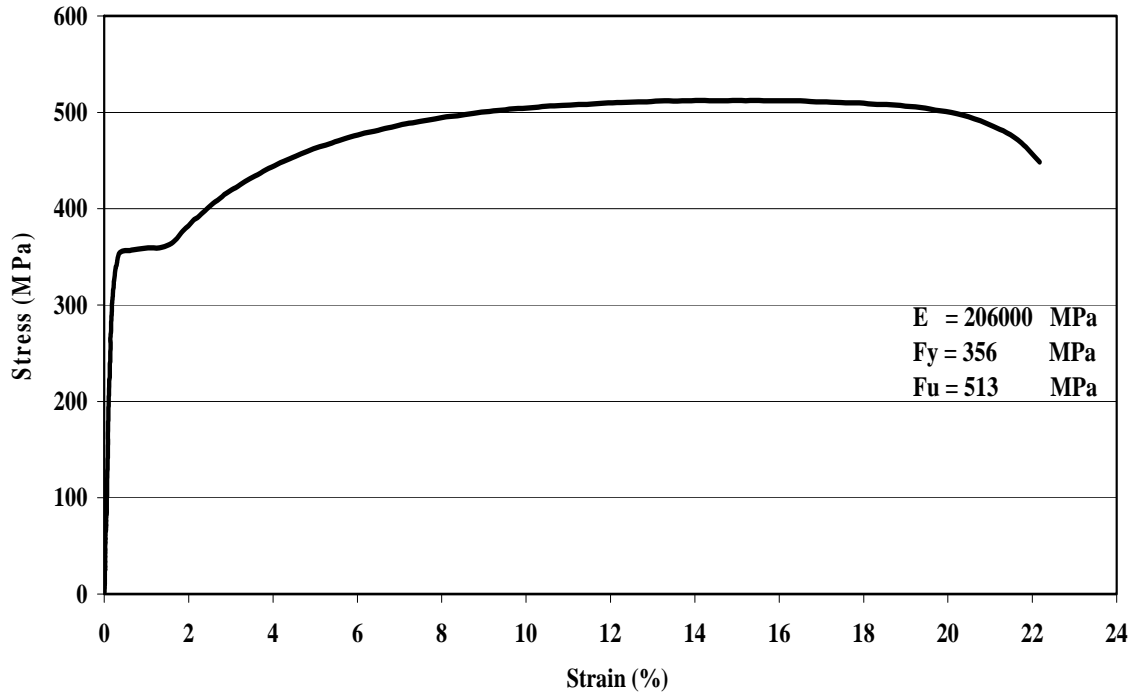


Figure B.3: Stress-Strain Curve for Specimen CP5-T3

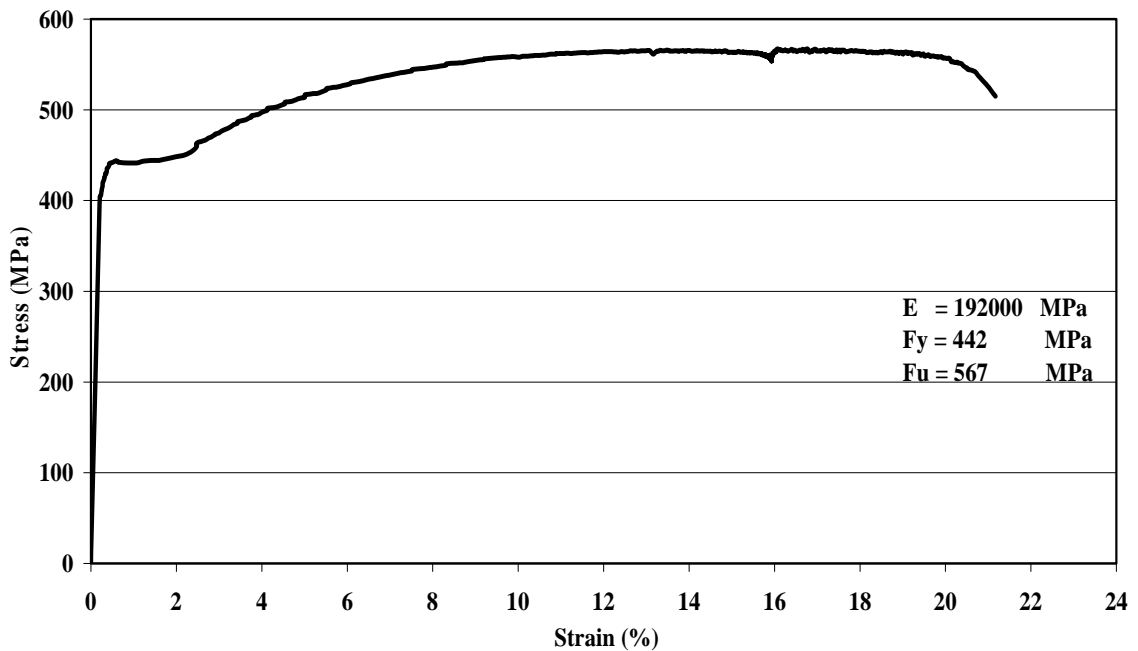


Figure B.4: Stress-Strain Curve for Specimen CP5-T4

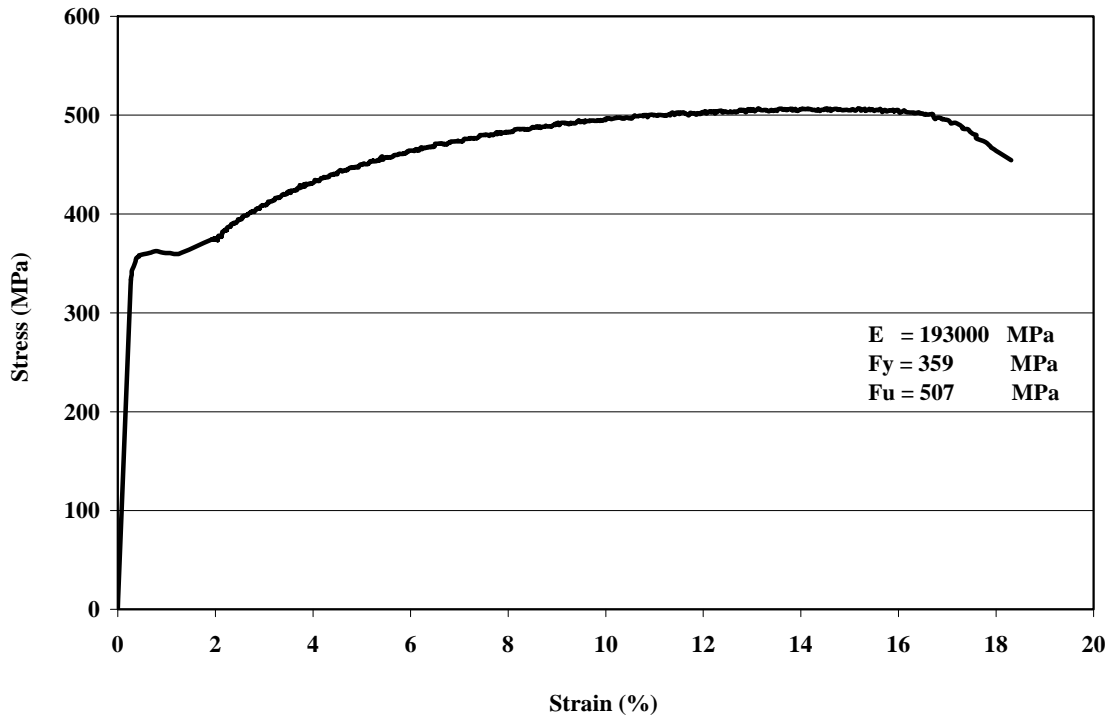


Figure B.5: Stress-Strain Curve for Specimen CP5-T5

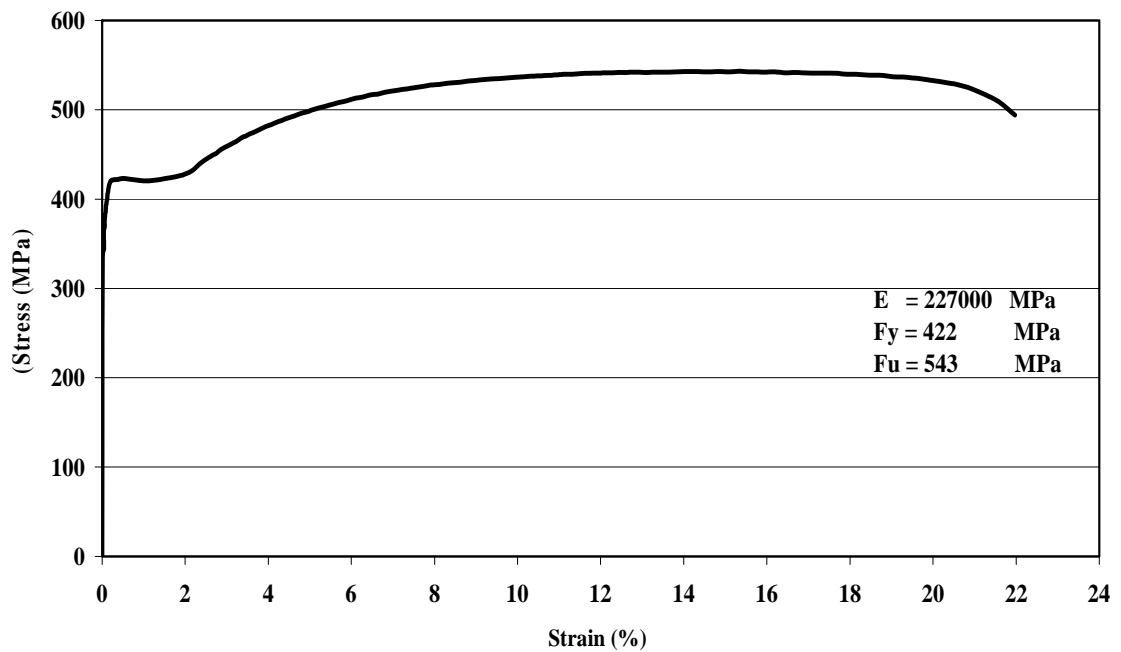


Figure B.6: Stress-Strain Curve for Specimen CP5-T6

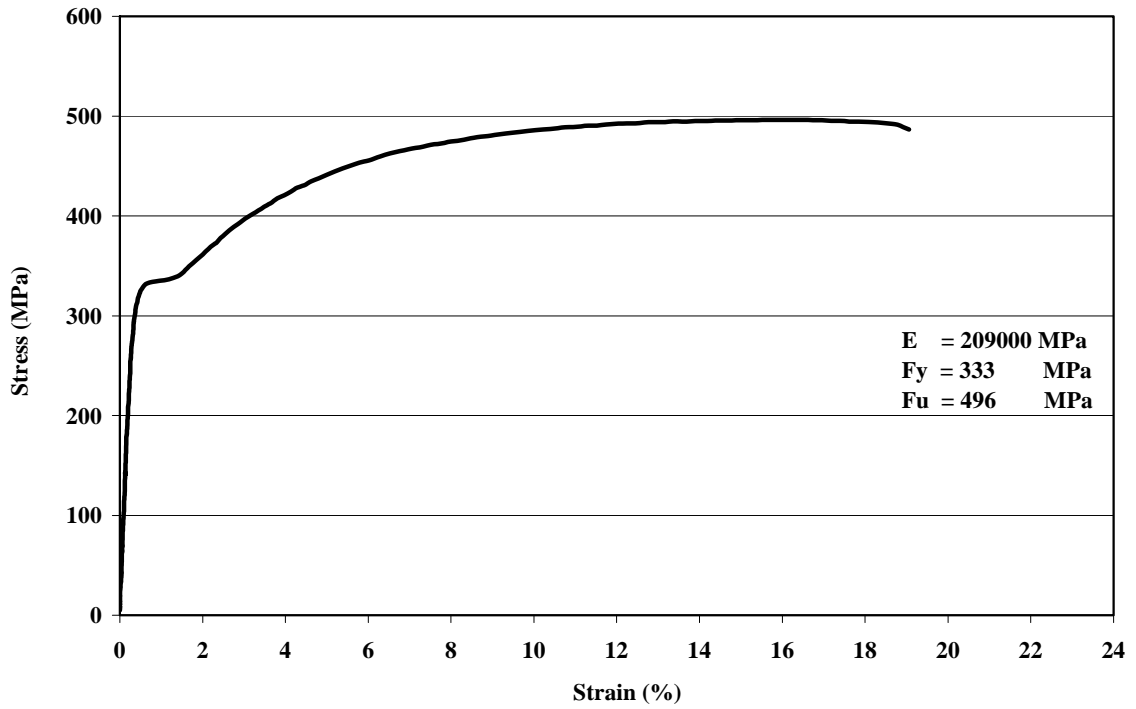


Figure B.7: Stress-Strain Curve for Specimen CP6-T7

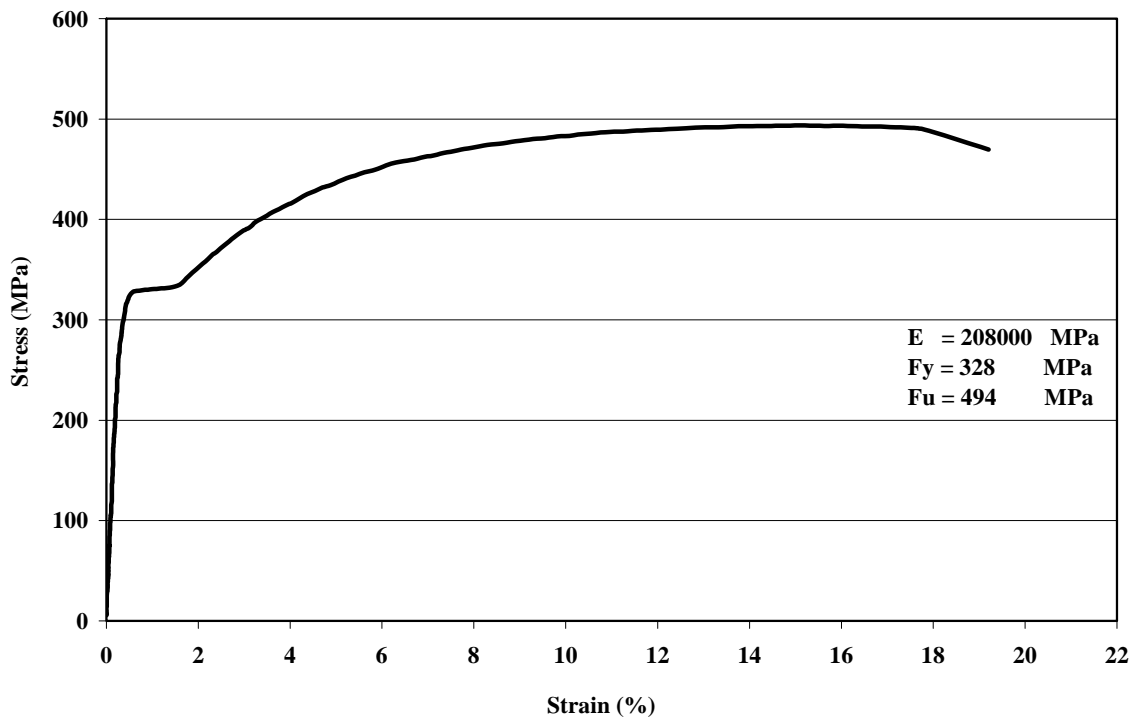


Figure B.8: Stress-Strain Curve for Specimen CP6-T8

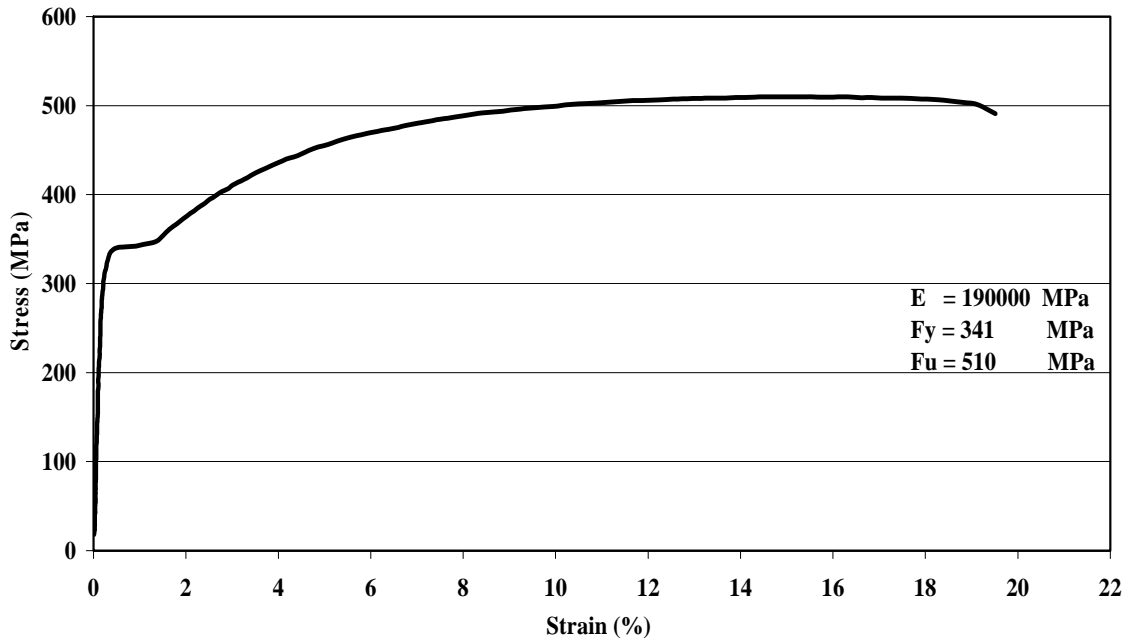


Figure B.9: Stress-Strain Curve for Specimen CP6-T9

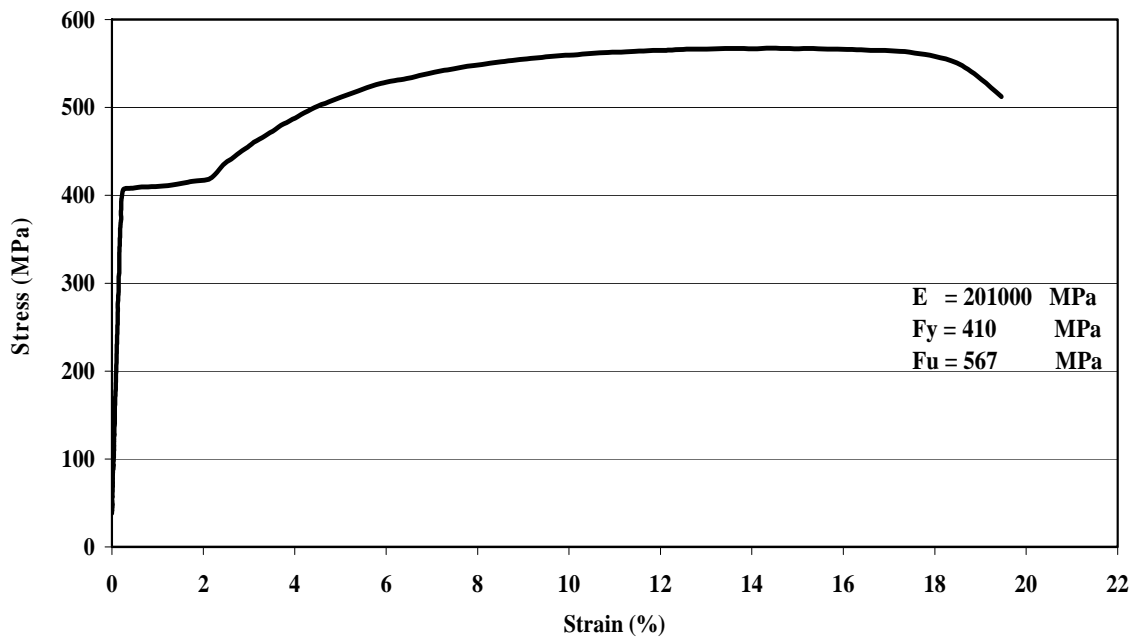


Figure B.10: Stress-Strain Curve for Specimen CP8-T10

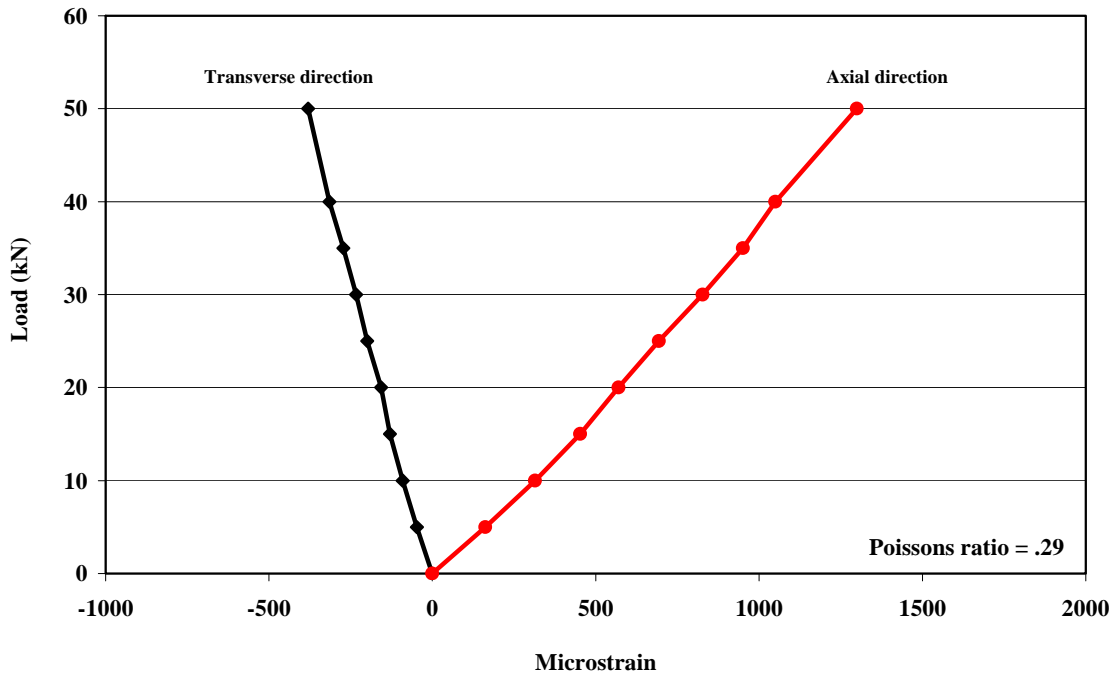


Figure B.11: Poisson's Ratio from Tensile Coupon Test CP5-T11

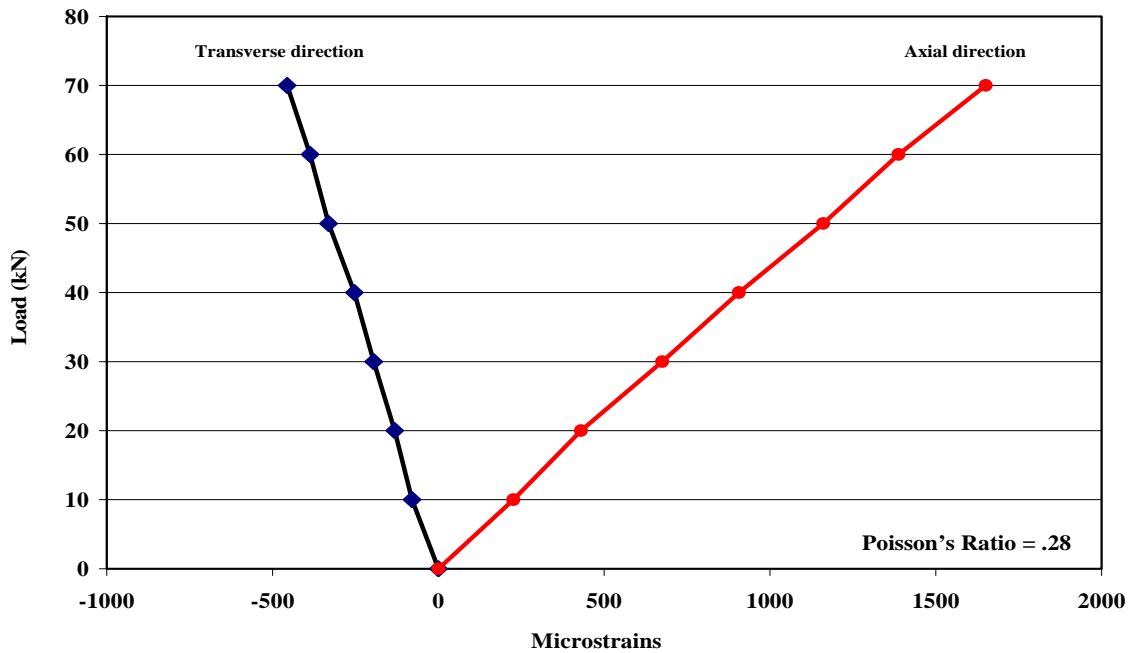


Figure B.12: Poisson's Ratio from Tensile Coupon Test CP6-T12

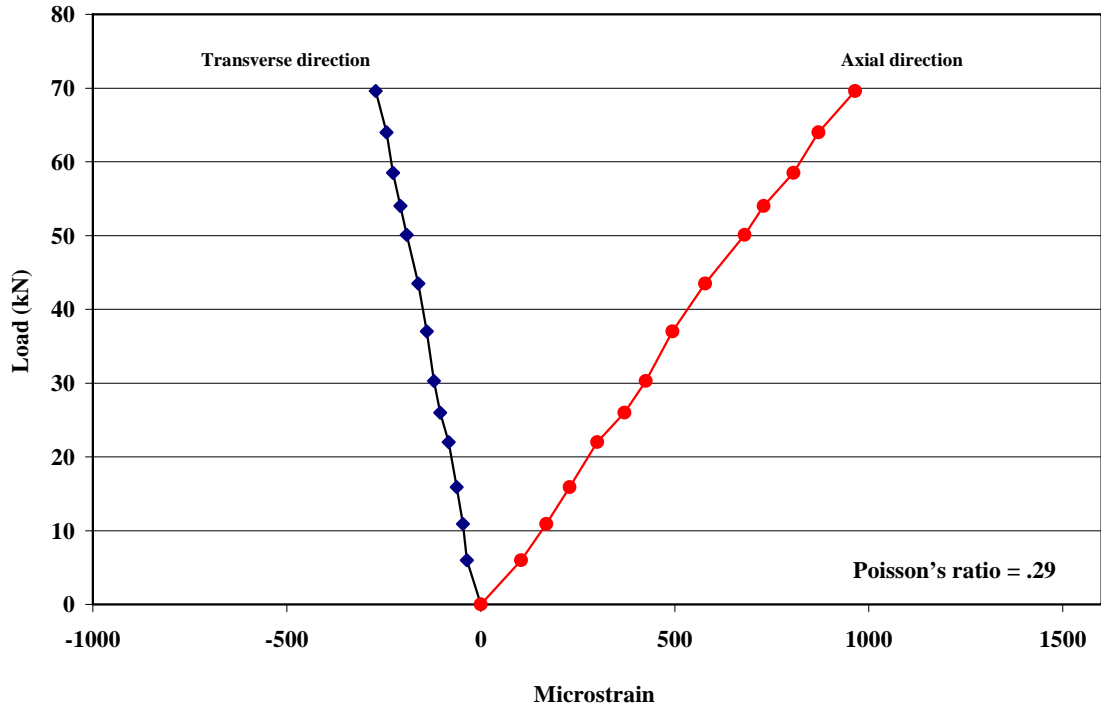


Figure B.13: Poisson's Ratio from Tensile Coupon Test CP8-T13

ملخص

تأثير اللحام على مقاومة انبعاج اللي الجانبى للجسور المصنعة على شكل I

اعداد

رجاء محمد سليمان يونس

المشرف

الأستاذ الدكتور ياسر محمد الحنيطي

المشرف المشارك

الأستاذ الدكتور غازي عبد الفتاح أبو فرسخ

لقد تم اجراء تجارب عملية لدراسة تأثير اللحام على تصرف الجسور المصنعة من صفائح فولاذية ملحومة أوتوماتيكياً. و قد أجريت هذه الاختبارات من خلال تحميل ١٩ جسراً" حملين شاقولين في الثلث الأوسط من الجائز. و لقد تم دراسة أنماط انهيار هذه الجسور و قدرتها على التحمل و مقارنتها مع المواصفات العالمية و الدراسات السابقة المماثلة.

أُستنتج من هذه الدراسة أن قدرة تحمل الجسور الملحومة من جهتين ليست دائماً" أعلى من قدرة تحمل جسور مماثلة لها ملحومة من جهة واحدة.